Fully Coupled Analysis of Large Scale Tracked Vehicle Systems with Flexible Link Chains

BY

MICHAEL WALLIN

B.S. in Mechanical Engineering, University of Illinois at Chicago, 2011

THESIS

Submitted as partial fulfillment of the requirements for the degree of
Doctor of Philosophy in Mechanical Engineering in the
Graduate College of the University of Illinois at Chicago, 2016

Chicago, Illinois

Defense Committee:

Professor Ahmed A. Shabana, Chair and Advisor, Mechanical and Industrial Engineering
Eduard Karpov, Civil and Materials Engineering
Sheng-Wei Chi, Civil and Materials Engineering
Ashraf Hamed, MSC Software
Paramsothy Jayakumar, U.S. Army RDECOM-TARDEC

Contribution of Authors

Chapter 2 represents a published manuscript (Ding, Jieyu, Wallin, Michael, Wei, Cheng, Recuero, Antonio M., Shabana, Ahmed A., 2014, “Use of Independent Rotation Field in the Large Displacement Analysis of Beams,” Journal of Computational and Nonlinear Dynamics, Vol. 76(3), pp. 1829-1843) for which I am the secondary author and main contributor to the writing. Jieyu Ding created the base code for which all the simulation results would eventually be found while Cheng Wei altered this code to match specific situational results, such as Figures 2.8 and 2.9 which add an extension force and a moment at the tip, respectively. Antonio Recuero contributed with advice, editing, and organizing subsections to be addressed, specifically with mapping out Section 2.5 on issues with the LRVF. My research advisor, Dr. Ahmed Shabana contributed to the writing of the manuscript.

Chapter 3 represents another published manuscript (Wallin, Michael, Aboubakr, Ahmed K., Jayakumar, Paramsothy, Letherwood, Michael D., Gorsich, David J., Hamed, Ashraf, Shabana, Ahmed A., 2013, "A Comparative Study of Joint Formulations: Application to Multibody System Tracked Vehicles," Journal of Computational and Nonlinear Dynamics, Vol. 74(3), pp. 783-800) for which I am the primary author. In this manuscript, I ran all rigid-bodied simulations, created the figures, and was the main contributor to the writing. Ahmed Aboubakr contributed with analysis of the results and further contributed with writing and organization. Paramsothy Jayakumar, Michael Letherwood, and David Gorsich of TARDEC contributed with funding for this project, suspension details to the tracked vehicle that was simulated, and, in Dr. Jayakumar’s case, helped with editing and the conclusions made based on the results. Ashraf Hamed contributed with his development and simulation of the ANCF flexible chain tracked

vehicle model and the calculation of the ANCF elastic forces used in Figures 3.11-3.14. My research advisor, Ahmed Shabana contributed to the writing of the manuscript.

Chapter 4 represents the final published manuscript (Wallin, Michael, Hamed, Ashraf M., Paramsothy, Jayakumar, Gorsich, David J., Letherwood, Michael D., Shabana, Ahmed, A., 2016, "Evaluation of the Accuracy of the Rigid Body Approach in the Prediction of the Dynamic Stresses of Complex Multibody Systems," International Journal of Vehicle Performance, Vol. 2(2), pp. 140-165) for which I am the primary author and main contributor to the writing. Ashraf Hamed helped with debugging the code I had written for the FFR post processing results and editing. Paramsothy Jayakumar, Michael Letherwood, and David Gorsich of TARDEC contributed with funding for this project. Paramsothy Jayakumar came up with the idea for comparing FFR and ANCF strain results for the track link of the tracked vehicle model and helped further with editing and suggestions for the investigation. My research advisor, Ahmed Shabana contributed to the writing of the manuscript.

TABLE OF CONTENTS

LIST OF TABLES

LIST OF FIGURES

SUMMARY

This thesis examines multiple multibody dynamic formulations and their effects in the large displacement analysis of flexible bodies. The second chapter will examine the effect of using independent finite rotation fields in the large displacement analysis of flexible beams first formulated 30 years ago. This finite rotation description is at the core of the large rotation vector formulation (LRVF), which has been used in the dynamic analysis of bodies experiencing large rotation and deformation. The LRVF employs two independently interpolated meshes for describing the flexible body dynamics: the position mesh and the rotation mesh. The use of these two geometrically independent meshes can lead to coordinate and geometric invariant redundancy that can be the source of fundamental problems in the analysis of large deformations. It is demonstrated in this thesis that the two geometry meshes can define different space curves, which can differ by arbitrary rigid body displacements. The material points of the two meshes occupy different positions in the deformed configuration, and as a consequence, the geometries of the two meshes can differ significantly. Other issues including energy conservation and the inextensibility of the rotation mesh will also be discussed. Simple examples are presented in order to shed light on these fundamental issues.

The third chapter of this thesis focuses on the dynamic formulation of mechanical joints using different approaches that lead to different models with different numbers of degrees of freedom. Some of these formulations allow for capturing the joint deformations using discrete elastic model while the others are continuum-based and capture joint deformation modes that cannot be captured using the discrete elastic joint models. Specifically, four types of joint formulations are considered in this chapter; the *ideal*, *penalty*, *compliant discrete element*, and *compliant continuum-based joint models*. The *ideal joint formulation*, or constrained dynamics

approach, which does not allow for deformation degrees of freedom in the case of rigid body or small deformation analysis, requires introducing a set of algebraic constraint equations that can be handled in computational multibody system (MBS). When the constrained dynamics approach is used, the constraint equations must be satisfied at the position, velocity, and acceleration levels. The *penalty method*, on the other hand, ensures that the same algebraic equations are satisfied at the position level only with a force-based approach. In the *compliant discrete element joint formulation*, no constraint conditions are used; instead the connectivity conditions between bodies are enforced using forces that can be defined in their most general form in MBS algorithms using bushing elements that allow for the definition of general nonlinear forces and moments. The new *compliant continuum-based joint formulation*, which is based on the finite element (FE) absolute nodal coordinate formulation (ANCF), has several advantages: (1) It captures modes of joint deformations that cannot be captured using the compliant discrete joint models; (2) It leads to linear connectivity conditions, thereby allowing for the elimination of the dependent variables at a preprocessing stage; (3) It leads to a constant inertia matrix in the case of chain like structure; and (4) It automatically captures the deformation of the bodies using distributed inertia and elasticity. The formulations of these three different joint models are compared in order to shed light on the fundamental differences between them. Numerical results of a detailed tracked vehicle model are presented in order to demonstrate the implementation of some of the formulations discussed in this chapter.

Because of the lack of computational methods that can be used for the direct calculation of the stresses of complex multibody systems such as tracked vehicles, the dynamic stresses of such systems are often evaluated at a post-processing stage using forces obtained from a rigid body analysis. With the recent developments in MBS dynamics, detailed flexible body models of

vehicle systems can be developed and used to evaluate, for the first time, the accuracy of the stress prediction based on the rigid body force calculations. It is, therefore, the objective of this chapter to use the finite element absolute nodal coordinate formulation, which automatically accounts for the dynamic coupling between the rigid body motion and the elastic deformation, to obtain the stress results. These results are then used to evaluate the accuracy of the stresses calculated at a post-processing stage using forces determined from a rigid body analysis. ANCF finite elements are used to perform the coupled dynamic analysis and obtain the stresses based on a fully nonlinear flexible body analysis. In order to obtain an accurate representation of the stresses in the case of the rigid body analysis, the floating frame of reference (FFR) formulation dynamic equations are used to define the inertia and joint reaction forces that must be used in the post-processing stress calculations. To this end, the rigid body accelerations, including the angular accelerations, as well as the joint reaction forces are first predicted using a rigid body analysis. The solution of the rigid body problem is then used to formulate the FFR equations associated with the elastic coordinates. These equations include the effect of the inertia, centrifugal, and Coriolis forces resulting from the rigid body displacements. The resulting linear second order ordinary differential equations associated with the FFR elastic coordinates are solved for the elastic accelerations which are integrated to determine the elastic coordinates and velocities. The obtained elastic coordinates are used to determine the stresses which are compared with the stresses obtained using the fully coupled ANCF analysis. The two approaches described are explained in detail and used in the stress analysis of the track links in a complex three-dimensional tracked vehicle model. One of the most common areas of failure for such tracked vehicles is attributed to the failure of the track link chains, and therefore, performing a

detailed fully coupled stress analysis, as the one described in this chapter, is necessary in order to obtain more accurate stress results and avoid failure of such complex vehicle systems.

ACKNOWLEDGEMENTS

I would like to thank Dr. Ahmed A. Shabana for his guidance throughout my professional and graduate career. I'd like to thank Dr. Ashraf Hamed, Dr. Ahmed Aboubakr, and Dr. Ulysses Contreras for all the work accomplished together on the tracked vehicle model I have presented so many times as well as everyone else in the Dynamic Simulation Laboratory I have worked with and learned from. I also want to thank Dr. Jayakumar for his contributions in thoroughly examining my results and investigations which led to my publications being of much higher quality. I'd also like to thank my remaining committee members Dr. Edward Karpov and Dr. Sheng-Wei Chi for their invaluable advice.

I would also like to thank the support I received from the US Army Tank-Automotive Research, Development, and Engineering Center (TARDEC).

CHAPTER 1

INTRODUCTION

1.1 LARGE DISPLACEMENT FORMULATIONS

The choice of the geometric description used in large displacement analysis can be a challenge, particularly in the case of finite rotations. An example of a large displacement analysis formulation is the floating frame of reference (FFR) formulation, which is widely used when the bodies experience finite rigid body rotation and small deformation. This formulation leads to a local linear elasticity problem that allows for exploiting model-order reduction techniques (Shabana, 2014). Because of the need for the simulation of rigid body motion and large deformation, several nonlinear theories were proposed in the two fields of computational mechanics and flexible multibody system (MBS) dynamics. In the co-rotational formulations, a coordinate system is used for each finite element to define both the elastic and inertia forces (Belytschko et al., 1977). In the absolute nodal coordinate formulation (ANCF), on the other hand, the rigid and flexible body motion is defined using global coordinates including Cartesian position and gradient coordinates (Bayoumy et al., 2013; Gerstmayr et al., 2013; Shabana, 2012). Another finite element (FE) formulation used for the description of large rotation and large deformation problems is the large rotation vector formulation (LRVF), which is supposed to be a non-incremental procedure intended mostly for beam and plate applications (Simo and Vu-Quoc, 1986). Simo and Vu-Quoc developed this formulation by describing the geometrically exact beam dynamics based on the Kirchhoff-Love model developed by Reissner (1972; 1973). Reissner's work represents the foundation of the large-displacement finite-strain theory of shear-deformable beams (Irschik and Gerstmayr, 2009). Reissner formulated a one-dimensional large-

strain beam theory for plane deformations by first deriving the local equations of beam equilibrium with the assumption of a plane and undistorted cross-section. He then developed generalized constitutive relations at the beam-theory level based on generalized strain measures such as the bending, axial force, and shear force strains. The virtual work of the internal, external, and boundary forces were then derived to obtain the governing equations. Simo and Vu-Quoc expanded upon this static theory to dynamics with the essence of this approach leading to accomplishing a fully nonlinear plane beam theory that can account for finite rotations as well as finite strains. Absolute positions and absolute finite angles are used as generalized coordinates. The position and rotation fields are interpolated independently in the LRVF, giving rise to questions with regard to the redundancy in the geometric description. The rotation field can be used to define a tangent vector that defines a space curve which possesses geometric properties, such as curvature and torsion, which can significantly differ from those obtained using the position field (Shabana, 2010). In fact, the nodes of the position-based (PB) interpolation can occupy positions in space that are different from the positions occupied by the nodes of the rotation-based (RB) interpolation. Furthermore, as will be shown in this thesis, the rotation mesh defines a beam that is inextensible, leading to an additional inconsistency in the LRVF geometry representation.

Several notable contributions by other authors were based on Simo and Vu-Quoc's geometrically exact beam theory, such as the work of Romero (2004) who examined the use of interpolation types for the rotation field. The interpolations types were discussed in terms of advantages and drawbacks using nonlinear rod models to provide qualitative and quantitative evaluation of four interpolation techniques with the goal to assess each method. The best overall properties were obtained with models using an orthogonal interpolation in the rotation group,

where the objectivity of the continuum model was preserved. This method was originally proposed by Crisfield and Jelenic (1999), where it was also shown that the application of linear interpolation techniques to finite rotation fields of either incremental or iterative rotations is non-objective and is path-dependent. Objectivity is achieved when the geometry is invariant under rigid body transformation. When this condition is met, the formulation is said to be objective, otherwise it is non-objective. In order to address this problem, simple algorithms that achieve objectivity were developed to test finite rotation formulations to help identifying the source of the problems and deal with the unavoidable singularities associated with the use of some finite rotation parameters (Bauchau et al., 2008). Although the algorithms can handle the finite rotations through a rescaling operation, the separation of displacement and rotation fields still exists.

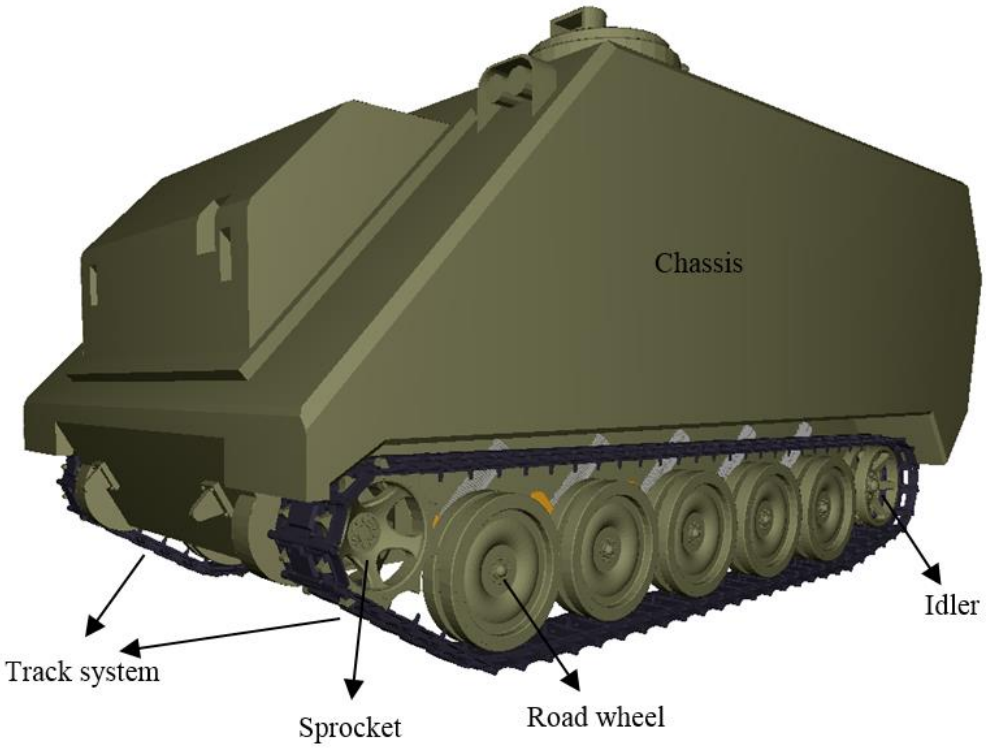

Figure 1.1: The SIGMA/SAMS tracked vehicle model

1.2 JOINT FORMULATION PRINCIPLES

Accurate formulation of mechanical joints is another necessity in the computer simulation of multibody systems that represent many technological and industrial applications. An example of these MBS applications, in which accurate modeling of joint compliance is necessary, is the tracked vehicle shown in Fig. 1.1. The links of the track chains of this vehicle are connected by pin joints that can be subjected to significant stresses during the vehicle functional operations. Nonetheless, there are different joint formulations that can lead to different dynamic models which have different numbers of degrees of freedom. This thesis will investigate the use of four different methods for formulating mechanical joints in MBS applications. These four methods are the ideal joint formulation, the penalty method, the compliant discrete element joint formulation, and the compliant continuum-based joint formulations.

The ideal joint formulation is based on a set of algebraic equations that do not account for the joint flexibility; this is regardless of whether or not the body is flexible. The algebraic joint equations are expressed in terms of the coordinates of the two bodies connected by the joint. These algebraic equations are considered as constraint equations which can be enforced using two fundamentally different methods; the constrained dynamics approach and the penalty method. In the constrained dynamics approach, the technique of Lagrange multipliers or a recursive method is used. In this case, the joint constraint equations must be satisfied at the position, velocity, and acceleration levels. The number of degrees of freedom of the model in this case is equal to the number of the system coordinates minus the number of the algebraic joint constraint equations. In the penalty method, on the other hand, the number of degrees of freedom of the model is not affected by the number of joint constraint equations. These joint algebraic

equations are enforced using high stiffness penalty coefficients that ensure that the algebraic constraint equations are satisfied at the position level. The penalty method does not ensure that the constraint equations are satisfied at the velocity and acceleration levels.

In the compliant discrete element joint formulation, no algebraic equations are used to describe the joints between bodies in the system. The connectivity between bodies is instead described using force elements that have forms defined by the user of the MBS code. MBS system codes have bushing elements that can be used to define general linear or nonlinear force and moment expressions. The stiffness and damping coefficients in the force and moment expressions can be selected by the user. The bushing elements can be used to model the joint compliance in the case of rigid and flexible body dynamics. It is important, however, to point out that adding bushing elements has no effect on the number of degrees of freedom of the model. Unlike the penalty method, the use of bushing element does not require the formulation of algebraic joint equations. Bushing elements allow for systematically introducing three force components and three moment components.

The new finite element (FE) absolute nodal coordinate formulation (ANCF) allows for systematically developing new joint formulations that capture modes of deformation that cannot be captured using the discrete joint models. It also allows for modeling body flexibility using new FE meshes that have constant inertia and linear connectivity conditions. Specifically, the compliant ANCF continuum-based joint formulation has the following advantages:

1. ANCF finite elements allow for developing new joint formulations that capture deformation modes that cannot be captured using compliant discrete joint formulations. The use of the ANCF gradient coordinates allows for developing different joint models with different numbers of degrees of freedom that allow for different strain modes.

2. The use of the ANCF gradient coordinates allows for developing linear joint constraint equations. These linear algebraic equations can be used to eliminate dependent variables at a preprocessing stage, thereby significantly reducing the model dimensionality.
3. ANCF finite elements can also be used to model the body deformation in addition to the joint compliance. Distributed inertia and elasticity are used for both body flexibility and joint compliance.
4. ANCF finite elements lead to new types of FE meshes that have constant inertia, a feature that can be exploited to develop a sparse matrix structure of the MBS dynamic equations.

1.3 STRESS ANALYSIS ON A COMPLEX TRACKED VEHICLE MODEL

Another contribution from this thesis, is an investigation into accurate predictions of the dynamic stresses in MBS simulations. This work is crucial in the design of many complex engineering systems. One system that is commonly modeled and tested because of its use in tough terrains and because of the high manufacturing and maintenance cost is the aforementioned tracked vehicle. One of the most complex and difficult to model sections of these vehicles is the track chain, which consists of multiple track links interconnected by revolute joints. As previously mentioned, these joints can be modeled using kinematic constraints or bushing elements to eliminate or constrain the necessary degrees of freedom and allow for a rotation about a single axis. Because of the difficulties of developing flexible link chain tracked vehicle models, the stress analysis of such systems has been performed by obtaining forces from a rigid body analysis of the vehicle. These forces are then used in a linear structural problem to obtain the track link stresses. With the recent developments in flexible MBS analysis techniques and the introduction of new finite element approaches, such as the absolute nodal coordinate

formulation, it is now feasible to build fully coupled flexible link chain tracked vehicle models. The results of these new nonlinear models, which account for the coupling between the rigid body motion and the elastic deformation, can be used to examine the accuracy of the models that ignore the effect of the elastic deformation on the rigid body motion of the track links. It is, therefore, another focus of this thesis to develop a fully nonlinear coupled ANCF stress analysis approach and use this approach to evaluate the stress results based on forces determined using the rigid body analysis.

1.3.1 Tracked Vehicle Development and Simulation

Choi et al. (1998) developed the first three-dimensional multibody tracked vehicle model utilizing nonlinear constrained dynamic equations of motion. Recursive kinematic equations for the vehicle were expressed in terms of independent joint coordinates using a velocity transformation matrix. Furthermore, three-dimensional nonlinear contact force models to describe the interaction between track links and the sprockets, road wheels, idlers and ground were developed and used to define the generalized contact forces associated with the vehicle generalized coordinates. Ryu et al. (2000) developed track link models using compliant elements based on experimental data from a high-speed tracked vehicle. Numerical difficulties encountered in the simulation of the tracked vehicle model due to high frequency contact forces were resolved by using explicit numerical integration methods with a variable time step size. Ryu et al. (2003) later validated the numerical results using real-life simulation data of the chassis and track link acceleration and track tension. Stiff compliant elements were used to represent the joints between the track links. An efficient contact search algorithm was used to detect the interactions between the track links and other vehicle components including the ground. Yamakawa and Watanabe (2004) developed a high-mobility rigid body tracked vehicle

model utilizing a torsion bar suspension system. The vehicle model was evaluated in terms of ride performance, steerability, and stability over rough terrain.

1.3.2 Dynamic Stress Analysis Comparison

As previously stated, one of the most widely accepted formulations used in flexible MBS applications is the FFR formulation. The FE/FFR formulation uses a coupled set of reference and elastic coordinates and allows for systematically filtering out complex shapes associated with high frequencies that have no significant effect on the solution. The reference coordinates define the location and orientation of a selected body reference while the elastic coordinates describe the body deformation with respect to the body reference (Nada et al., 2009; Shabana, 2014). The choice of the body reference is an important issue in defining the stresses and strains in the FFR formulation and this issue will be discussed further in the following section. The FFR formulation was used by Campanelli and Shabana (1998) to study the vibration and dynamic stresses of the track links of tracked vehicles. A detailed three-dimensional FE model of a track link was developed and used to determine the natural frequencies and mode shapes. An explanation of the terms representing the rigid body inertia, centrifugal and Coriolis forces in the equations of motion associated with the elastic coordinates of the track was provided. Furthermore, a computational procedure for determining the generalized constraint forces associated with the elastic coordinates of the deformable chain link was presented. Hamed et al. (2015) simplified the modeling of a heavily constrained tracked vehicle model by using flexible ANCF finite elements and linear connectivity conditions. The elimination of joint constraint equations at a preprocessing stage was discussed and attributed to solving a fundamental singularity problem with closed loop systems. Results of rigid- and flexible-linked chains were compared, including rigid body motion and constraint forces. It is impractical to develop a

detailed flexible link tracked vehicle model using the FFR formulation. It is important, however, to point out that in the case of small deformation problems, as it is the case with the track links, the results obtained using the two approaches (FFR and ANCF) have been compared in the literature. The reported results show that the two formulations agree well in the case of small deformations (Shabana and Schwertassek, 1998; Shabana, 2014; Dibold et al., 2009). Dibold et al. (2009), in particular, gave a detailed comparison between the ANCF and FFR using small and large static deformation problems, as well as small and large deformation dynamic problems. Included in this comparison are examples of a cantilever beam with a tip load, a pendulum subjected to the effect of gravity, and a slider-crank mechanism. Using the fact that the two formulations give similar results in the case of small deformation problems and the fact that it is impractical to develop an FFR tracked vehicle model with flexible link chain, the fully nonlinear model that will be developed in this thesis will employ ANCF finite elements that facilitate developing such complex tracked vehicle models.

1.4 SCOPE AND ORGANIZATION OF THIS THESIS

The second chapter analytically and numerically examines and demonstrates the fundamental LRVF redundancy problem. It is will be shown that the use of two independent interpolations for the position and rotation leads to two independent meshes with nodes that occupy different positions in space in the deformed configuration. As a consequence, the material points of the rotation mesh are different from the material points of the position mesh. Furthermore, the space curve resulting from the rotation mesh is inextensible regardless of the axial load applied. Another contribution of this chapter is to show that, while shear is an independent mode of deformation, the independent position and rotation interpolations cannot, in general, lead to the

same geometric representation. As a consequence, the use of curvature defined using the rotation mesh to describe the bending of the position mesh cannot be justified. Numerical examples are presented to shed light on these fundamental issues and concepts.

Chapter 2 is organized as follows. Section 2.2 demonstrates using a simple example that two independent kinematic descriptions cannot be used, in general, to obtain the same geometry. The brief discussion presented in Section 2.2 is necessary in order to clearly understand the LRVF kinematic assumptions and the potential problems which can develop from using independent interpolations for the position and rotation. Section 2.3 shows that a rotation mesh implicitly defines another space curve whose geometric properties may differ from an independently interpolated position mesh in a three-dimensional case. The LRVF kinematic description and equations of motion are presented in Section 2.4 for the planar case, where the definitions of the strains are also included. Section 2.5 compares the curvatures obtained using the PB and RB interpolations and shows how they can vary significantly. This section will also show additional complications resulting from using an independent RB interpolation such as the rotation field's inextensibility when some assumptions related to the definition of the tangent vector are made. Section 2.6 presents numerical results obtained using the LRVF, including a robot arm subjected to a specified angular motion and an axial load. The numerical results obtained, which demonstrate that the nodes of the two meshes occupy different positions in space, shed light on the fundamental redundancy issue in the definition of inertia and strains. Conclusions are presented in Section 2.7.

The objective of the third chapter of this thesis is to provide a comprehensive study of different joint formulations and demonstrate the fundamental differences between them when applied to the analysis of complex tracked vehicle system models. Better understanding of these

formulations can lead to more accurate, and possibly faster, computer simulations that can be the basis for more reliable performance evaluation of the vehicles. The tracked vehicles considered in this chapter are assumed to consist of interconnected bodies that can have arbitrary displacements. These results are obtained using the general purpose MBS computer code SIGMA/SAMS (Shabana, 2010) which allows for systematically modeling MBS applications using the augmented formulation, penalty method, bushing elements, and ANCF finite elements. In the augmented formulation, the technique of Lagrange multipliers is used to determine the unknown accelerations and joint forces. The computational algorithm used in SIGMA/SAMS ensures that the algebraic constraint equations are satisfied at the position, velocity, and acceleration levels.

Chapter 3 is organized as follows. Section 3.2 gives background analysis into high mobility tracked vehicle models, including major developments in MBS applications. Such examples include force implementations, suspension development and testing, three-dimensional modeling, and complex contact algorithm development. Section 3.3 describes two separate methods that can be used to model a system of algebraic constraint equations. In the first method, the augmented formulation, the dynamic equations of motion explicitly show the constraint forces in terms of redundant coordinates. This approach leads to a general MBS structure though also increases problem dimensionality. The second formulation is the recursive formulation, which eliminates redundant coordinates and leads to a minimum set of differential algebraic equations. This method uses the joint degrees of freedom in the dynamic equations of motion, and although isn’t as general as the previous method, lowers problem dimensionality and increases computational efficiency. Section 3.4 emphasizes the importance of understanding the relationship and difference between generalized and Cartesian moments. Section 3.5 contains

four subsections, each describing a specific joint formulation used to model each track system used in the simulation of the tracked vehicle shown in Fig. 1.1. As described in the abstract of this thesis, the track systems are created using the algebraic constraint method, the penalty method, the compliant discrete element method, and the compliant continuum-based method. Section 3.6 outlines the components and component properties used for all the tracked vehicle models, then uses numerical results to compare each model in terms of position, velocity, and joint forces. Conclusions are presented in Section 3.7.

Developing a three-dimensional rigid body tracked vehicle model remains a challenging task. As will be shown in Chapter 4, this is mainly due to the complexity of the joints in these models and the high frequency forces resulting from the contact forces. For this reason, one cannot find in the literature a flexible link chain tracked vehicle model based on the FFR formulation (Sherif et al., 2011, 2012; Irshik et al., 2009; Shabana, 2014). The FFR formulation leads to a highly nonlinear mass matrix and to a significant increase in the complexity of the joint formulations. The Coriolis and centrifugal forces also have complex expressions that depend nonlinearly on the coordinates and velocities. As a result, developing an FFR tracked vehicle model that takes into account the dynamic coupling between the rigid body motion and the small elastic deformations of the links has been recognized as impractical, and for this reason, the development of such a model has not been pursued in the literature. Instead, the chain link stresses are calculated using decoupled analysis that employs forces obtained from the rigid body simulation of the tracked vehicle. This was the only practical approach available. Nonetheless, the accuracy of this approach has never been evaluated by comparison with a fully nonlinear coupled analysis because of the above mentioned limitations of the existing approaches.

The use of ANCF finite elements (Abbas et al., 2010; Liu et al., 2011; Nachbaguaer, 2012, Olshevskiy et al., 2013; Yoo et al., 2004, 2005; Tian et al., 2009, 2010; von Dombrowski, 1997), allows for developing detailed flexible-link tracked vehicle models. The use of ANCF finite elements allowed for formulating the joint constraints at a preprocessing stage, thereby eliminating the dependent variables before the start of the simulation and also eliminating the need for formulating such equations during the dynamic simulation. The concerns regarding the nonlinearity of the inertia forces are also addressed since ANCF finite elements lead to a constant inertia matrix which can be converted to an identity matrix if the ANCF Cholesky coordinates are used (Shabana et al., 2012). Using ANCF finite elements, a fully coupled analysis of complex tracked vehicle systems with flexible link chains can be performed efficiently. The dynamic stresses can be calculated and used to shed light on the response of the vehicle to different loading conditions. These new fully coupled tracked vehicle models can also be used to evaluate the accuracy of the stress calculation procedures that ignore the effect of the elastic deformation on the rigid body motion of the track links. The objective of this chapter is therefore to develop two stress analysis approaches; the first is based on a fully coupled ANCF approach that accounts for the complete coupling between the rigid body motion and the elastic deformations, while the second is based on a linearization procedure that neglects the effect of the elastic deformation on the rigid body motion of the track link. The governing equations used in both approaches are developed and a comparative numerical study is presented in order to evaluate the accuracy of the stresses and strains obtained from forces determined using rigid body vehicle simulations.

Chapter 4 is organized as follows. Section 4.2 describes the motion description in both the ANCF and FFR formulations, including the four coordinates systems used for each finite

element and the deformation and rotation restrictions held in the FFR formulation. Section 4.3 describes the post processing stress analysis using the FFR formulation. It is important to note that this section describes the FFR equations used in terms of deformation coordinates and doesn't refer to the more commonly used modal analysis. This section will show how the kinematic equations are used to determine the highly nonlinear mass matrix, as well as how each force vector is determined and the assumptions made in the calculation of each component of the equations of motion. Section 4.4 will define the fully coupled, nonlinear deformation analysis accomplished by the ANCF. Similarly to the previous section, the mass matrix and force vector calculations are shown for the ANCF. Several advantages to this approach are also pointed out, including problem dimension reduction and a constant mass matrix which leads to zero Coriolis and centrifugal forces. Section 4.5 displays numerical results from two separate simulations: a lower velocity simulation and a higher velocity simulation. The numerical results presented in this section will compare between the FFR post processing and ANCF tracked vehicle models in terms of positions, velocities, and, most importantly, axial stress and strain. Conclusions are presented in Section 4.6.

CHAPTER 2

INDEPENDENT ROTATION FIELDS IN LARGE DISPLACEMENT ANALYSIS

(Previously published as Ding, Jieyu, Wallin, Michael, Wei, Cheng, Recuero, Antonio M., Shabana, Ahmed A., 2014, "Use of Independent Rotation Field in the Large Displacement Analysis of Beams," Journal of Computational and Nonlinear Dynamics, Vol. 76(3), pp. 1829-1843)

2.1 INITIAL LARGE ROTATION VECTOR FORMULATION OBSERVATIONS

This chapter examines multiple multibody dynamic formulations and their effects in the large displacement analysis of flexible bodies. More specifically, the effect of using independent finite rotation fields in the large displacement analysis of flexible beams first formulated 30 years ago will be examined. This finite rotation description is at the core of the large rotation vector formulation (LRVF), which has been used in the dynamic analysis of bodies experiencing large rotation and deformation. The LRVF employs two independently interpolated meshes for describing the flexible body dynamics: the position mesh and the rotation mesh. The use of these two geometrically independent meshes can lead to coordinate and geometric invariant redundancy that can be the source of fundamental problems in the analysis of large deformations. It is demonstrated in this chapter that the two geometry meshes can define different space curves, which can differ by arbitrary rigid body displacements. The material points of the two meshes occupy different positions in the deformed configuration, and as a consequence, the geometries of the two meshes can differ significantly. Other issues including energy conservation and the

inextensibility of the rotation mesh will also be discussed. Simple examples are presented in order to shed light on these fundamental issues.

2.2 FUNDAMENTAL KINEMATIC DESCRIPTIONS EXAMPLE

In this section, a simple example is used to demonstrate that two independent kinematic descriptions can possess significantly different geometries. This issue is fundamental in understanding the basic assumptions and the redundancy problem associated with the use of some large displacement FE formulations. There are two types of redundancies; one which can be eliminated systematically using a constraint or penalty approach, while the other cannot be eliminated and this second type can pose fundamental problems since it is in violation of basic mechanics motion description principles.

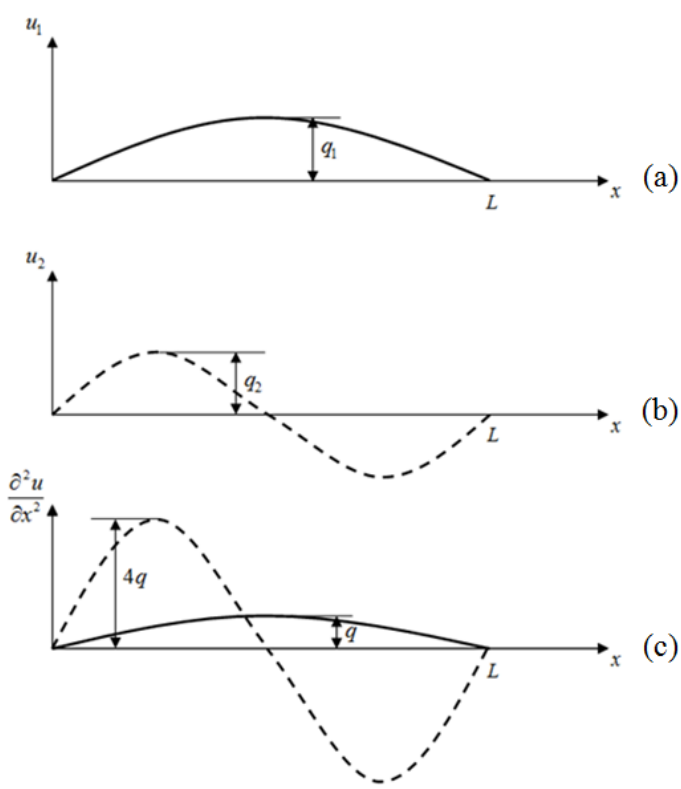

Figure 2.1: Mode shape displacement and curvature

In order to explain the second type of redundancy which cannot be resolved, the two modes of deformation shown in Fig. 2.1 are considered. Figure 2.1a shows an example of a simple mode shape that defines a displacement field $u_1(x,t)=\left(\sin\left(\frac{\pi x}{L}\right)\right)q_1(t)$, while Fig. 2.1b shows a second mode shape that defines another displacement field $u_2(x,t)=\left(\sin\left(\frac{2\pi x}{L}\right)\right)q_2(t)$ with q_1 and q_2 being the amplitudes of the first and second independent mode shapes, respectively, for an element of length L with x as the axial coordinate of the beam, and t as time. Even in this simple case, the two independent fields u_1 and u_2 have significantly different geometric properties. By applying forces or constraints, u_1 and u_2 cannot be brought to be the same. As a consequence, the material points of the curve defined by the field u_1 will occupy positions that are different from the positions occupied by the material points of the curve defined by the field u_2 regardless of the forces and the constraints used. For example, the constraint condition that $u_1(x,t)=u_2(x,t)$ leads to the trivial solution $q_1(t)=q_2(t)=0$ which corresponds to the undeformed reference configuration. One can also show, using the simple example of this section, that the geometric properties of two independent fields can be significantly different. As a consequence, it cannot be justified to assume that the geometric properties, obtained using one field, are the same as those of the other field. For example, using the assumption of small change in the length of the beam, the curvatures of the curves defined by the two fields $u_1(x,t)$ and $u_2(x,t)$ can be approximated by differentiating twice with respect to the parameter x as $\left(\partial^2 u_1/\partial x^2\right)=\left(\pi^2/L^2\right)\left(\sin\left(\frac{\pi x}{L}\right)\right)q_1(t)$ and

$\left(\partial^2 u_2/\partial x^2\right)=\left(4\pi^2/L^2\right)\left(\sin\left(\frac{2\pi x}{L}\right)\right)q_2(t)$. These two equations show that for the same amplitudes, the values of the curvature of u_2 is different from the values of the curvature of u_1. The differences in curvature can be seen clearly in Fig. 2.1c where the same coordinate amplitude q is used for the two fields.

The concept discussed in this section is important to understand when nodes in the position and rotation meshes are shown in later sections of this chapter to occupy different positions in space. While the displacement solution obtained using the position mesh in the LRVF may compare favorably with the solution obtained using other formulations, further investigation into derived geometric properties such as curvature and torsion can show greater geometric inconsistency that sheds light on more fundamental formulation issues.

2.3 ROTATION-BASED GEOMETRIC REPRESENTATION

In the preceding section, it was shown, using a simple example, that in general two different shapes cannot be brought together perfectly regardless of the magnitude of the forces or type of constraints applied. In the LRVF, two independent interpolations are used for the position and finite rotation fields. The curve defined using the rotation field has geometric properties different from those of the curve defined by the position field. This section explains how the rotation field can be used to define a space curve (another position field) expressed in terms of finite rotations.

A three-dimensional space curve can be systematically defined in a global coordinate system XYZ by introducing a rotation field that defines the orientation of coordinate systems at points on the space curve. One can then choose an appropriate sequence of the three Euler angle successive rotations to reach any orientation in space. For example, if s is the space curve arc

length parameter, one can use the interpolated rotation vector $\boldsymbol{\theta}(s)=\left[\psi(s) \quad \phi(s) \quad \theta(s)\right]^T$ to define the orientation of coordinate systems with origins attached to material points on the space curve. If $X^iY^iZ^i$ is the coordinate system at an arbitrary material point i defined by the arc length parameter s on the space curve, one can use the Euler angle sequence defined by an angle ψ (yaw) about the Z^i axis, followed by a second rotation ϕ (roll) about the $-Y^i$ axis, followed by a third and final rotation θ (pitch) about the $-X^i$ axis (Shabana, 2010). Using this sequence of rotations, the transformation matrix that defines the orientation of the coordinate system at s can be written as (Ratho and Shabana, 2006)

$$\mathbf{A}=\begin{bmatrix} \cos\psi\cos\theta & -\sin\psi\cos\phi+\cos\psi\sin\theta\sin\phi & -\sin\psi\sin\phi-\cos\psi\sin\theta\cos\phi \\ \sin\psi\cos\theta & \cos\psi\cos\phi+\sin\psi\sin\theta\sin\phi & \cos\psi\sin\phi-\sin\psi\sin\theta\cos\phi \\ \sin\theta & -\cos\theta\sin\phi & \cos\theta\cos\phi \end{bmatrix} \tag{2.1}$$

In order to construct a curve using the rotation field, the first column of the transformation matrix can be considered as the unit tangent to the space curve at s. Let $\mathbf{r}(s)=\left[x \quad y \quad z\right]^T$ be the vector that defines the space curve. The location of an arbitrary point on the space curve as a function of the arc length can be determined by integrating the equation $d\mathbf{r}=\mathbf{t}ds$. This equation with the use of Eq. 2.1 can be written as $\mathbf{r}(s)=\mathbf{r}_0+\int \mathbf{t}ds$. Substituting the tangent vector $\mathbf{t}$ into this equation leads to

$$\mathbf{r}(s)=\mathbf{r}_0+\int_{s_0}^{s}\begin{bmatrix} \cos\psi(s)\cos\theta(s) \\ \sin\psi(s)\cos\theta(s) \\ \sin\theta(s) \end{bmatrix}ds \tag{2.2}$$

where subscript 0 refers to an initial value, and $\mathbf{t}=\left[\cos\psi\cos\theta \quad \sin\psi\cos\theta \quad \sin\theta\right]^T$ is the unit

tangent vector at the arbitrary point i on the space curve. The preceding equation can be used to define a curve based on the rotation field without resorting to a position based interpolation. It is important to note that, even in the case of using a linear rotation field, the space curve of Eq. 2.2 is a highly nonlinear function since it contains trigonometric functions. Differentiating the tangent vector with respect to the parameter s defines the curvature vector as

$$\frac{d\mathbf{t}}{ds} = \begin{bmatrix} -\psi' \sin\psi \cos\theta - \theta' \cos\psi \sin\theta \\ \psi' \cos\psi \cos\theta - \theta' \sin\psi \sin\theta \\ \theta' \cos\theta \end{bmatrix} \tag{2.3}$$

where $\psi' = \partial\psi / \partial s$ and $\theta' = \partial\theta / \partial s$. The norm of this vector defines the curve curvature as

$$\kappa = \left| \frac{d\mathbf{t}}{ds} \right| = \sqrt{(\psi' \cos\theta)^2 + (\theta')^2} \tag{2.4}$$

Furthermore, the normal vector can be defined using Eqs. 2.3 and 2.4 as

$$\mathbf{n} = \frac{(d\mathbf{t}/ds)}{|d\mathbf{t}/ds|} = \frac{1}{\kappa} \begin{bmatrix} -\psi' \sin\psi \cos\theta - \theta' \cos\psi \sin\theta \\ \psi' \cos\psi \cos\theta - \theta' \sin\psi \sin\theta \\ \theta' \cos\theta \end{bmatrix} \tag{2.5}$$

The curve torsion can then be evaluated by differentiating the curvature vector of Eq. 2.3 with respect to s one more time. Therefore, the geometric properties of the curve can be uniquely defined. Furthermore, if the angles are functions of time, the curvature will also change as function of the angles, and therefore, an arbitrary large deformation can be captured.

The curvature and torsion, obtained using the finite rotation interpolation, are often used to formulate the strains in the large rotation vector formulations. It is implicitly assumed that the RB curvature and torsion are the same as the curvature and torsion of another space curve obtained using an independent position interpolation. This important issue will be discussed in more detail in later sections of this chapter.

2.4 LARGE ROTATION VECTOR FORMULATION

While in the preceding section, general three-dimensional analysis is used to define a space curve using the finite rotation interpolation, the LRVF considered in this chapter can be clearly addressed without delving into the details of the spatial analysis. The LRVF incorporates two independent interpolations, one PB and one RB; this brings up the issue of redundancy despite the fact that shear is an independent deformation mode. As previously shown, two independent meshes cannot be brought together regardless of the constraints and forces used. In this section, the kinematics and dynamic equations of the large rotation vector formulation are explained using planar analysis in order to better understand and interpret the results of the examples that will be presented in later sections of this chapter. To this end, consider a two-dimensional flexible beam of length L, with one end at the origin of the inertial frame XY. The beam is allowed to rotate about the Z axis, but the entire motion of the beam is constrained to the XY plane.

2.4.1 LRVF Kinematics

In the large rotation vector formulation, two independent interpolations are used for the position and finite rotations. These two independent fields can be written, respectively, as $\mathbf{r}_0(x,t)=\mathbf{S}_r(x)\mathbf{e}_r(t)$ and $\theta(x,t)=\mathbf{S}_\theta(x)\mathbf{e}_\theta(t)$, where x is the axial coordinate, t is time, subscript 0 refers to the beam centerline, $\mathbf{S}_r$ and $\mathbf{S}_\theta$ are shape function matrices, and $\mathbf{e}_r$ and $\mathbf{e}_\theta$ are vectors of nodal coordinates. The position vector of an arbitrary point P on a finite element j may be defined as follows

$$\mathbf{r}_P^j(x,t)=\mathbf{r}_0(x,t)+y\mathbf{t}_2(x,t) \tag{2.6}$$

where $\mathbf{r}_0(x,t) = \begin{bmatrix} x+u & v \end{bmatrix}^T$ denotes the deformed position of the beam axis (see Fig. 2.2), y is a coordinate that defines the locations of points on the planar cross sections, and $\mathbf{t}_2$ is a vector in the direction of the cross section. Scalars u and v represent the displacements of the beam material points along the global axes *X* and *Y*, respectively. The position vector $\mathbf{r}_0$ and the moving vectors $\mathbf{t}_1$ and $\mathbf{t}_2$ are defined with respect to the inertial frame. The moving vectors are parameterized by means of the time dependent finite angle θ as

$$\mathbf{A} = \begin{bmatrix} \mathbf{t}_1 & \mathbf{t}_2 \end{bmatrix}, \ \mathbf{t}_1 = \begin{bmatrix} \cos\theta \\ \sin\theta \end{bmatrix}, \quad \mathbf{t}_2 = \begin{bmatrix} -\sin\theta \\ \cos\theta \end{bmatrix} \tag{2.7}$$

In Eq. 2.7, $\mathbf{A}$ is the orientation matrix defined at a point on the beam centerline. The orientation of the cross section is therefore kinematically uncoupled from the position field in order to allow accounting for the shear deformation.

It is important to point out that while the LRVF kinematic description accounts for the shear deformation, the beam cross section in this description is assumed to be rigid and planar. An axial force or stretch of the beam does not lead to a change in the cross section dimensions. This formulation is, therefore, conceptually different from the absolute nodal coordinate formulation (ANCF) which allows for the shear and warping using fully parameterized elements. The two formulations capture different modes of deformation, and therefore, the LRVF and the ANCF can be compared only when using very specific and simplified examples.

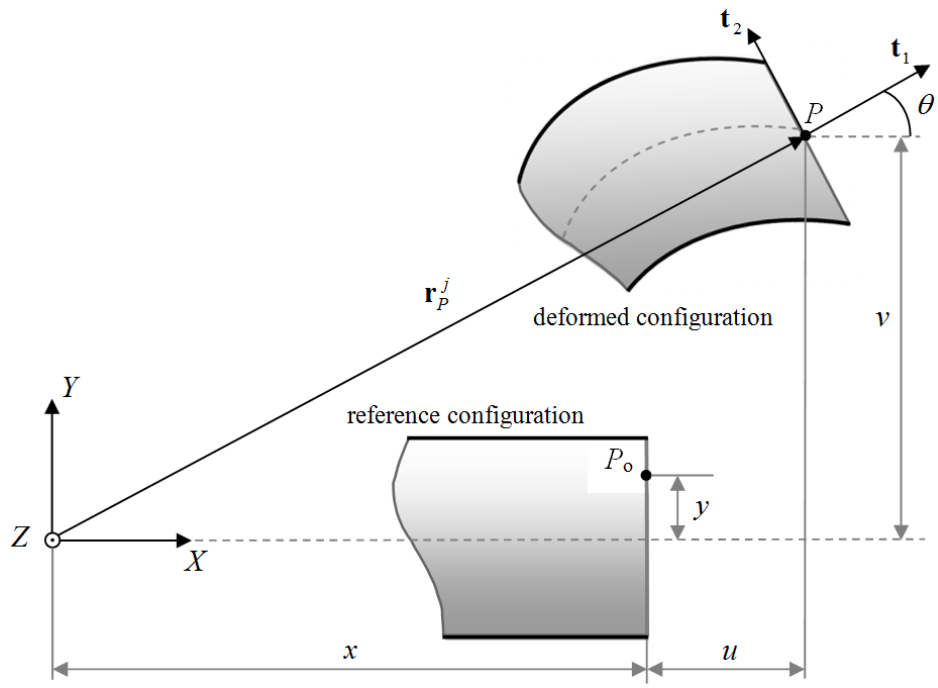

Figure 2.2: Kinematic definition of a beam in the large rotation vector formulation

2.4.2 Energy Expressions

For the most part, the LRVF implementation is based on the co-rotational approach. Following the work presented in (Simo and Vu-Quoc, 1986) and using the co-rotational procedure description, no distinction is made in most LRVF investigations between the spatial coordinate x and the beam centerline arc length s. It is important, however, to point out that in the case of large deformation and when non-incremental solution procedure is used, one must distinguish between x and s in order to accurately define the beam geometry. Based on the kinematic description in Eq. 2.6, the kinetic energy of a beam can be written as (Simo and Vu-Quoc, 1986)

$$T = \frac{1}{2}\int_0^L (A_\rho \dot{\mathbf{r}}_0^T \dot{\mathbf{r}}_0 + I_\rho \dot{\theta}^2) dx \tag{2.8}$$

where L is the length of the element in the longitudinal direction, and the inertia constants are

defined as $A_\rho = \int_{-h/2}^{h/2} \rho(x,y)dy$ and $I_\rho = \int_{-h/2}^{h/2} \rho(x,y)y^2 dy$, respectively, where ρ is the mass density and h is the beam height. The resulting LRVF mass matrix is constant only in the case of planar analysis. In the case of three-dimensional analysis, the resulting LRVF mass matrix is highly nonlinear. This is another fundamental difference between the LRVF and ANCF since ANCF finite elements always lead to a constant mass matrix.

The LRVF potential energy, however, becomes nonlinear and is defined by the axial, bending, and shear components as

$$V = \frac{1}{2}\int_0^L \left(EA\varepsilon_{xx}^2 + GA_s\varepsilon_{xy}^2 + EI\left(\frac{d\theta}{dx}\right)^2 \right) dx \tag{2.9}$$

where EA, GA_s, and EI are the axial, shear, and flexural stiffnesses of the beam, and ε_{xx} and ε_{xy} are the axial and shearing strains, respectively, which can be defined as

$$\varepsilon_{xx} = \mathbf{t}_1^T \mathbf{r}_0' - 1, \quad \varepsilon_{xy} = \mathbf{t}_2^T \mathbf{r}_0' \tag{2.10}$$

where $\mathbf{r}_0' = \partial \mathbf{r}_0 / \partial x = \left(\partial \mathbf{r}_0 / \partial s\right)\left(\partial s / \partial x\right)$, where s is the arc length of the beam centerline. From Eq. 2.10, it is clear that the strains are defined using both interpolation meshes which can have very different geometry. If the independent rotation mesh is used with the assumption that $x \approx s$, then $\mathbf{r}_0' = \mathbf{t}_1$ and when $\mathbf{r}_0'$ is substituted into Eq. 2.10, the axial and shearing strains become $\varepsilon_{xx} = \mathbf{t}_1^T \mathbf{t}_1 - 1 = 0$ and $\varepsilon_{xy} = \mathbf{t}_2^T \mathbf{t}_1 = 0$, respectively, and are therefore constant. For a consistent geometry description, the two meshes should yield the same location for the material points at which the strains are computed. This presents a brief proof of the inextensibility of a beam when using independent angular coordinates and can easily be generalized to the three-dimensional case which poses an inconsistency in the LRVF geometry representation. Further analysis into

beam inextensibility, as well as other issues associated with independent rotation interpolations, will be shown in greater detail in Section 2.5.

2.4.3 Equations of Motion

The equations of motion of a planar body in the large rotation vector formulation utilize uncoupled inertia terms and can be systematically obtained by means of Hamilton's principle (Simo and Vu-Quoc, 1986). Accordingly, it is required that

$$L = \int_{t_1}^{t_2} (T - V)dt \tag{2.11}$$

be stationary for arbitrary paths connecting two points at time t_1 and t_2 in the configuration space. Substituting the kinetic and potential energies previously defined in Eqs. 2.8 and 2.9, respectively, into Eq. 2.11 with standard manipulations yields the following equations for the planar case

$$\begin{aligned} A_\rho \ddot{\mathbf{r}}_0 - \left[\mathbf{ACA}^T \begin{bmatrix} 1 + u' - \cos\theta \\ v' - \sin\theta \end{bmatrix} \right]' - \bar{\mathbf{n}} = 0 \\ I_\rho \ddot{\theta} - EI\theta'' - \begin{bmatrix} -v' \\ 1 + u' \end{bmatrix}^T \mathbf{ACA}^T \begin{bmatrix} 1 + u' - \cos\theta \\ v' - \sin\theta \end{bmatrix} - \bar{m} = 0 \end{aligned} \tag{2.12}$$

where EA and GA_s are the axial and shear stiffness of the beam, respectively, A_ρ and I_ρ are the respective inertia constants defined in the previous subsection, and $(\bullet)' = d(\bullet)/dx$. The external force vector and external moment acting on the deformed cross section of the beam are represented in these equations as $\bar{\mathbf{n}} = \begin{bmatrix} \bar{n}_1 & \bar{n}_2 \end{bmatrix}^T$ and $\bar{m}$, respectively, while the transformation matrix **A** is defined previously in Eq. 2.7, and **C** is given as

$$\mathbf{C} = \begin{bmatrix} EA & 0 \\ 0 & GA_s \end{bmatrix} \tag{2.13}$$

Note that the equations shown in Eq. 2.12 constitute the system of nonlinear partial differential equations governing the response of the system and neglect the effects of viscous friction.

2.5 COMMENTS ON THE ROTATION INTERPOLATION

The interpolation of angles with application to the analysis of large displacement of beams and plates has posed a number of challenges with regard to its use in computer simulations. This section intends to provide discussions on some limitations and difficulties which are characteristic of the interpolation of large rotations in flexible multibody systems.

The LRVF uses two independent meshes which can cause redundancy in the geometric definition. This issue especially affects the definition of the strains of the beam, which is at the core of the formulation and its applicability. Another issue, even though algorithmically avoidable, is the singularity that appears when parameterizing rotations using a minimal set of angular parameters. The mesh defined by these angular parameters is can be shown to be inextensible, which makes it unsuitable to capture axial deformation. Other methods that employ linearized angles, such conventional beams used with the co-rotational formulation, do not face some of the problems discussed in this section. Nonetheless, the use of linearized angles entails approximations that can burden the computational efficiency and accuracy and limits the applicability of the method in the case high rotational speeds (Shabana, 1996). The subsections presented hereafter discuss these problems in more detail either by deriving simple proofs or including state-of-the-art solutions to the aforesaid problems.

2.5.1 Redundancy of the Strain Definition

The use of two independent meshes to describe the same geometry causes redundancy in the definition of strains since two independent shapes cannot be brought together, as shown in Section 2.2. This issue can be easily exemplified using the strains by deriving the expressions for the curvature using both finite element meshes. In the case of planar beam elements, the tangent vector along the space curve $\mathbf{t}_1$, defined in Eq. 2.7, can be differentiated with respect to parameter s to determine the curvature vector as

$$\frac{d\mathbf{t}_1}{ds} = \begin{bmatrix} -\theta' \sin\theta \\ \theta' \cos\theta \end{bmatrix} \tag{2.14}$$

where $\theta' = \partial\theta / \partial s$. The norm of this vector defines the RB curvature as

$$\kappa^{rot} = \left| \frac{d\mathbf{t}_1}{ds} \right| = \theta' \tag{2.15}$$

The preceding definition of the curvature is based on the rotation mesh. If an independent position field is used, there exists, however, a different definition of the geometry invariants that depend on the assumed field of the position mesh. The geometric curvature based on the position mesh may be defined by the following equation

$$\kappa^{pos} = \left| \mathbf{r}_{ss} \right| = \frac{\left| \mathbf{r}_x \times \mathbf{r}_{xx} \right|}{\left| \mathbf{r}_x \right|^3} \tag{2.16}$$

where the subscript x denotes a spatial derivative with respect to the beam longitudinal coordinate. The definition in Eq. 2.16 requires the computation of second spatial derivatives, which are geometrically unrelated to the expression in Eq. 2.15, based on the rotation mesh. Equations 2.15 and 2.16 are an example of the redundancy in the geometry definition that results from the use of two independent meshes. The preceding two equations demonstrate that the use

of two independent meshes leads to two different sets of geometry invariants (curvature and torsion). In the LRVF, the curvature shown in Eq. 2.15 is commonly used to define the elastic forces.

2.5.2 Singularities in the Three-Dimensional Analysis of Beams

The study of the three-dimensional body rotation requires addressing the known problem of singularities. Flexible multibody formulations that use angles to describe large deformation can make use of minimal (e.g. Euler angles) or non-minimal (e.g. Euler parameters) rotation parameters to this end. When singularities occur, the simulation of the motion of the system does not proceed smoothly and this often causes the simulation to stop. Romero (2004) discussed different rotation interpolation strategies in four different methods in a series of tests for geometrically exact rods. Romero found in his work that two of his interpolation strategies (orthogonal interpolation by local rotation updates and non-orthogonal interpolation) possess singularities. The purpose of these investigations and several others was to cut down on extra computational costs and avoid any potential error accumulation. Within the context of the large rotation vector formulation, rescaling operations of a minimal set of rotation parameters have been suggested in order to avoid the singularities associated with the interpolation of rotation (Bauchau et al., 2008). In the latter publication, Bauchau and his collaborators (2008) analyzed the interpolation of finite rotations by developing and testing two algorithms dealing with geometrically exact beams. The first algorithm interpolated the rotation field by its rotation parameters at the nodes of each finite element and removed any possible effects of rescaling from the interpolation process. The second algorithm interpolated the rotation field by incremental nodal rotations defined by the rotation parameters at the nodes of each finite

element. In both algorithms, the task of rescaling is mandatory to avoid simulation failure. In summary, the treatment of the interpolation of rotations requires the use of algorithms specifically devised to avoid the accumulation of error and the well-known singularities associated with minimal sets of rotation parameters. This problem can be avoided by using non-rotation based finite element formulations such as the absolute nodal coordinate formulation.

2.5.3 Inextensibility of the Rotation Field

The large rotation vector formulation relies on both the rotation and position mesh for the calculation of strains. When calculating the strains, both meshes contribute to the geometric definition of strains (see Eq. 2.10 or (Simo and Vu-Quoc, 1986)). In the large deformation analysis of beams, a consistent description of geometry is necessary since strains can reach high values. However, rotation-based meshes can be inextensible, which adds a significant anomaly in the LRVF description of the large deformation. Another issue with regard to the use of a RB position representation is its inability to capture accurately axial and shearing strains in various applications. This can be especially problematic in situations where the beam stiffness is particularly low. Beam inextensibility when using a rotation mesh can be proven in multiple ways by using a two-dimensional beam element example. For a RB mesh $\theta(x,t)$ that employs the axial coordinate x as a parameter, one can write $d\mathbf{r}_0 = (\partial\mathbf{r}_0/\partial x)dx$ and use this equation to define a space curve. If $\partial\mathbf{r}_0/\partial x$ is assumed to be the first column of a rotation matrix based on the assumed rotation field, the position vector of an arbitrary point can be defined by rotation parameters instead of the previously defined position coordinates u and v as

$$\mathbf{r}_0(x,t)=\begin{bmatrix} x+\int_0^x\left(\cos\theta(\bar{x},t)-1\right)d\bar{x} \\ \int_0^x \sin\theta(\bar{x},t)\,d\bar{x} \end{bmatrix} \tag{2.17}$$

where x is the axial parameter of the beam, and t is time. Note that in Eq. 2.7, it is assumed that $\partial\mathbf{r}_0/\partial x$ is a unit tangent. Figure 2.2 shows that $u'=\cos\theta-1$ and $v'=\sin\theta$ in the rotation mesh, which leads to $\mathbf{r}_0'(x,t)=\left[1+\left(\cos\theta(x,t)-1\right)\quad \sin\theta(x,t)\right]^T=\left[\cos\theta(x,t)\quad \sin\theta(x,t)\right]^T=\mathbf{t}_1$, where $\mathbf{r}_0'=\partial\mathbf{r}_0/\partial x$. The strain measures of a beam using a RB mesh can then be defined as

$$\left.\begin{aligned} \varepsilon_{xx}^{rot}&=\mathbf{t}_1^T\mathbf{r}_0'-1=\left[\cos\theta\quad \sin\theta\right]\left[\cos\theta\quad \sin\theta\right]^T-1=0 \\ \varepsilon_{xy}^{rot}&=\mathbf{t}_2^T\mathbf{r}_0'=\left[-\sin\theta\quad \cos\theta\right]\left[\cos\theta\quad \sin\theta\right]^T=0 \\ \kappa^{rot}&=\frac{d\theta(x,t)}{dx}=\theta' \end{aligned}\right\} \tag{2.18}$$

where ε_{xx}^{rot} and ε_{xy}^{rot} are the axial and shearing strains, respectively, and κ^{rot} is the RB curvature. The moving vectors $\mathbf{t}_1$ and $\mathbf{t}_2$ are defined in Eq. 2.7 with respect to the inertial frame and shown in Fig. 2.2. Equation 2.18 shows that the axial and shearing strains are constant throughout.

A second proof of beam inextensibility when using the rotation mesh can be shown by defining the current length of a beam as $dl^2=d\mathbf{r}_0^T d\mathbf{r}_0=dx\left[\cos\theta(x,t)\quad \sin\theta(x,t)\right]\left[\cos\theta(x,t)\quad \sin\theta(x,t)\right]^T dx=\left(dx\right)^2=\left(dl_0\right)^2$. This shows that, when using the RB mesh parameter to define a unit tangent as the first column of the rotation matrix, the current length of a beam l will be equal to its initial length. Therefore, the described beam cannot be stretched and will retain its original length, which leads to inaccuracy when capturing the precise deformation of a beam. A specific example highlighting beam inextensibility of the rotation mesh will be shown in the numerical results section to better shed

light on this fundamental issue.

The fact that a RB interpolation leads to an inextensible beam can be also demonstrated in the case of spatial analysis. Using the rotation coordinates, the tangent vector can always be defined as the first column of a rotation matrix. This column is always a unit vector regardless of the parameterization used (x or s). The angles at an arbitrary point on the beam centerline can be defined in terms of any parameter; coordinates in the reference configuration are often used as parameters to define the rotation mesh (Lagrangian description). The use of parameters defined in the current deformed configuration will require different treatment and different solution procedure. Nonetheless, the first column of the rotation matrix expressed in terms of these angles remains a unit vector.

2.5.4 Energy Conservation

One widespread field of research within the context of flexible multibody dynamics is linked to the study of energy and momentum preserving schemes. The total energy of a non-dissipative system must remain constant throughout the simulation. When the LRVF description was systematically incorporated into flexible multibody systems codes, the use of constraints became mandatory. These constraints cause non-physical high frequency oscillations in the solution. These oscillations, in turn, together with the conservation of energy and momentum of the integration algorithms, have been studied in numerous investigations. One such investigation using beams was presented by Bauchau et al. (1995). In their work, it was discussed that high frequency oscillations hindered the convergence of the equations of motion and that a smaller time step did not necessarily help this problem. The higher frequency oscillations also made strict total energy preservation strenuous to accomplish. Bauchau and Theron (1996) later discussed an energy decaying scheme for non-linear beam models with the main focus being on

the derivation of an algorithm presenting with high frequency dissipation. The derived energy decay algorithms followed the parameter that the total energy at a time step must be equal to or less than that of the previous time step. It was also mentioned that this approach could be used as a time step control parameter with the concept that if the total energy was larger than it was at the previous time step, then a smaller time step would be used. Some of this theory was used by Romero and Armero (2002) when they developed a finite element formulation using geometrically exact rods. These rods used a time-stepping algorithm which improved the rod's dynamics by using the preservation of total linear and angular momentum, as well as the conservation of the total mechanical energy H (or Hamiltonian: $H = T + V$, where T and V are the kinetic and potential energy, respectively).

Besides the challenge of an energy and momentum preserving numerical integration, the definition of the strains using two independent meshes can lead to an inconsistent definition of the strain energy, which utilizes strain measures defined by the two meshes, when large deformation occurs. This can be attributed to the inextensibility of the rotation field in the way presented in the preceding subsection. According to the axial and shearing stresses defined in Eq. 2.10, the potential energy definition uses independently interpolated position and rotation meshes. As shown earlier, these meshes should describe the same geometry. However, the beam material points using LRVF cannot be properly and uniquely associated with the rotation and position meshes, and the same material point can greatly differ in location between the two meshes. This can cause inaccuracies in the definition of the strain energy. As a beam moves during a simulation, the differences in the position and rotation meshes can become considerably large and this may cause some sort of energy drift. While the kinematics used in the LRVF, as traditionally used by the finite element community, can be accurate for the description of small

deformation, the study of the geometry of large deformation on the basis of two independent meshes can lead to inconsistency.

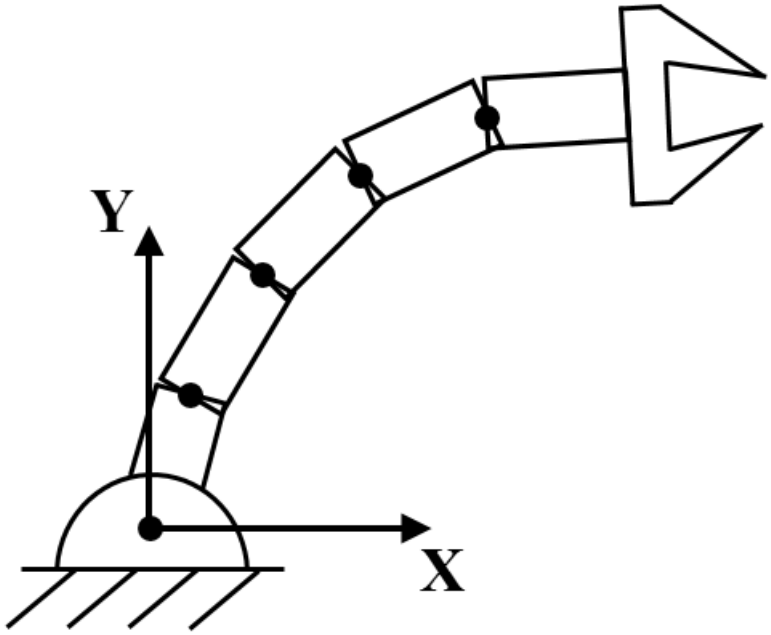

Figure 2.3: Flexible robot arm example

2.6 NUMERICAL RESULTS

A flexible robot arm rotating about one end, similar to the one shown in Fig. 2.3, is considered to illustrate the effect of the use of the rotation interpolation in the large rotation-large deformation analysis of beams. To this end, the large rotation vector formulation is used, as detailed in by Simo and Vu-Quoc (1986). The robot arm is represented by a beam whose first node is connected to the ground by a revolute joint. Several cases of an angle-driven flexible robot arm are considered to better demonstrate the redundancy of the geometry definition. For the figures in this section, Eq. 2.2 is used to obtain the space curve from the rotation mesh. The dimensions of the beam are assumed to be the same as reported by (Simo and Vu-Quoc, 1986), while the axial, shear, and flexural stiffnesses of the arm for each case are shown in Table 2.1. The finite

element mesh consists of 10 elements of equal length with linear interpolation functions for both displacement and rotation. The equations of motion are obtained using selective Gauss quadrature.

Table 2.1: Model parameters

	Figure 2.4 Parameters	Figures 2.5 and 2.6 Parameters	Figures 2.7, 2.8, and 2.9 Parameters
EA	1.00×10^9 N	1.00×10^7 N	1.00×10^6 N
GA_s	5.00×10^8 N	5.00×10^6 N	5.00×10^5 N
EI	8.33×10^7 N·m^2	8.33×10^5 N·m^2	8.33×10^4 N·m^2

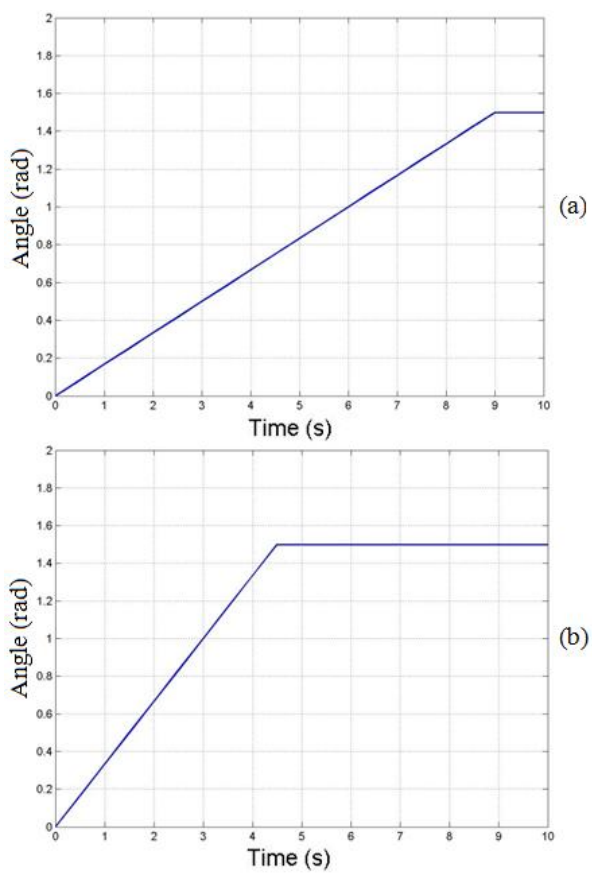

Figure 2.4: Rotation angle at the revolute joint

In the first case, the robot arm is repositioned to an angle of 1.5 rad from its initial

position by prescribing the rotation angle as a linear function of time, as shown in Fig. 2.4a. The sequence of motion during this repositioning stage is depicted in Fig. 2.5, where one snapshot of the beam is depicted at each second. This figure shows that when the stiffness is high and the angular velocity is low, the material point position results obtained using the position and rotation meshes can be in a good agreement. In the second case, the same prescribed rotational displacement is used with lower element stiffness. More significant differences may be observed between the two curves in this case, as shown in Fig. 2.6. The differences between geometry representations can be observed from the first steps of the simulation. The third case involves the robot arm repositioning to an angle of 1.5 rad from its initial position in 4.5 sec, as shown in Fig. 2.4b, with the elemental stiffness being the same as in the previous simulation model. Figure 2.7 shows that the increased angular velocity with a low stiffness leads to the meshes differing greatly in terms of curvature and nodal position. Figure 2.8 shows further differences between the position and rotation-based meshes when incorporating an axial load at the tip of the flexible arm. The tip load of 100 kN is applied in the axial direction of the last element of the arm at each time step. The results presented in this last figure show that the rotation-based interpolation cannot capture the stretch in the elements, whereas the independent position-based interpolation is actually stretched.

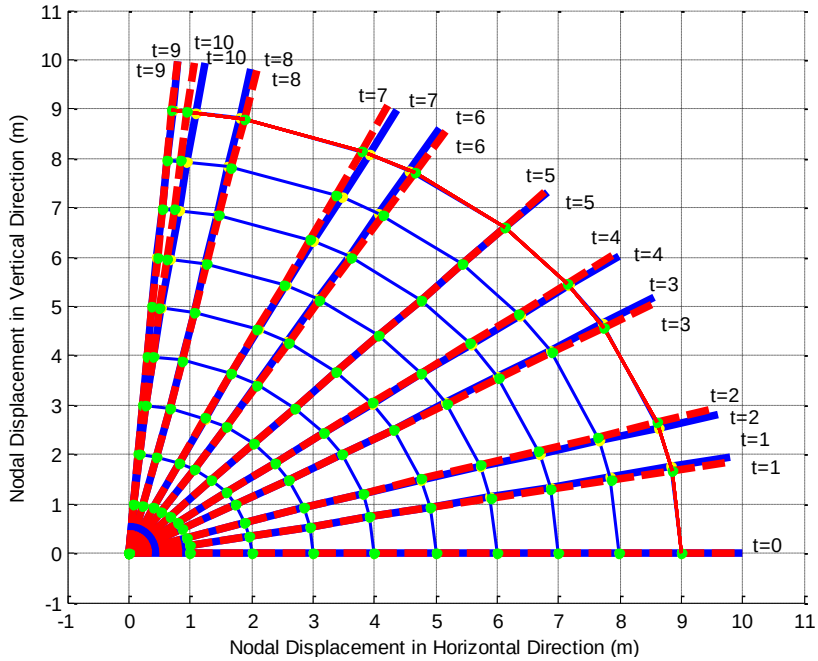

Figure 2.5: Repositioning sequence in LRVF: high stiffness

(— position-based curve, ---- rotation-based curve)

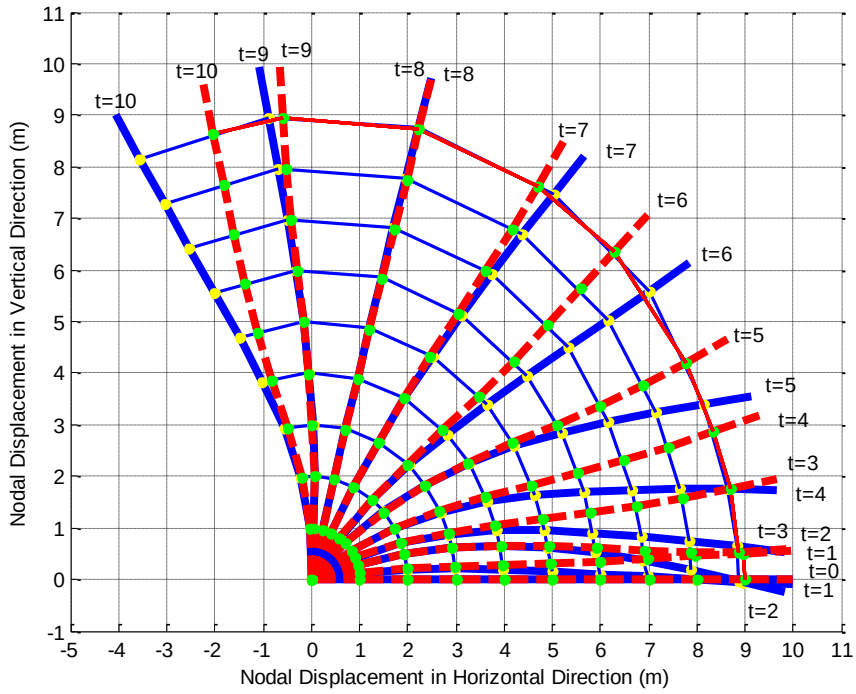

Figure 2.6: Repositioning sequence in LRVF: medium stiffness

(— position-based curve, ---- rotation-based curve)

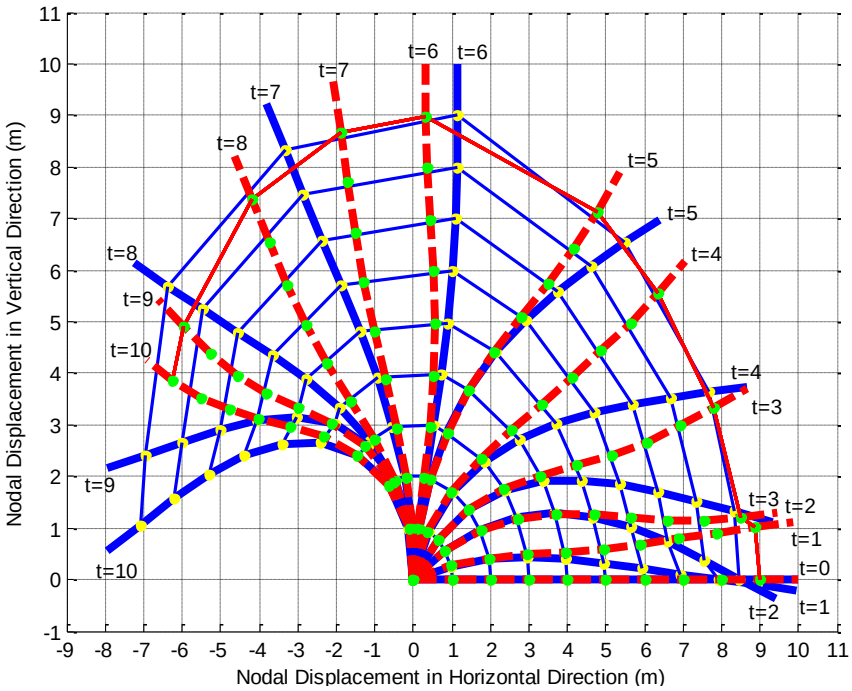

Figure 2.7: Repositioning sequence in LRVF: low stiffness

(— position-based curve, ---- rotation-based curve)

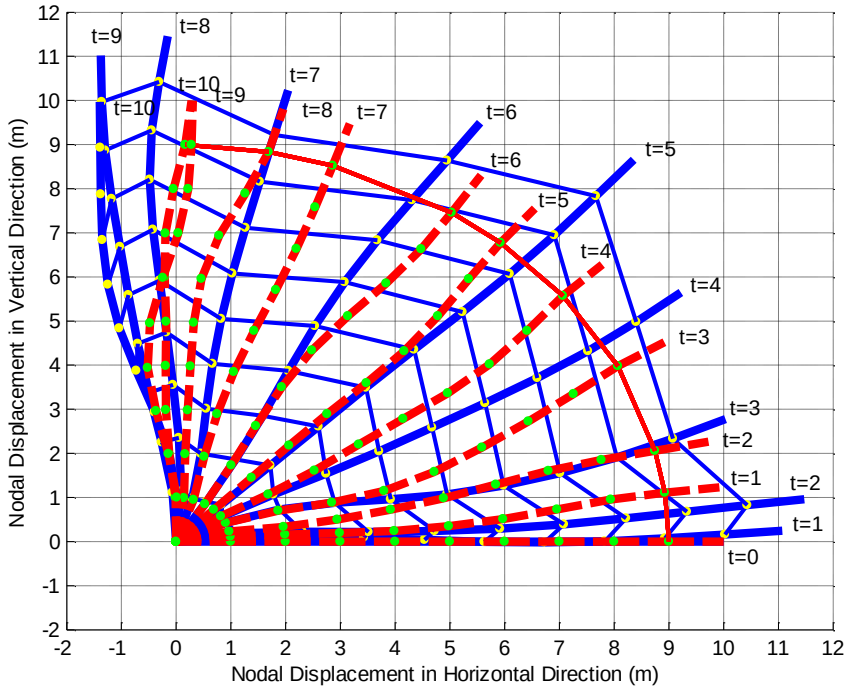

Figure 2.8: Repositioning sequence in LRVF: axial load

(— position-based curve, ---- rotation-based curve)

Another example using the same beam model is depicted in Figure 2.9. In this second example, the clamped boundary conditions are assumed at the first node. A constant external moment of 30 kN·m is applied at the free tip of the beam. The generalized moment is applied on the rotation coordinate of the node at the tip. The definition of axial and shear strains in Eq. 2.10 involve both position and rotation meshes. For this reason, the applied moment can generate axial and shear stresses. However, this aforesaid coupling is not sufficient to bring the two meshes together, as shown in Figure 2.9. It is clear from the results presented in this figure that the curvature obtained using the rotation-based mesh is not a good representative of the curvature of the position-based mesh. Figure 2.10 displays the values of the RB curvature at 20 sec. When using the rotation-based mesh, the curvature is nonzero and constant within the elements. However, because of the linear interpolation, the PB mesh always yields null curvature at every point within the element, which is in contrast to the large values obtained from the other mesh. It can also be seen in Fig. 2.10 that the curvature used to account for bending deformation in the LRVF does not possess inter-elemental continuity. More specifically, the use of independent position and rotation meshes in the LRVF makes it difficult to create strategies to enforce higher-order derivative continuity.

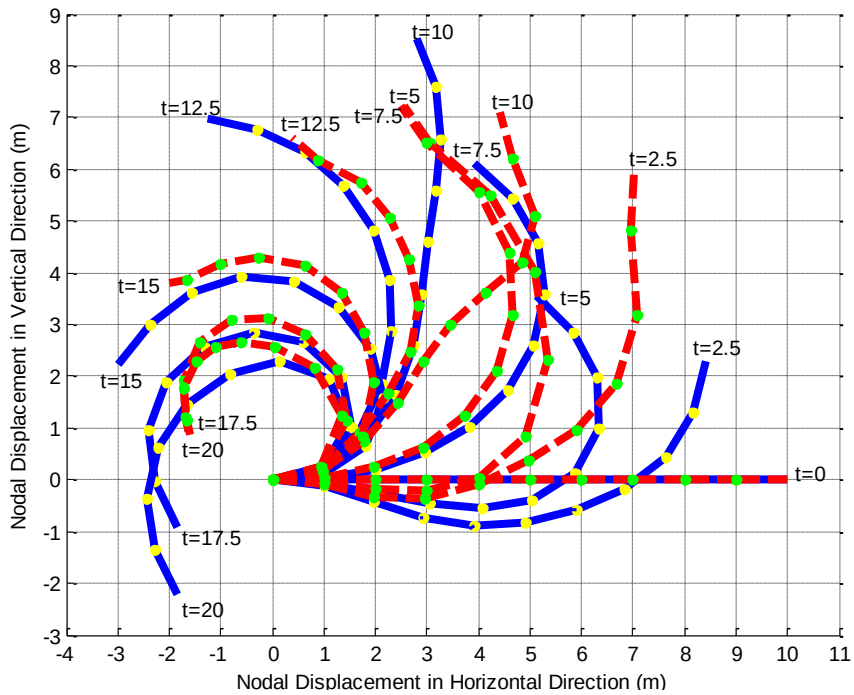

Figure 2.9: Cantilever beam with a moment applied at the tip

(— position-based curve, ---- rotation-based curve)

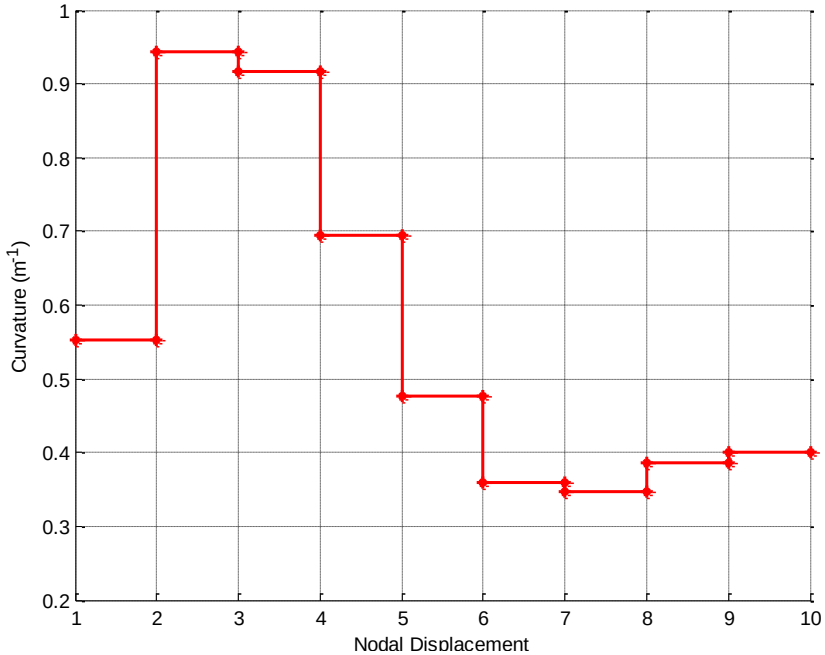

Figure 2.10: Curvature of rotation-based mesh at t = 20 s (the position-based curvature remains zero all the simulation due to the linear interpolation of the displacements)

2.7 CONCLUDING REMARKS

This chapter highlights some issues on the interpolation of rotations in the analysis of large deformation of bodies in flexible multibody system dynamics and presents results of the large rotation vector formulation. The focus is on the geometry issues arising from the use of two interpolation meshes: the position mesh and the rotation mesh. These two meshes lead to different space curves that can differ by an arbitrary rigid body displacement and have different geometric properties. The examples demonstrate the known fact that the rotation mesh of the LRVF is inextensible and that the material points of a rotation-based position mesh occupy different positions from the material points of the position mesh. The consequences of the redundancy in the geometry definition can negatively affect the accuracy of the strain energy and the inertia of the bodies. These inconsistencies become more apparent in the case of larger deformations and are not circumvented by the inclusion of elastic forces or imposing kinematic constraints. This is mainly due to the fact that two different assumed displacement fields cannot, in general, be brought to the same configuration as previously illustrated.

It is important to point out that this chapter is concentrated on a fundamental issue related to the use of the large rotation vector formulation. This chapter is not intended to provide a comparison of the LRVF with other formulations. Nonetheless, it is worth mentioning that several other approaches have been used in the large displacement analysis of structural systems. These formulations include the absolute nodal coordinate formulation (ANCF) and methods based on B-spline representation. For example, a more recent approach for flexible beams in multibody systems employs elastic beams modeled using dynamic splines (Theetten et al., 2008; Valentini and Pennestri, 2011). This approach is based on the Qin and Terzopoulos's work with D-NURBS (Qin and Terzopoulos, 1996), which is a physics-based generalization of non-uniform

rational B-Splines. D-NURBS combines physics-based constraint equations with spline geometry to improve the overall design process. Theetten et al. (2008) used this concept to develop geometrically exact dynamic splines (GEDS), which extends the mechanical accuracy with the use of geometrically exact formal expressions along with analytical spline expressions for real-time, computer-aided models. Valentini and Pennestri (2011) further advanced this approach by developing a dynamic spline formulation which could be suitable for MBS dynamics implementation of flexible beams undergoing large displacement.

CHAPTER 3

A COMPARATIVE STUDY OF JOINT FORMULATIONS

(Previously published as Wallin, Michael, Aboubakr, Ahmed K., Jayakumar, Paramsothy, Letherwood, Michael D., Gorsich, David J., Hamed, Ashraf, Shabana, Ahmed A., 2013, "A Comparative Study of Joint Formulations: Application to Multibody System Tracked Vehicles," Journal of Computational and Nonlinear Dynamics, Vol. 74(3), pp. 783-800)

3.1 JOINT CHAIN MODELS

The third chapter of this thesis focuses on the dynamic formulation of mechanical joints using different approaches that lead to different models with different numbers of degrees of freedom. Some of these formulations allow for capturing the joint deformations using discrete elastic models while the others are continuum-based and capture joint deformation modes that cannot be captured using the discrete elastic joint models. In the first chain formulation, referred to in this chapter as the ideal joint chain model, kinematic joints between the track links are described using nonlinear constraint equations that lead to significant reduction in the number of vehicle degrees of freedom. This joint model does not require assuming stiffness and damping for the track link connectivity, and therefore, does not allow for flexibility between the track links; it requires, however, the solution of a system of differential and algebraic equations if redundant coordinate formulations are used. Redundant coordinate algorithms based on the Lagrangian augmented form of the equations of motion require the use of Newton-Raphson method in order to ensure that the constraint equations are satisfied at the position level. Recursive and joint variables methods can also be used instead of redundant coordinate formulations in order to

avoid Newton-Raphson algorithm. Another approach that can be used to enforce the constraint equations at the position level is the penalty method. This model does not lead to reduction in the number of the system degrees of freedom. Two other approaches that capture the joint compliance are also considered in this chapter. The first is the compliant discrete element method that employs MBS bushing elements to define the connectivity between the track links. This approach, as in the case of the penalty method, requires assuming stiffness and damping coefficients at the connection, and therefore allows for the flexibility between the track links. In the second, the compliant continuum-based joint formulation that employs ANCF finite elements is used. This approach, which captures new joint deformation modes, leads to linear connectivity conditions allowing for an efficient elimination of the dependent variables which can be applied a single time at a preprocessing stage; this leads to a constant inertia matrix and zero Coriolis and centrifugal forces (Shabana et al., 2012). This approach leads to new types of FE chain meshes that have desirable characteristics.

3.2 TRACKED VEHICLES: BACKGROUND

High mobility tracked vehicle such as military battle tanks and armored personal carriers are designed for the mobility over rough and off-road terrains. Investigations on the dynamic analysis of such tracked vehicles shown in Fig. 1.1 have been limited because of the complexity of the forces resulting from interaction between the vehicle components. These forces are impulsive in nature, and their dynamic modeling requires sophisticated computational capabilities. Several two dimensional models for the analysis of tracked vehicle have been developed. Galaitsis (1984) demonstrated that the dynamic track tension and suspension loads in high speed tracked vehicles developed by analytical methods are useful in evaluating the

dynamic characteristics of the tracked vehicle components. Bando et al. (1991) outlined a procedure for the design and analysis of rubber tracked small-size bulldozers, and produced a computer simulation which was used in the evaluation of the vehicle performance. Both steel and continuous rubber tracks are modeled by discretizing them into several rigid bodies connected by compliant elements. The simulation results indicate that the vehicle has favorable characteristics, such as less damage to the road surface, and reduced vibration and noise. Murray and Canfield (1992) used general purpose multibody computer codes to model a simple track link and sprocket system. The behavior of the interaction between the track link and the sprocket was illustrated graphically and it was found that the computer time can be significantly reduced by using supercomputers. Nakanishi et al. (1994) developed a two dimensional contact force model for planar analysis of multibody tracked vehicle systems. Modal parameters such as modal stiffness and damping, and the mode shapes, are found experimentally and utilized to simulate a multibody tracked vehicle model consisting of interconnected rigid and flexible components. The theoretical foundation for using the modal parameters of the assembled vehicle to obtain the component modal parameters of the chassis is explained in depth. Also presented is the set of modal and reference generalized coordinates used to formulate the equations of motion of the full vehicle system.

A number of approaches have been proposed in the literature for developing three-dimensional MBS models. Choi et al. (1998) developed the nonlinear dynamic equations of motion of the three-dimensional multibody tracked vehicle systems, taking into consideration the degrees of freedom of the track chains. To avoid the solution of a system of differential and algebraic equations, the recursive kinematic equations of the vehicle are expressed in terms of the independent joint coordinates. In order to take advantage of sparse matrix algorithms, the

independent differential equations of the three-dimensional tracked vehicles are obtained using the velocity transformation method. Three-dimensional nonlinear contact force models that describe the interaction between the track links and the vehicle components such as the road wheels, sprockets, and idlers as well as the interaction between the track links and the ground are developed and used to define the generalized contact forces associated with the vehicle generalized coordinates. A computer simulation of a tracked vehicle in which the track is assumed to consist of track links connected by a single degree of freedom revolute joint is presented in order to demonstrate the use of the formulations presented in their study. Ryu et al. (2000) developed compliant track link models and investigated the use of these models in the dynamic analysis of high-speed, high-mobility tracked vehicles. The characteristics of the compliant elements used in this investigation to describe the track joints are measured experimentally. A numerical integration method having a relatively large stability region is employed in order to maintain the solution accuracy, and a variable step size integration algorithm is used in order to improve the efficiency. The dimensionality problem is solved by decoupling the equations of motion of the chassis and track subsystems. Recursive methods are used to obtain a minimum set of equations for the chassis subsystem. Several simulations scenarios including an accelerated motion, high-speed motion, braking, and turning motion of the high-mobility vehicle are tested in order to demonstrate the effectiveness and validity of the methods proposed. Ozaki and Shabana (2003) evaluated the performance of different formulations using a tracked vehicle model that is subjected to impulsive forces. They developed joint constraints models and the resulting contact forces from the interactions between the track chains and other vehicle components, such as the sprocket and road wheels, as well as between the track chains and ground. In this study, the nonlinear contact force models used were

developed and presented with the formulations of the generalized forces associated with the generalized coordinates. Ryu et al (2003) investigated the nonlinear dynamic modeling methods for the virtual design of tracked vehicles by using MBS dynamic simulation techniques. The results include high oscillatory signals resulting from the impulsive contact forces and the use of stiff compliant elements to represent the joints between the track links. Each track link is modeled as a body which has six degrees of freedom, and two compliant bushing elements are used to connect track links. Efficient contact search and kinematics algorithms in the context of the compliance contact model are developed to detect the interactions between track links, road wheels, sprockets, and ground for the sake of speedy and robust solutions. Rubinstein and Hitron (2004) developed a three-dimensional multibody model for predicting dynamic behavior of off-road tracked vehicles using LMS-DADS. Each track link is considered a rigid body and is connected to its neighboring track link via a revolute joint. The road-wheel track-link interaction is described using three-dimensional contact force elements, and the track-link terrain interaction is modeled using a pressure-sinkage relationship. An efficient contact search algorithm was used to detect the interactions between the track links and other vehicle components including the ground. Yamakawa and Watanabe (2004) developed a high-mobility rigid body tracked vehicle model utilizing a torsion bar suspension system. The vehicle model was evaluated in terms of ride performance, steerability and stability over rough terrain.

3.3 ALGEBRAIC CONSTRAINT EQUATIONS

In the methods of *constrained dynamics*, there are two approaches that are often used to model ideal mechanical joints that do not account for the effect of elasticity and damping. These two methods are the *augmented formulation* that employs the technique of Lagrange multipliers or

the *recursive formulation* which allows for systematic elimination of the dependent variables using the algebraic equations. These two formulations are briefly discussed in this section.

3.3.1 Augmented Formulation

In the augmented formulation, the constraint forces explicitly appear in the dynamic equations which are expressed in terms of redundant coordinates (Shabana, 2010). Unknown accelerations and constraint forces are solved for using the constraint relationships with the differential equations of motion. While this approach leads to a sparse matrix structure, it has the drawback of increasing the problem dimensionality and it requires more sophisticated numerical algorithms to solve the resulting system of differential and algebraic equations (DAE). Using the generalized coordinates, the equations of motion of a body i can be written as (Roberson and Schwertassek, 1988; Shabana et al., 2008)

$$\mathbf{M}^i\ddot{\mathbf{q}}^i = \mathbf{Q}_e^i + \mathbf{Q}_c^i + \mathbf{Q}_\upsilon^i \tag{3.1}$$

where $\mathbf{M}^i$ is the mass matrix of the body, $\ddot{\mathbf{q}}^i = \left[\ddot{\mathbf{R}}^{iT} \;\; \ddot{\boldsymbol{\theta}}^{iT}\right]^T$ is the vector of the accelerations of the body with $\mathbf{R}^i$ and $\boldsymbol{\theta}^i$ defining the body translation and orientation, respectively, $\mathbf{Q}_e^i$ is the vector of external forces, $\mathbf{Q}_c^i$ is the vector of the constraint forces which can be written in terms of Lagrange multipliers $\boldsymbol{\lambda}$ as $\mathbf{Q}_c^i = -\mathbf{C}_{\mathbf{q}^i}^T\boldsymbol{\lambda}$, $\mathbf{C}_{\mathbf{q}^i}$ is the constraint Jacobian matrix associated with the coordinates of body i, and $\mathbf{Q}_\upsilon^i$ is the vector of the inertia forces that absorb the quadratic terms in the velocities. The constraint equations at the acceleration level can be written as $\mathbf{C}_{\mathbf{q}^i}\ddot{\mathbf{q}}^i = \mathbf{Q}_d^i$, where $\mathbf{Q}_d^i$ is a vector that absorbs first derivatives of the coordinates. Using Eq. 3.1 with the constraint equations at the acceleration level, one obtains

$$\begin{bmatrix} \mathbf{M} & \mathbf{C}_{\mathbf{q}}^{T} \\ \mathbf{C}_{\mathbf{q}} & \mathbf{0} \end{bmatrix} \begin{bmatrix} \ddot{\mathbf{q}} \\ \boldsymbol{\lambda} \end{bmatrix} = \begin{bmatrix} \mathbf{Q}_{e} + \mathbf{Q}_{\upsilon} \\ \mathbf{Q}_{d} \end{bmatrix} \tag{3.2}$$

The matrices and vectors that appear in this equation are the system matrices and vectors that are obtained by assembling the body matrices and vectors. The unknown accelerations and Lagrange Multipliers in Eq. 3.2, which guarantees the constraint equations are satisfied at the acceleration level, can then be found. To ensure that the algebraic kinematic constraints are satisfied for both the positions and velocities, the independent accelerations $\ddot{\mathbf{q}}_i$ are recognized and integrated to calculate the independent coordinates and velocities $\mathbf{q}_i$ and $\dot{\mathbf{q}}_i$, respectively. From the numerical integration the independent coordinates can be determined, while the dependent coordinates $\mathbf{q}_d$ can be calculated from the nonlinear constraint equations using an iterative Newton-Raphson algorithm requiring the solution of the system $\mathbf{C}_{\mathbf{q}_d} \Delta \mathbf{q}_d = -\mathbf{C}$, where $\Delta \mathbf{q}_d$ is the vector of Newton differences, and $\mathbf{C}_{\mathbf{q}_d}$ is the constraint Jacobian matrix partition only associated with the dependent coordinates. With the independent velocities, the dependent velocities $\dot{\mathbf{q}}_d$ can be determined by simply solving the set of linear algebraic constraint equations at the velocity level. This system of equations can be written as $\mathbf{C}_{\mathbf{q}_d} \dot{\mathbf{q}}_d = -\mathbf{C}_{\mathbf{q}_i} \dot{\mathbf{q}}_i - \mathbf{C}_t$; where $\mathbf{C}_{\mathbf{q}_i}$ is the Jacobian constraint matrix associated with the independent coordinates and $\mathbf{C}_t = \partial \mathbf{C} / \partial t$ is the partial derivative of the constraint functions with respect to time.

Lagrange multipliers can be used to obtain the generalized constraint equations acting on a body. The generalized constraint forces acting on body i from a given joint k, can be determined by the equation

$$\left(\mathbf{Q}_c^i\right)_k = -\left(\mathbf{C}_k\right)_{\mathbf{q}^i}^T \boldsymbol{\lambda}_k = \left[\mathbf{F}_k^{iT} \quad \mathbf{T}_k^{iT}\right]^T \tag{3.3}$$

where $\mathbf{F}_k^i$ and $\mathbf{T}_k^i$ are the generalized joint forces associated with the translation and orientation coordinates of body i, respectively. Using the results of the previous equation and the concept of equipollent forces, the reaction forces at the joint definition point can be determined.

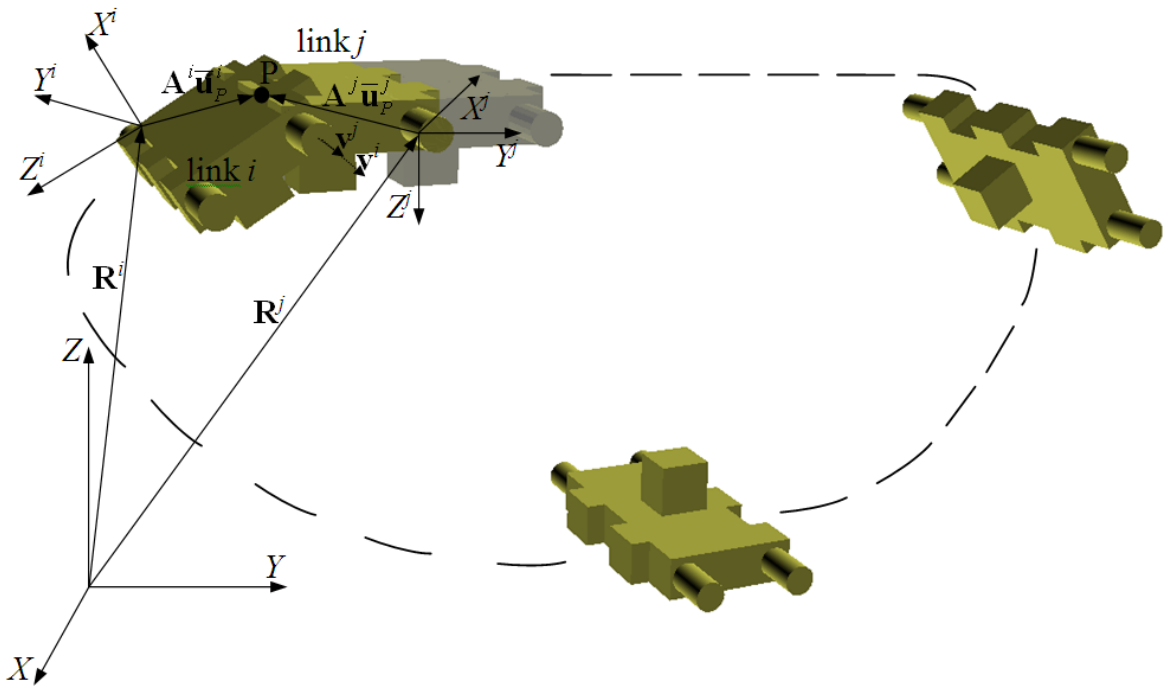

Figure 3.1: Revolute joint

3.3.2 Recursive Formulation

Another alternate approach for formulating the equations of motion of constrained mechanical systems is the recursive method, wherein the equations of motion are formulated in terms of the joint degrees of freedom. This formulation leads to a minimum set of differential equations from which the workless constraint forces are automatically eliminated (Roberson and Schwertassek, 1988; Shabana, 2010). The numerical procedure used in solving these differential equations is much simpler than the procedure used in the solution of the mixed system of differential and algebraic equations resulting from the use of the augmented formulation. In the recursive

formulation, the equations of motion are formulated in terms of joint degrees of freedom. In this formulation, the multibody system is assumed to consist of subsystems, as in the case of the track chains shown in Fig. 3.1. The absolute coordinates and velocities of an arbitrary body i in a subsystem are expressed in terms of the independent joint variables as well as the absolute coordinates and velocities of body j. If body i is connected to body j through a revolute joint, which is the case in this subsystem, the relative rotation is the only degree of freedom represented between the bodies. The connectivity between bodies i and body j can then be described using the kinematic relationships

$$\left.\begin{aligned} &\mathbf{R}^i + \mathbf{A}^i\bar{\mathbf{u}}_P^i - \mathbf{R}^j - \mathbf{A}^j\bar{\mathbf{u}}_P^j = \mathbf{0} \\ &\boldsymbol{\omega}^i = \boldsymbol{\omega}^j + \boldsymbol{\omega}^{i,j} \end{aligned}\right\} \tag{3.4}$$

where $\mathbf{R}^i$ is the global position vector of the origin of body I; $\mathbf{A}^i$ is the transformation matrix that defines the body orientation and can be expressed in terms of Euler parameters; $\bar{\mathbf{u}}_P^i$ and $\bar{\mathbf{u}}_P^j$ are the local position vectors of point P defined in the coordinate systems of body I and j, respectively, $\boldsymbol{\omega}^i$ and $\boldsymbol{\omega}^j$ are, respectively, the absolute angular velocity vectors of bodies i and j, and $\boldsymbol{\omega}^{i,j}$ is the angular velocity vector of body I with respect to body j which can be defined as $\boldsymbol{\omega}^{i,j} = \dot{\phi}^i\mathbf{v}^j$, with $\mathbf{v}^j = \mathbf{A}^j\bar{\mathbf{v}}^j$ where $\bar{\mathbf{v}}^j$ is a unit vector along the axis of rotation defined in the coordinate system of body j, and ϕ^i is the angle of relative rotation. By differentiating the first equation in Eq. 3.4 twice and the second once with respect to time, one obtains

$$\left.\begin{aligned} &\ddot{\mathbf{R}}^i = -\boldsymbol{\omega}^i \times (\boldsymbol{\omega}^i \times \mathbf{u}_P^i) - \boldsymbol{\alpha}^i \times \mathbf{u}_P^i + \ddot{\mathbf{R}}^j + \boldsymbol{\omega}^j \times (\boldsymbol{\omega}^j \times \mathbf{u}_P^j) + \boldsymbol{\alpha}^j \times \mathbf{u}_P^j \\ &\boldsymbol{\alpha}^i = \boldsymbol{\alpha}^j + \mathbf{v}^j\ddot{\phi}^i + (\boldsymbol{\omega}^j \times \mathbf{v}^j)\dot{\phi}^i \end{aligned}\right\} \tag{3.5}$$

In this equation, $\boldsymbol{\alpha}^k$ is the absolute angular acceleration vector of body k. Using the kinematic equations obtained in this section, one can systematically eliminate the dependent variables in

order to obtain a number of differential equations of motion equal to the number of the system degrees of freedom. Using this approach, one obtains a dense inertia matrix in a system of dynamic equations that does not have constraint forces. A second, alternative approach is to use the kinematic equations developed in this section to determine all the system absolute coordinates and velocities. One can then construct Eq. 3.2, which can be solved for the accelerations and Lagrange multipliers. Using the absolute acceleration relationships of Eq. 3.5, one can determine the relative joint accelerations. The joint accelerations can be integrated forward in time in order to determine the joint coordinates and velocities.

3.4 GENERALIZED FORCES

In defining the joint forces between the track links, it is important to understand the relationship and differences between the generalized and the Cartesian moments (Roberson and Schwertassek, 1988; Shabana, 2010). This is important in interpreting the reaction forces of the ideal joints and also important in the implementation of the penalty method and bushing elements. Let $\mathbf{F}^i$ be a force vector that acts at a point P^i on a rigid body *i*. If this force vector is assumed to be defined in the global coordinate system, then the virtual work of this force vector can be written as $\delta W_e^i = \mathbf{F}^{i^T} \delta \mathbf{r}_P^i$, where $\delta \mathbf{r}_P^i$ can be found using the virtual change in the position vector of an arbitrary point on rigid body i as

$$\delta \mathbf{r}_P^i = \begin{bmatrix} \mathbf{I} & -\mathbf{A}^i \tilde{\bar{\mathbf{u}}}_P^i \bar{\mathbf{G}}^i \end{bmatrix} \begin{bmatrix} \delta \mathbf{R}^i \\ \delta \boldsymbol{\theta}^i \end{bmatrix} \tag{3.6}$$

In this equation, $\mathbf{A}^i$ is the transformation matrix that defines the body orientation, $\tilde{\bar{\mathbf{u}}}_P^i$ is the skew symmetric matrix associated with the vector $\bar{\mathbf{u}}_P^i$ that defines the local coordinates of the point P^i,

and $\bar{\mathbf{G}}^i$ is the matrix that relates the angular velocity vector $\bar{\boldsymbol{\omega}}^i$ defined in the body coordinate system to the time derivatives of the orientation coordinates, that is $\bar{\boldsymbol{\omega}}^i = \bar{\mathbf{G}}^i \dot{\boldsymbol{\theta}}^i$. Note that since $\tilde{\mathbf{u}}_P^i = \mathbf{A}^i \tilde{\bar{\mathbf{u}}}_P^i \mathbf{A}^{i^T}$, Eq. 3.6 can be written as $\delta \mathbf{r}_P^i = \delta \mathbf{R}^i - \tilde{\mathbf{u}}_P^i \mathbf{G}^i \delta \boldsymbol{\theta}^i$. Using this equation in the virtual work expression, one obtains $\delta W_e^i = \mathbf{F}^{i^T} \delta \mathbf{R}^i - \mathbf{F}^{i^T} \tilde{\mathbf{u}}_P^i \mathbf{G}^i \delta \boldsymbol{\theta}^i$, which can be written as

$$\delta W_e^i = \mathbf{F}_R^{i^T} \delta \mathbf{R}^i + \mathbf{F}_\theta^{i^T} \delta \boldsymbol{\theta}^i \tag{3.7}$$

where $\mathbf{F}_R^i = \mathbf{F}^i$, and $\mathbf{F}_\theta^i = -\mathbf{G}^{i^T} \tilde{\mathbf{u}}_P^{i^T} \mathbf{F}^i$. These equations imply that a force that acts at an arbitrary point on the rigid body I is equipollent to another system defined at the reference point that consists of the same force and a set of generalized forces, defined by $\mathbf{F}_\theta^i = -\mathbf{G}^{i^T} \tilde{\mathbf{u}}_P^{i^T} \mathbf{F}^i$ associated with the orientation coordinates of the body (Roberson and Schwertassek, 1988; Shabana, 2010).

Since $\tilde{\mathbf{u}}_P^i$ is a skew-symmetric matrix, it follows that $\tilde{\mathbf{u}}_P^i = -\tilde{\mathbf{u}}_P^{i^T}$. Using this identity, one can show that the generalized moment can be written as $\mathbf{F}_\theta^i = \mathbf{G}^{i^T} (\mathbf{u}_P^i \times \mathbf{F}^i)$, where $\mathbf{M}_a^i = \mathbf{u}_P^i \times \mathbf{F}^i$ is the Cartesian moment resulting from the application of the force $\mathbf{F}^i$, and $\mathbf{G}^i$ is the matrix that relates the angular velocity vector $\boldsymbol{\omega}^i$ defined in the global coordinate system to the time derivatives of the orientation coordinates, that is $\boldsymbol{\omega}^i = \mathbf{G}^i \dot{\boldsymbol{\theta}}^i$. It follows that the relationship between the generalized and Cartesian moment is $\mathbf{F}_\theta^i = \mathbf{G}^{i^T} \mathbf{M}_a^i$. If the components of the moment vector are defined in the body coordinate system, one has $\mathbf{F}_\theta^i = \bar{\mathbf{G}}^{i^T} \bar{\mathbf{M}}_a^i$, where $\bar{\mathbf{M}}_a^i = \mathbf{A}^{i^T} \mathbf{M}_a^i$. The relationships developed in this section will be used in the formulation of the joint forces in the case of the penalty method. These relationships will also be used in the computer implementation of the bushing element in general MBS algorithms.

3.5 JOINT FORMULATIONS

In this chapter, four different joint models are considered; two models are based on algebraic equations that require the use of the methods of constrained dynamics or the penalty method. In the case of constrained dynamics, an alternative to the use of Lagrange multipliers is the use of the recursive methods, as previously discussed. When Lagrange multiplier technique or the recursive methods are used, the constraint equations must be satisfied at the position, velocity, and acceleration levels. The penalty method, on the other hand, satisfies the algebraic constraint equations at the position level only.

3.5.1 Constraint Equations

The revolute (pin) joint is used in this section as an example to demonstrate the formulation of the algebraic constraint equations. This joint has been used in the literature in the modeling of the track chains. As shown in Fig. 3.1, the track chain can be assumed to consist of links connected to each other by a pin joint that allows for the relative rotation between them. General MBS algorithms allow for the nonlinear algebraic equations that define the pin joint to be expressed in terms of the absolute coordinates of the two bodies i and j interconnected. The five algebraic constraint equations that eliminate five degrees of freedom can be written in terms of the absolute Cartesian coordinates of the two bodies as (Shabana, 2010)

$$\mathbf{C}\left(\mathbf{q}^i,\mathbf{q}^j\right)=\left[\mathbf{v}_1^{iT}\mathbf{v}^j \quad \mathbf{v}_2^{iT}\mathbf{v}^j \quad \mathbf{v}_1^{iT}\mathbf{r}_P^{ij} \quad \mathbf{v}_2^{iT}\mathbf{r}_P^{ij} \quad \mathbf{r}_P^{ijT}\mathbf{r}_P^{ij}-k_\theta\right]^T=\mathbf{0} \tag{3.8}$$

where $\mathbf{v}^i$ and $\mathbf{v}^j$ are two vectors defined along the joint axis on bodies i and j, respectively; $\mathbf{v}^i,\mathbf{v}_1^i,\mathbf{v}_2^i$ form an orthogonal triad defined on body i; k_θ is a constant (Shabana, 2010); and

$$\mathbf{r}_P^{ij} = \mathbf{r}_P^i - \mathbf{r}_P^j = \mathbf{R}^i + \mathbf{A}^i \bar{\mathbf{u}}_P^i - \mathbf{R}^j - \mathbf{A}^j \bar{\mathbf{u}}_P^j \tag{3.9}$$

In this equation, $\mathbf{A}^i$ and $\mathbf{A}^j$ are the transformation matrices that define the orientation of bodies i and j, respectively, and $\bar{\mathbf{u}}_P^i$ and $\bar{\mathbf{u}}_P^j$ are the local position vectors of points P^i and P^j with respect to bodies i and j, respectively. Points P^i and P^j are defined on the axis of the pin joint on bodies i and j, respectively. One can show that the Jacobian matrix of the pin joint constraints is defined as

$$\mathbf{C}_{\mathbf{q}} = \begin{bmatrix} \mathbf{C}_{\mathbf{q}^i} & \mathbf{C}_{\mathbf{q}^j} \end{bmatrix} = \begin{bmatrix} \mathbf{v}^{jT}\mathbf{H}_1^i & \mathbf{v}_1^{iT}\mathbf{H}^j \\ \mathbf{v}^{jT}\mathbf{H}_2^i & \mathbf{v}_2^{iT}\mathbf{H}^j \\ \mathbf{r}_P^{ijT}\mathbf{H}_1^i + \mathbf{v}_1^{iT}\mathbf{H}_P^i & -\mathbf{v}_1^{iT}\mathbf{H}_P^j \\ \mathbf{r}_P^{ijT}\mathbf{H}_2^i + \mathbf{v}_2^{iT}\mathbf{H}_P^i & -\mathbf{v}_2^{iT}\mathbf{H}_P^j \\ 2\mathbf{r}_P^{ijT}\mathbf{H}_P^i & -2\mathbf{r}_P^{ijT}\mathbf{H}_P^j \end{bmatrix} \tag{3.10}$$

where $\mathbf{C}_{\mathbf{q}^i}$ and $\mathbf{C}_{\mathbf{q}^j}$ are the constraint Jacobian matrices associated with the coordinates of bodies i and j, respectively; and other vectors and matrices that appear in the preceding equation are

$\mathbf{H}_P^i = \begin{bmatrix} \mathbf{I} & \mathbf{A}^i \tilde{\bar{\mathbf{u}}}_P^{i\,T} \bar{\mathbf{G}}^i \end{bmatrix}$, $\mathbf{H}_P^j = \begin{bmatrix} \mathbf{I} & \mathbf{A}^j \tilde{\bar{\mathbf{u}}}_P^{j\,T} \bar{\mathbf{G}}^j \end{bmatrix}$, $\mathbf{H}_1^i = \dfrac{\partial \mathbf{v}_1^i}{\partial \mathbf{q}^i} = \dfrac{\partial}{\partial \mathbf{q}^i}\left(\mathbf{A}^i \bar{\mathbf{v}}_1^i\right)$, $\mathbf{H}_2^i = \dfrac{\partial \mathbf{v}_2^i}{\partial \mathbf{q}^i} = \dfrac{\partial}{\partial \mathbf{q}^i}\left(\mathbf{A}^i \bar{\mathbf{v}}_2^i\right)$,
$\mathbf{H}^j = \dfrac{\partial \mathbf{v}^j}{\partial \mathbf{q}^j} = \dfrac{\partial}{\partial \mathbf{q}^j}\left(\mathbf{A}^j \bar{\mathbf{v}}^j\right)$.

An alternate approach for formulating the revolute (pin) joint constraints is to consider a special case of the spherical joint in which the relative rotation between the two bodies is allowed only along a single joint axis. If point P is the joint definition point, and $\mathbf{v}^i$ and $\mathbf{v}^j$ are two vectors defined along the joint axis on bodies i and j, respectively, the constraint equations of the revolute joint can be written as $\mathbf{C}\left(\mathbf{q}^i, \mathbf{q}^j\right) = \begin{bmatrix} \mathbf{r}_P^{ij} & \mathbf{v}_1^{iT}\mathbf{v}^j & \mathbf{v}_2^{iT}\mathbf{v}^j \end{bmatrix}^T = \mathbf{0}$. The first equation ensures no displacement between the two bodies to within a given tolerance. The last

two equations guarantee the vectors $\mathbf{v}^i$ and $\mathbf{v}^j$ remain parallel and, in so doing, eliminates the relative rotation between the two bodies in two perpendicular directions.

3.5.2 Penalty Method

The constraint equations that describe the connectivity between the track links can be enforced using the penalty approach. In this case, these algebraic equations are satisfied only at the position level. The penalty method does not lead to elimination of degrees of freedom, and therefore, it is conceptually different from the case of Lagrange multiplier technique or the recursive approach. In order to demonstrate the penalty approach, the violations in the constraint equations of a revolute joint k can be written as

$$\mathbf{d}_k = \begin{bmatrix} \mathbf{r}_P^{ij} & \mathbf{v}_1^{iT}\mathbf{v}^j & \mathbf{v}_2^{iT}\mathbf{v}^j \end{bmatrix}^T \tag{3.11}$$

Using this violation $\mathbf{d}_k$, a restoring force vector can then be defined as $\mathbf{f}_k = k_k\,\mathbf{d}_k + c_k\dot{\mathbf{d}}_k$, where k_k, and c_k are assumed penalty stiffness and damping coefficients, respectively, and $\dot{\mathbf{d}}_k$ is the time derivative of the violation vector $\mathbf{d}_k$. The virtual work of this restoring force $\mathbf{f}_k$ can then be written as $\delta W_k^{ij} = -\mathbf{f}_k{}^T\delta\mathbf{d}_k$, which can be written as

$$\delta W_k^{ij} = -\mathbf{F}_B^T\delta\mathbf{r}_p^{ij} - F_1\delta\left(\mathbf{v}_1^{iT}\mathbf{v}^j\right) - F_2\delta\left(\mathbf{v}_2^{iT}\mathbf{v}^j\right) \tag{3.12}$$

where $\delta\mathbf{r}_p^{ij} = \delta\mathbf{R}^i - \tilde{\mathbf{u}}_P^i\mathbf{G}^i\delta\boldsymbol{\theta}^i - \delta\mathbf{R}^j + \tilde{\mathbf{u}}_P^j\mathbf{G}^j\delta\boldsymbol{\theta}^j$, $\mathbf{F}_B = k_k\mathbf{r}_p^{ij} + c_k\dot{\mathbf{r}}_p^{ij}$, $\delta(\mathbf{v}_1^{iT}\mathbf{v}^j) = \mathbf{v}^{jT}\delta\mathbf{v}_1^i + \mathbf{v}_1^{iT}\delta\mathbf{v}^j$,

$\delta(\mathbf{v}_2^{i\,T}\mathbf{v}^j) = \mathbf{v}^{jT}\delta\mathbf{v}_2^i + \mathbf{v}_2^{i\,T}\delta\mathbf{v}^j$, $F_1 = k_k\left(\mathbf{v}_1^{iT}\mathbf{v}^j\right) + c_k\dfrac{d\left(\mathbf{v}_1^{iT}\mathbf{v}^j\right)}{dt}$, and $F_2 = k_k\left(\mathbf{v}_2^{iT}\mathbf{v}^j\right) + c_k\dfrac{d\left(\mathbf{v}_2^{iT}\mathbf{v}^j\right)}{dt}$.

Equation 3.12 can be used to define a set of generalized forces acting on bodies I and j that maintain the connectivity between the two bodies as

$$\delta W_k^{ij} = \mathbf{Q}_R^{i\,T}\delta\mathbf{R}^i + \mathbf{Q}_\theta^{i\,T}\delta\boldsymbol{\theta}^i + \mathbf{Q}_R^{j\,T}\delta\mathbf{R}^j + \mathbf{Q}_\theta^{j\,T}\delta\boldsymbol{\theta}^j \tag{3.13}$$

Which can be rewritten in a compact form as $\delta W = \mathbf{Q}_B^{i\,T}\delta\mathbf{q}^i + \mathbf{Q}_B^{j\,T}\delta\mathbf{q}^j$, where $\mathbf{q}^i$ and $\mathbf{q}^j$ are the generalized coordinates of bodies i and j, and

$$\left.\begin{aligned} \mathbf{Q}_B^i &= \begin{bmatrix} \mathbf{Q}_R^i \\ \mathbf{Q}_\theta^i \end{bmatrix} = \begin{bmatrix} -\mathbf{F}_B \\ \mathbf{G}^{iT}\tilde{\mathbf{u}}_P^{i\,T}\mathbf{F}_B + \mathbf{G}^{iT}\mathbf{M}_1^i + \mathbf{G}^{iT}\mathbf{M}_2^i \end{bmatrix} \\ \mathbf{Q}_B^j &= \begin{bmatrix} \mathbf{Q}_R^j \\ \mathbf{Q}_\theta^j \end{bmatrix} = \begin{bmatrix} \mathbf{F}_B \\ -\mathbf{G}^{jT}\tilde{\mathbf{u}}_P^{j\,T}\mathbf{F}_B - \mathbf{G}^{jT}\mathbf{M}_1^i - \mathbf{G}^{jT}\mathbf{M}_2^i \end{bmatrix} \end{aligned}\right\} \tag{3.14}$$

where $\mathbf{M}_1^i = -F_1\tilde{\mathbf{v}}_1^i\mathbf{v}^j$, $\mathbf{M}_1^j = F_1\tilde{\mathbf{v}}_1^i\,\mathbf{v}^j$, $\mathbf{M}_2^i = -F_1\tilde{\mathbf{v}}_2^i\,\mathbf{v}^j$, and $\mathbf{M}_2^j = F_1\tilde{\mathbf{v}}_2^i\,\mathbf{v}^j$. Equation 14 defines the generalized forces associated with the absolute Cartesian coordinates due to the revolute joint connection between bodies i and j. With a proper selection of the penalty coefficients, these forces ensure that the constraint equations are satisfied at the position level.

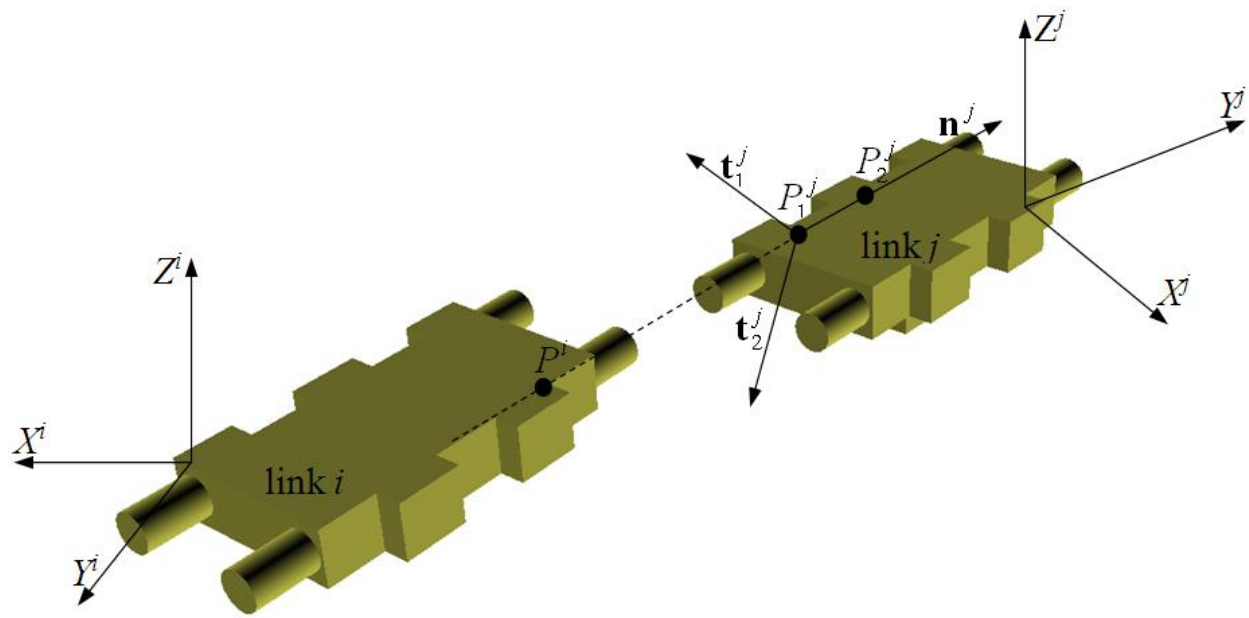

Figure 3.2: Bushing element

3.5.3 Compliant Discrete Element Joint Formulation

The compliant discrete element joint formulation allows for introducing joint deformations. In this approach, no algebraic equations are enforced. In most MBS computer codes, the compliant discrete element joint method can be applied using the standard MBS bushing element that allows for introducing three force and three moment components that can be linear or nonlinear functions of the body coordinates. As shown in Fig. 3.2, the position vectors $\bar{\mathbf{u}}_{P_1}^j$ and $\bar{\mathbf{u}}_{P_2}^j$ of two points, P_1^j and P_2^j on body *j*, can be used to define one axis of the coordinate system of the bushing element as $\bar{\mathbf{n}}^j = \left(\bar{\mathbf{u}}_{p_1}^j - \bar{\mathbf{u}}_{p_2}^j\right) \Big/ \left|\bar{\mathbf{u}}_{p_1}^j - \bar{\mathbf{u}}_{p_2}^j\right|$, where $\bar{\mathbf{n}}^j$ is one of the bushing axes defined in the body j coordinate system. This axis can then be defined in the global coordinate system as $\mathbf{n}^j = \mathbf{A}^j \bar{\mathbf{n}}^j$, where $\mathbf{A}^j$ is the transformation matrix that defines the orientation of the coordinate system of body j in the global system. Using this axis, one can define the directional properties of the bushing element with the other two axes of the bushing coordinate system being defined using the transformation matrix $\bar{\mathbf{A}}^{bj} = \begin{bmatrix} \bar{\mathbf{t}}_1^j & \bar{\mathbf{t}}_2^j & \bar{\mathbf{n}}^j \end{bmatrix}$ where $\bar{\mathbf{t}}_1^j$ and $\bar{\mathbf{t}}_2^j$ are the two unit vectors that complete the three orthogonal axes of the bushing element coordinate system. Assuming that body j is a rigid body, the bushing coordinate system can be defined with respect to the global coordinate system as $\mathbf{A}^{bj} = \mathbf{A}^j \bar{\mathbf{A}}^{bj}$. Choosing points P^i and P_1^j to initially coincide; one can define the bushing deformation and rate of deformation vectors in the bushing coordinate system as $\bar{\boldsymbol{\delta}}^{bij} = \mathbf{A}^{bj^T} \mathbf{r}^{ij}$, and $\dot{\bar{\boldsymbol{\delta}}}^{bij} = \mathbf{A}^{bj^T} \dot{\mathbf{r}}^{ij}$, respectively, where $\mathbf{r}^{ij} = \mathbf{r}_P^i - \mathbf{r}_{P_1}^j$ is the position vector of point P_1^j with respect to point P^i.

The rotational deformation of the bushing element can be obtained using the transformation matrix that defines the orientation of the bushing coordinate system on body i

with respect to the bushing coordinate system on body j. This matrix is defined as $\mathbf{A}^{bij} = \mathbf{A}^{bj^T}\mathbf{A}^{bi}$, where $\mathbf{A}^{bj}$ is the orientation matrix of the bushing coordinate system on body j, while $\mathbf{A}^{bi}$ is the orientation matrix of the bushing coordinate system with respect to the coordinate system of body i that is defined as $\mathbf{A}^{bi} = \mathbf{A}^{i}\overline{\mathbf{A}}^{bi}$. Assuming that the relative rotations between bodies i and j are small, the relative rotation matrix, $\mathbf{A}^{bij}$ can be used to extract three relative rotations defined in the bushing coordinate system, $\overline{\boldsymbol{\theta}}^{bij} = \left[\theta_x^{bij} \; \theta_y^{bij} \; \theta_z^{bij}\right]^T$. The relative angular velocity between the two bodies defined in the bushing coordinate system can also be written as $\overline{\boldsymbol{\omega}}^{bij} = \mathbf{A}^{bj^T}(\boldsymbol{\omega}^i - \boldsymbol{\omega}^j)$, where $\boldsymbol{\omega}^i$ and $\boldsymbol{\omega}^j$ are the absolute angular velocity vectors of bodies i and j, respectively, defined in the global coordinate system. The bushing stiffness and damping coefficients are often determined using experimental testing, and these coefficients are defined generally in the bushing coordinate system. Let $\mathbf{K}_r$ and $\mathbf{C}_r$ be the translational stiffness and damping matrices, respectively, defined with respect to the bushing coordinate system; and assume that the rotational stiffness and damping matrices are $\mathbf{K}_\theta$ and $\mathbf{C}_\theta$, respectively. In terms of translational and rotational stiffness and damping matrices, the force vector defined in the bushing coordinate system can be written as

$$\begin{bmatrix} \overline{\mathbf{F}}_R^b \\ \overline{\mathbf{M}}_\theta^b \end{bmatrix} = \begin{bmatrix} \mathbf{K}_r & \mathbf{0} \\ \mathbf{0} & \mathbf{K}_\theta \end{bmatrix} \begin{bmatrix} \overline{\boldsymbol{\delta}}^{bij} \\ \overline{\boldsymbol{\theta}}^{bij} \end{bmatrix} + \begin{bmatrix} \mathbf{C}_r & \mathbf{0} \\ \mathbf{0} & \mathbf{C}_\theta \end{bmatrix} \begin{bmatrix} \dot{\overline{\boldsymbol{\delta}}}^{bij} \\ \overline{\boldsymbol{\omega}}^{bij} \end{bmatrix} \tag{3.15}$$

This force vector can then be defined in the global coordinate system, and the results can be used to define the generalized bushing forces and moments acting on the two bodies as previously described in this chapter.

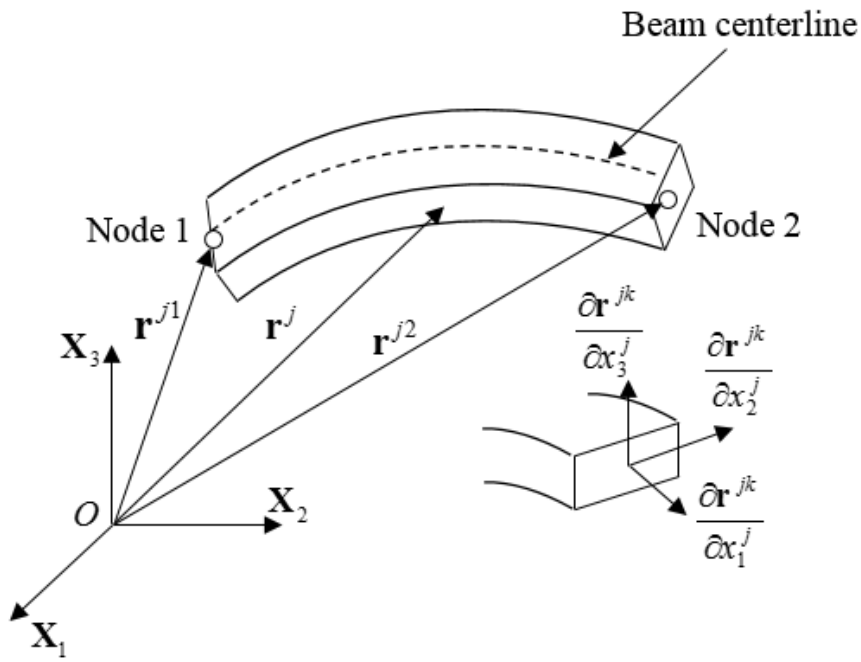

Figure 3.3: ANCF beam element coordinates

3.5.4 Compliant Continuum-Based Joint Formulation

The compliant continuum-based joint formulation allows capturing joint strain modes that cannot be captured using the compliant discrete element joint method. When ANCF finite elements are used, one can develop new FE meshes that have linear connectivity and constant inertia (Shabana et al., 2012). This allows for systematically eliminating dependent variables at a preprocessing stage, and as a result, there is no need for the use of joint formulations in the main processor. This approach can be used to develop new spatial chain models where the modes of deformations at the definition points of the joints that allow for rigid body rotations between ANCF finite elements can be captured. The displacement field of an ANCF finite element, as the one shown in Fig. 3.3, can be written as $\mathbf{r}(x, y, z, t) = \mathbf{s}(x, y, z)\mathbf{e}(t)$ where x, y, and z are the element spatial coordinates; t is time; $\mathbf{S}$ is the element shape function matrix, and $\mathbf{e}$ is the vector of element nodal coordinates. Using this displacement field, the equations of a pin joint

between elements i and j can be written using the six scalar equations $\mathbf{r}^i = \mathbf{r}^j, \mathbf{r}^i_\alpha = \mathbf{r}^j_\alpha$, where α is the coordinate line that defines the joint axis; α can be x, y, or z or any other coordinate line. The six scalar equations eliminate six degrees of freedom; three translations, two rotations, and one deformation mode. Therefore, this joint has five modes of deformation that include stretch and shear modes. This ANCF revolute joint model ensures C^1 continuity with respect to the coordinate line α and C^0 continuity with respect to the other two parameters. It follows that the Lagrangian strain component $\varepsilon_{\alpha\alpha} = \left(\mathbf{r}^T_\alpha \mathbf{r}_\alpha - 1\right)/2$ is continuous at the joint definition point, while the other five strain components can be discontinuous. The resulting joint constraint equations are linear, and therefore, can be applied at a preprocessing stage to systematically eliminate the dependent variables. Using these equations, one can develop a new kinematically linear FE mesh for flexible-link chains in which the links can have arbitrarily large relative rotations.

In the numerical investigation presented in this chapter, a three-dimensional cable element is used to model the flexibility of the chain links. For the three-dimensional cable element used in the compliant continuum-based model, the nodal coordinates can be written as $\mathbf{e}^j = \left[\mathbf{r}^{j^T}(x^j_1 = 0) \quad \mathbf{r}^{j^T}_{x_1}(x^j_1 = 0) \quad \mathbf{r}^{j^T}(x^j_1 = l) \quad \mathbf{r}^{j^T}_{x_1}(x^j_1 = l)\right]^T$, with the element shape function defined as $\mathbf{S}^j = \left[s_1\mathbf{I} \quad s_2\mathbf{I} \quad s_3\mathbf{I} \quad s_4\mathbf{I}\right]$ where $\mathbf{I}$ is the 3×3 identity matrix (Gerstmayr and Shabana, 2006). The shape functions s_i, for I = 1, 2, 3, 4, are defined as

$$\begin{aligned} s_1 &= 1 - 3\xi^2 + 2\xi^3, \quad s_2 = l(\xi - 2\xi^2 + \xi^3), \\ s_3 &= \quad 3\xi^2 - 2\xi^3, \quad s_4 = l(-\xi^2 + \xi^3), \end{aligned} \tag{3.16}$$

where $\xi = x_1^j / l$ and l is the length of the element. The constraint forces, $\mathbf{Q}_C^j$, can then be found using the equation of motion for a single body (element) j as $\mathbf{M}^j \ddot{\mathbf{e}}^j = (\mathbf{Q}_s^j + \mathbf{Q}_{con}^j + \mathbf{Q}_e^j) + \mathbf{Q}_C^j$, where $\mathbf{Q}_s^j$, $\mathbf{Q}_{con}^j$, and $\mathbf{Q}_e^j$ are the elastic forces, forces of contacts between the chain links and other bodies in the system, and gravity forces, respectively, associated with the element nodal coordinates $\mathbf{e}^j$ and $\mathbf{M}^j$ is the symmetric mass matrix of the finite element j defined as $\mathbf{M}^j = \int_{V^j} \rho^j \mathbf{S}^{j^T} \mathbf{S}^j dV^j$, where ρ^j is the mass density of the material points of the element and V^j is the element volume. Since the shape function for a three-dimensional cable element only depends on the x_1 spatial coordinate, the mass matrix can then be defined as

$$\mathbf{M}^j = \int_{\frac{-d}{2}}^{\frac{d}{2}} \int_{\frac{-h}{2}}^{\frac{h}{2}} \int_0^l \rho_0^j \mathbf{S}^{j^T} \mathbf{S}^j dx_1 dx_2 dx_3 = d^j h^j \rho_0^j \int_0^l \mathbf{S}^{j^T} \mathbf{S}^j dx_1 \tag{3.17}$$

For the cable element, this mass matrix can be written explicitly as

$$\mathbf{M}^j = d^j h^j \rho_0^j \begin{bmatrix}
\frac{13}{35}l & 0 & 0 & \frac{11}{210}l^2 & 0 & 0 & \frac{9}{70}l & 0 & 0 & -\frac{13}{420}l^2 & 0 & 0 \\
0 & \frac{13}{35}l & 0 & 0 & \frac{11}{210}l^2 & 0 & 0 & \frac{9}{70}l & 0 & 0 & -\frac{13}{420}l^2 & 0 \\
0 & 0 & \frac{13}{35}l & 0 & 0 & \frac{11}{210}l^2 & 0 & 0 & \frac{9}{70}l & 0 & 0 & -\frac{13}{420}l^2 \\
\frac{11}{210}l^2 & 0 & 0 & \frac{1}{105}l^3 & 0 & 0 & \frac{13}{420}l^2 & 0 & 0 & -\frac{1}{140}l^3 & 0 & 0 \\
0 & \frac{11}{210}l^2 & 0 & 0 & \frac{1}{105}l^3 & 0 & 0 & \frac{13}{420}l^2 & 0 & 0 & -\frac{1}{140}l^3 & 0 \\
0 & 0 & \frac{11}{210}l^2 & 0 & 0 & \frac{1}{105}l^3 & 0 & 0 & \frac{13}{420}l^2 & 0 & 0 & -\frac{1}{140}l^3 \\
\frac{9}{70}l & 0 & 0 & \frac{13}{420}l^2 & 0 & 0 & \frac{13}{35}l & 0 & 0 & -\frac{11}{210}l^2 & 0 & 0 \\
0 & \frac{9}{70}l & 0 & 0 & \frac{13}{420}l^2 & 0 & 0 & \frac{13}{35}l & 0 & 0 & -\frac{11}{210}l^2 & 0 \\
0 & 0 & \frac{9}{70}l & 0 & 0 & \frac{13}{420}l^2 & 0 & 0 & \frac{13}{35}l & 0 & 0 & -\frac{11}{210}l^2 \\
-\frac{13}{420}l^2 & 0 & 0 & -\frac{1}{140}l^3 & 0 & 0 & -\frac{11}{210}l^2 & 0 & 0 & \frac{1}{105}l^3 & 0 & 0 \\
0 & -\frac{13}{420}l^2 & 0 & 0 & -\frac{1}{140}l^3 & 0 & 0 & -\frac{11}{210}l^2 & 0 & 0 & \frac{1}{105}l^3 & 0 \\
0 & 0 & -\frac{13}{420}l^2 & 0 & 0 & -\frac{1}{140}l^3 & 0 & 0 & -\frac{11}{210}l^2 & 0 & 0 & \frac{1}{105}l^3
\end{bmatrix} \tag{3.18}$$

where $d^j, h^j,$ and ρ_0^j are the width, height, and initial density, respectively, of element *j*. It is important to note that the mass matrix is constant in both two-dimensional and three-dimensional cases and leads to zero centrifugal and Coriolis forces when the body experiences an arbitrary large deformation and finite rotation. The virtual work of the elastic forces can then be defined as

$$\delta W_s = \int_0^l EA\varepsilon_{11}\delta\varepsilon_{11}dx_1 + \int_0^l EI\kappa\delta\kappa dx_1 \tag{3.19}$$

where E is the modulus of elasticity, A is the element cross section, I is the second moment of area and κ is the curvature. The elastic forces of the cable element can also be evaluated using the following expression for the strain energy $U = \int_0^l EA(\varepsilon_{11})^2 dx_1 + \int_0^l EI(\kappa)^2 dx_1$ as $\mathbf{Q}_s = \left(\frac{\partial U}{\partial \mathbf{e}}\right)^T$.

Similarly, the gravity forces can be found using the virtual work of the gravity forces, $\delta W_e = \int_V \begin{bmatrix} 0 & 0 & -\rho_0 g \end{bmatrix} \mathbf{S}\delta\mathbf{e} dV$. Substituting in the shape functions and integrating over the volume leads to $\delta W_s = -mg\begin{bmatrix} 0 & 0 & \frac{1}{2} & 0 & 0 & \frac{l}{12} & 0 & 0 & \frac{1}{2} & 0 & 0 & \frac{-l}{12} \end{bmatrix}\delta\mathbf{e}$, which leads to

$$\mathbf{Q}_e = -mg\begin{bmatrix} 0 & 0 & \frac{1}{2} & 0 & 0 & \frac{l}{12} & 0 & 0 & \frac{1}{2} & 0 & 0 & \frac{-l}{12} \end{bmatrix} \tag{3.20}$$

Using the principle of virtual work with the mass matrix and nodal accelerations as previously defined, the joint forces for a specific element can then be easily calculated.

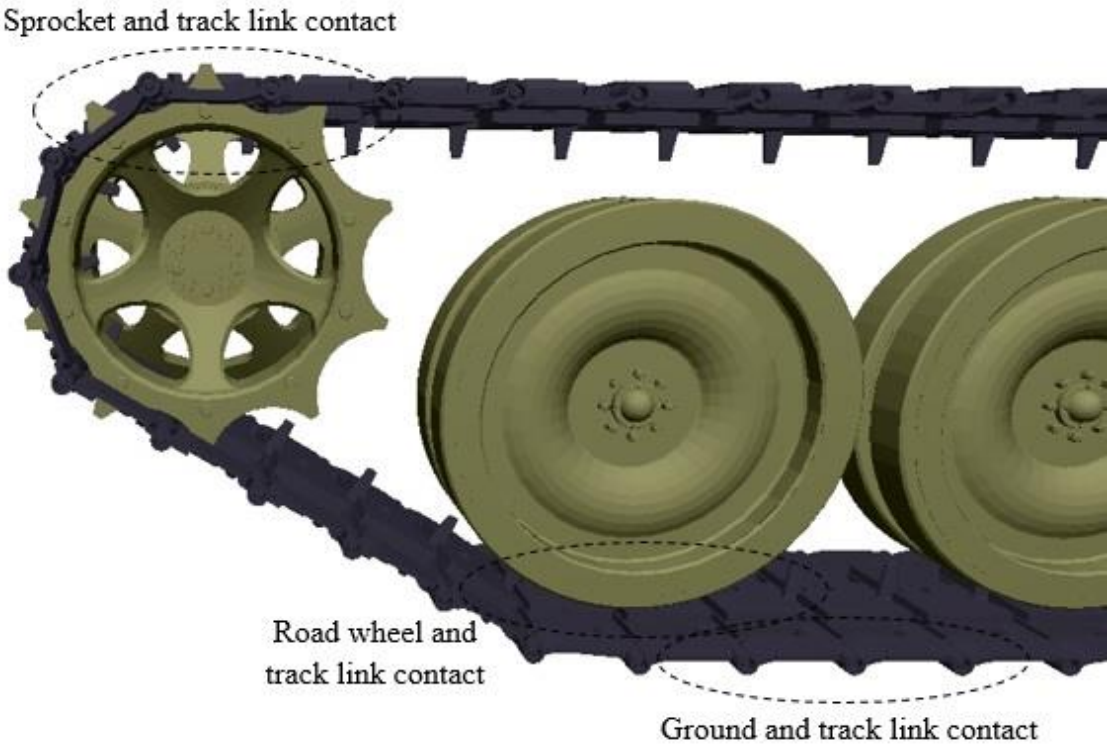

Figure 3.4: Tracked vehicle contact models

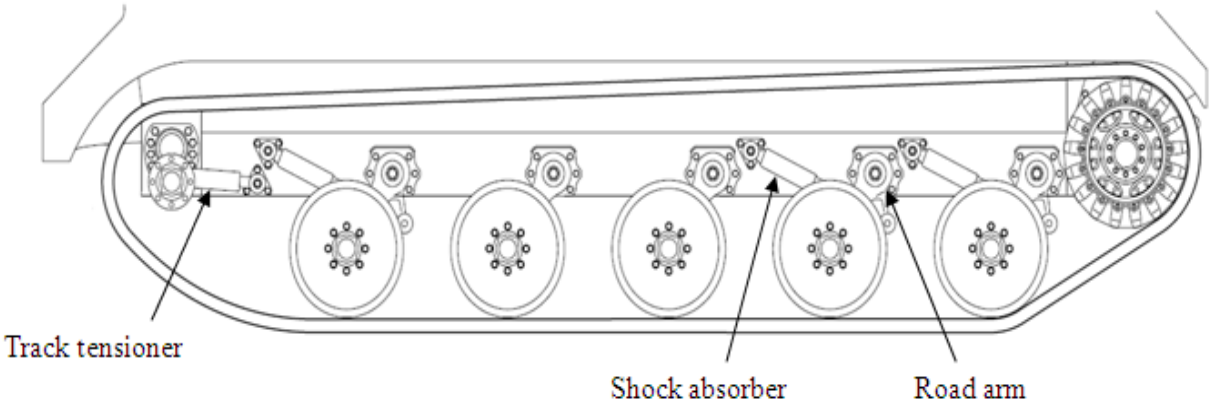

Figure 3.5: Suspension system layout of the tracked vehicle
(www.combatreform.org/SoucyBandTrackInstallationA-654RB.pdf)

Table 3.1: Mass and inertia values for tracked vehicle parts

Part	Mass (kg)	I_{xx} (kg.m^2)	I_{yy} (kg.m^2)	I_{zz} (kg.m^2)	I_{xy}, I_{xz}, I_{yz} (kg.m^2)
Chassis	5489.2	1786.9	10450	10721	0
Sprocket	436.67	13.868	12.216	12.216	0
Idler	429.57	14.698	12.545	12.545	0
Road Wheel	561.07	26.063	19.819	19.819	0
Road Arm	75.264	0.77085	0.37632	0.77085	0
Track Link	18.024	0.04113	0.22463	0.25256	0

Table 3.2: Contact Parameters

Parameters	Sprocket-Track Contact	Road Wheel-Track Contact	Ground-Track Contact
k	2.00×10^6 N/m	2.00×10^6 N/m	2.00×10^6 N/m
c	5.00×10^3 N·s/m	5.00×10^3 N·s/m	5.00×10^3 N·s/m
μ	0.150	0.100	0.300

Table 3.3: Suspension properties

Constants	Spring/Shock Absorber	Track Tensioner
Stiffness Coefficient, k	1.00×10^6 N/m	1.00×10^6 N/m
Damping Coefficient, c	1.50×10^4 N·s/m	1.40×10^4 N·s/m
Initial Length, l	0.508 m	0 m

3.6 NUMERICAL RESULTS

In this section, numerical results, obtained using the tracked vehicle model shown in Fig. 1.1, are used to compare the different joint formulations presented in this chapter. The tracked vehicle modeled is an armored personnel carrier that consists of a chassis, idler, sprocket, 5 road-wheels, and 64 track links on each track side (right and left). Figure 3.4 shows the engagement of the track links with some of the vehicle components, while more details about the road wheel arrangement and the configuration of the suspension system of the tracked vehicle model are shown in Fig. 3.5. Table 3.1 shows the inertia properties for all the tracked vehicle model components used in this simulation. More specifications of this vehicle can be obtained from open sources (M113, 2003). The vehicle has a suspension system that consists of road arms placed between the road wheels and chassis as well as shock absorbers connected to each road arm. Table 3.2 shows the stiffness and the damping coefficients of the contact models used. Initially two different simulation scenarios, one with the suspension system and the other without the suspension system, will be considered to study the effect of using the suspension system on the results. The road arms and the sprockets are connected to the chassis by revolute joints, and the road arms are connected to the road-wheels by revolute joints. The track links are connected to each other using revolute joints, which can be modeled using the constraint equations, penalty method, bushing element, or ANCF finite elements as previously mentioned. Tensioners are added to the system by connecting each idler to a tensioner with a revolute joint and connecting the tensioner to the chassis with a prismatic joint to ensure only translation between them. Table 3.3 shows the properties of the suspension system of each model used in the simulation. The angular velocities of the sprockets of the vehicle model considered in this numerical section are

assumed to increase after 1 sec until they reach a constant value of 25 rad/sec after 8 seconds as shown in Fig. 3.6.

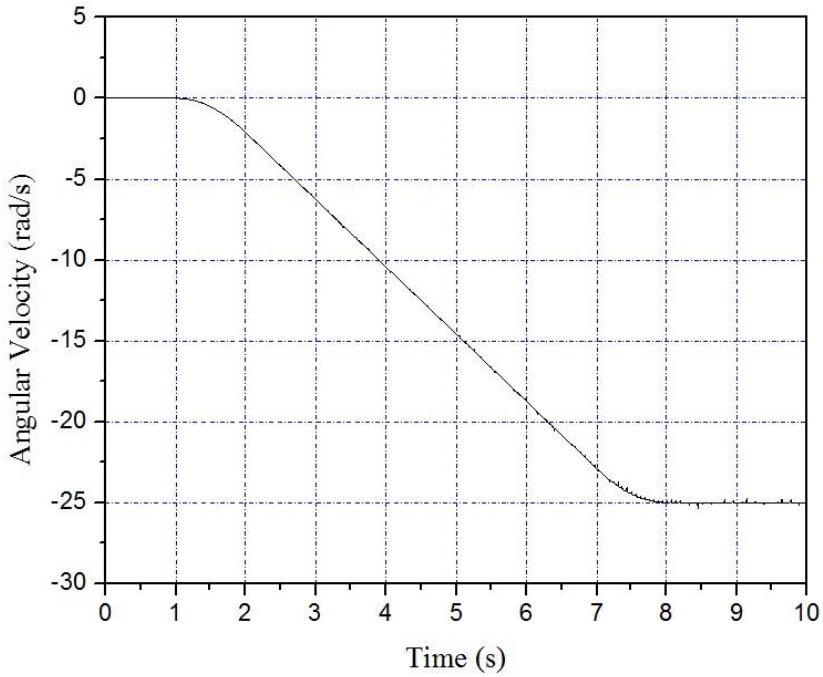

Figure 3.6: Sprocket angular velocity

Figure 3.7 shows the chassis vertical displacement using the joint model with and without the suspension system. The results presented in this figure show that the model with a suspension system allows for more vibration (a 7 cm initial drop compared to 0.64 cm), which helps make the model more realistic as compared to the previously unsuspended model. The ANCF finite element for the track links used is a three-dimensional steel cable element with a modulus of rigidity of 76.9 Gpa, a Young's modulus of 200 Gpa, and a mass density of 7.80×10^3 kg/m^3. Figures 3.8 and 3.10 show, respectively, the chassis forward position and velocity results obtained using different joint models. While the results presented in these figures show good agreement, the computational time varies when these different models are used. The constrained joint model takes less computational time compared to the penalty, bushing element, and ANCF

joint models; the penalty model CPU time is six times that of the constraint model CPU time, while the bushing model CPU time is three times, and the ANCF joint model CPU time is 5 times that of the constraint model CPU time. This increase in the penalty and bushing element CPU time is attributed to the high stiffness coefficients used in both of these models. Efforts are currently being made to improve the efficiency of the ANCF model.

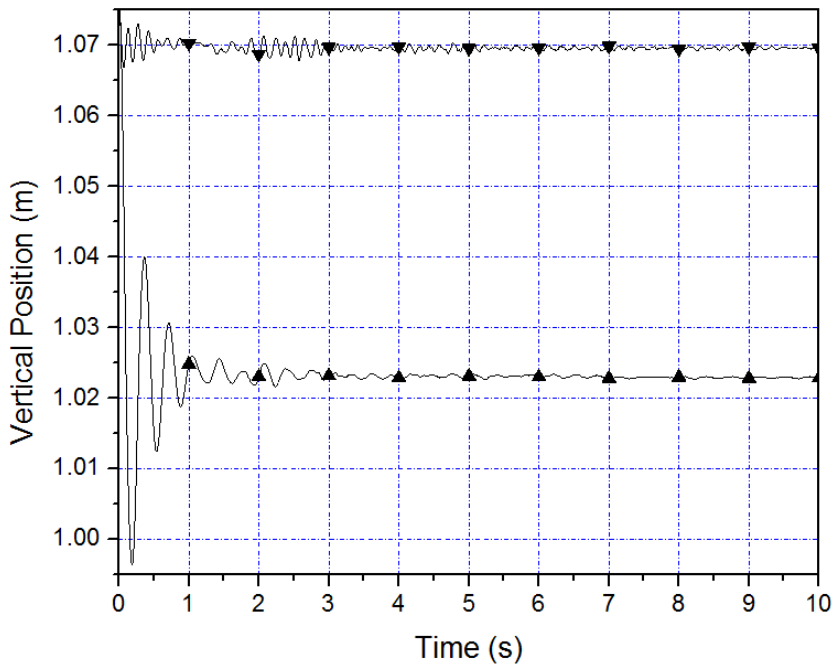

Figure 3.7: Chassis vertical displacement
(—▲— with suspension, —▼— without suspension)

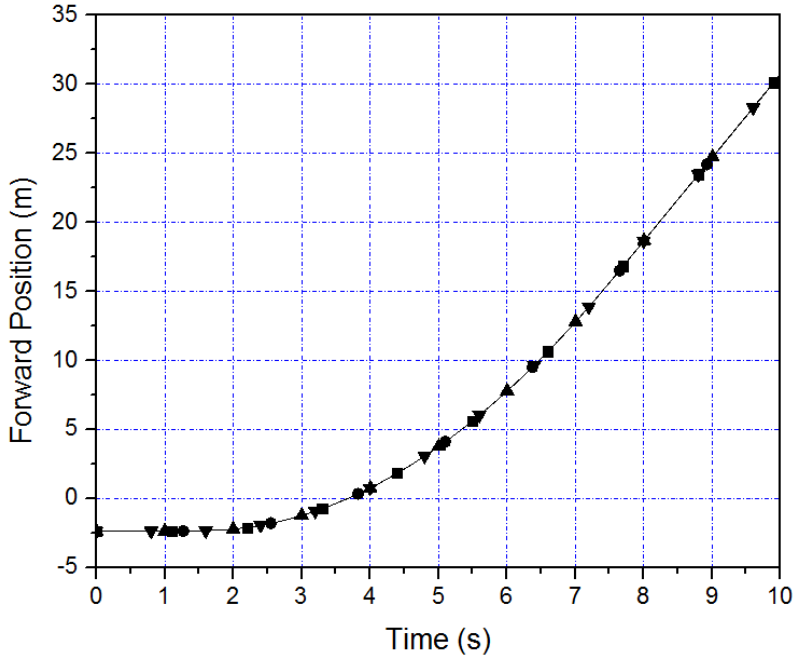

Figure 3.8: Chassis forward position
(—▲— Constrained joint model, —▼— Penalty method model, —■— Bushing element model, —●— ANCF model)

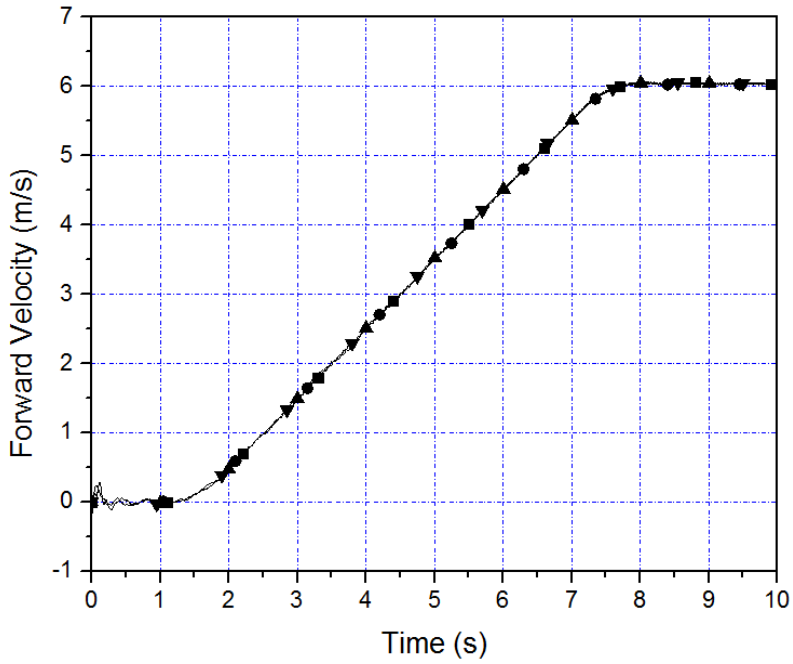

Figure 3.9: Chassis forward velocity
(—▲— Constrained joint model, —▼— Penalty method model, —■— Bushing element model, —●— ANCF model)

Figure 3.10 shows the motion trajectory of a track link in the chassis coordinate system using the constraint model, the penalty model, the bushing element model, and the ANCF joint model, respectively. The results in this figure show good, although not exact, agreement between the different models and emphasize differences between the penalty method and bushing element models, which both use forces to enforce the connectivity conditions between bodies. Figures 3.11 – 3.15 show the joint forces in the longitudinal and the vertical directions, respectively, obtained using the constrained, penalty, and ANCF joint models. The variation from positive to negative values in Figs. 3.11a and 3.11b are defined in the global coordinate system and they occur when the track links rotate in opposite directions. The changes in the orientation of the links, shown in Figs 3.12a and 3.12b, explain the change from positive to negative of the sign of the spikes in the constraint forces after 4 seconds. Very high frequencies were filtered out in all models using a low pass FFT with a cut-off frequency of 30 Hz in order to show clearly the nominal values of the joint forces presented in Figs. 3.11b and 3.12b. The results presented in these figures are obtained using a stiffness coefficient of 1×10^9 N/m and damping coefficient of 1×10^5 N.s/m for the penalty method model. The results show good agreement between the constrained and penalty joint models with the ANCF joint model, as expected, showing lower force magnitude due to the flexibility of the elements. Figures 3.13 and 3.14 show the same results in the case of a stiffness coefficient of 1×10^7 N/m and damping coefficient of 1×10^5 N.s/m for the penalty method model. The results of Figs. 3.13 and 3.14, which show significant differences between the two ideal joint models, demonstrate the drawback of the penalty method when the penalty stiffness coefficient is reduced. Similar results can be expected in the case of the bushing element models where the forces obtained also depend on the stiffness and damping coefficient of the joint. Figure 3.15 shows the joint deformation predicted using the penalty

model using different stiffness coefficients. The penalty model with a stiffness coefficient of 1×10^9 N/m shows much less deformation, less than 0.075 mm, while the penalty model with a stiffness of 1×10^7 N/m has much more deformation, over 1.5 mm, between the track links. The results presented in Figs. 3.13-3.15 explain the differences that can be accumulated as a result of user defined stiffness coefficients in the penalty force joint formulation.

Table 3.4: Joint model characteristics

Joint model type	Number of Coordinates	Number of DOF	Number of Constraints
Pin Joint	1092	168	924
Penalty Method	1092	798	294
Bushing Element	1092	798	294
ANCF	1227	1060	167

Table 3.4 shows the data of each type of the joint formulations used. These data include the number of coordinates, the number of degrees of freedom (DOF), and the number of constraints. In this chapter, four Euler parameters are used to describe the orientation of each body in the model. In Table 3.4, the constraints include the Euler parameters constraints; one for each body.

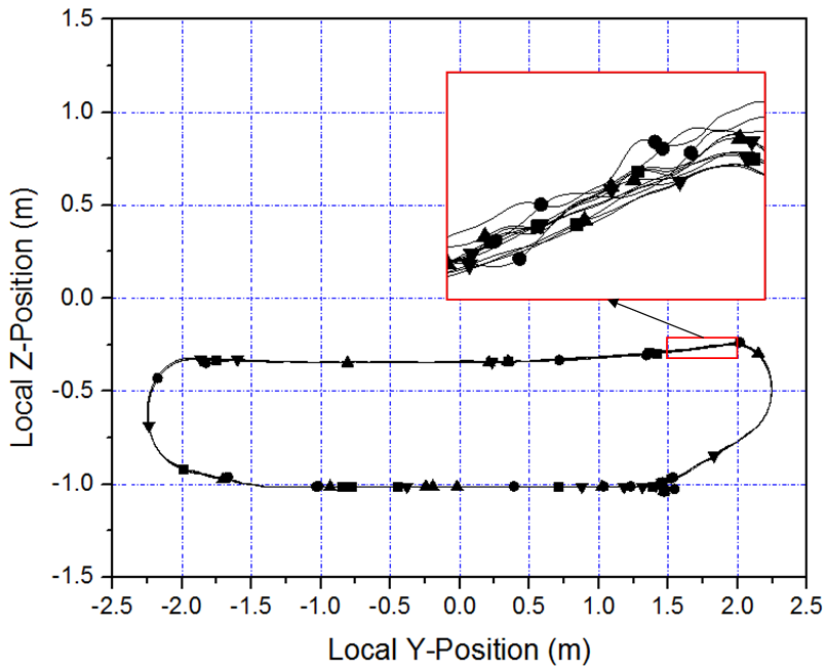

Figure 3.10: Trajectory motion of a track link in the chassis coordinate system
(—▲— Constrained joint model, —▼— Penalty method model, —■— Bushing element model, —●— ANCF model)

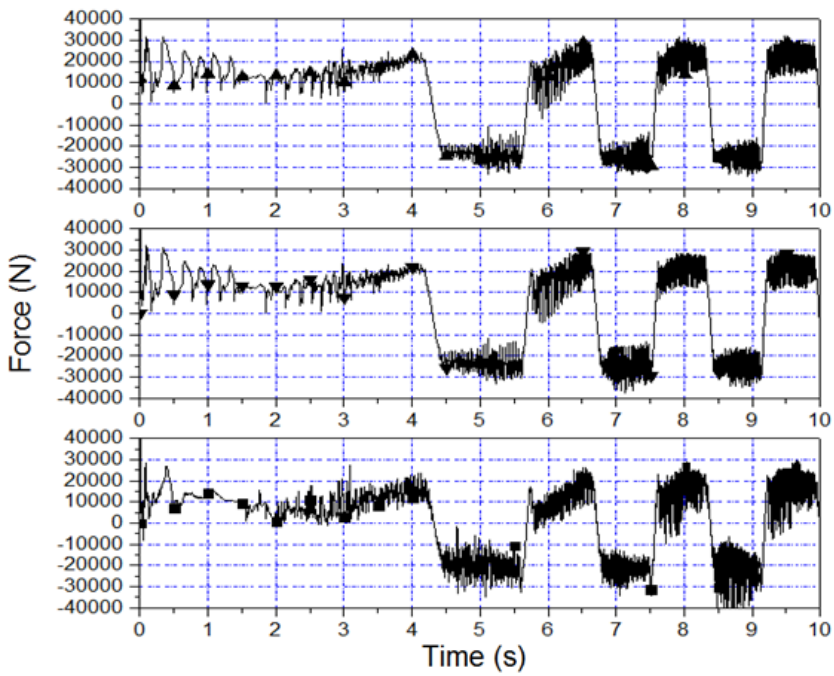

Figure 3.11a: Joint longitudinal forces
(—▲— Constrained joint model, —▼— Penalty method model k = 1×10^9 N/m, —■— ANCF model)

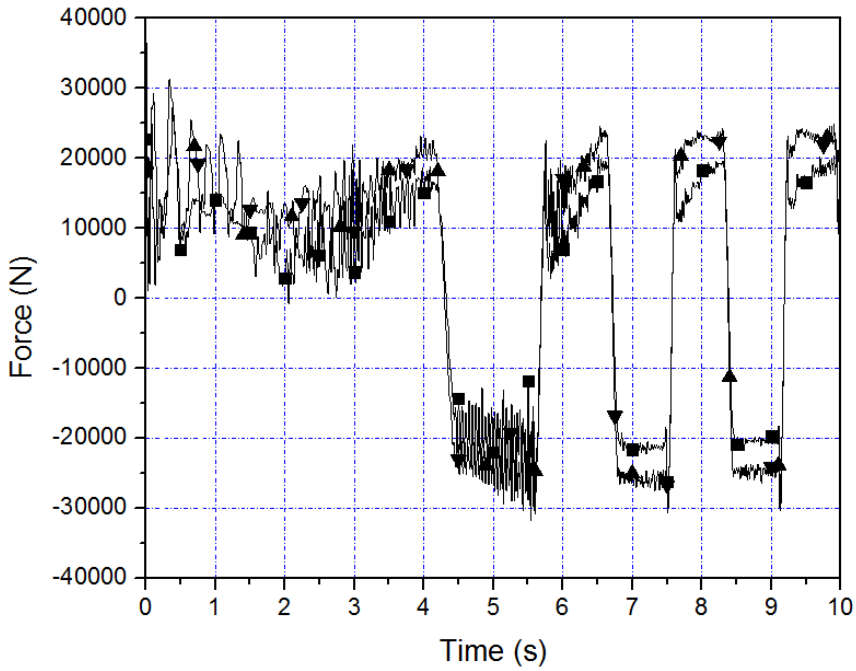

Figure 3.11b: Filtered joint longitudinal forces using FFT
(—▲— Constrained joint model, —▼— Penalty method model k = 1×10^9 N/m, —■— ANCF model)

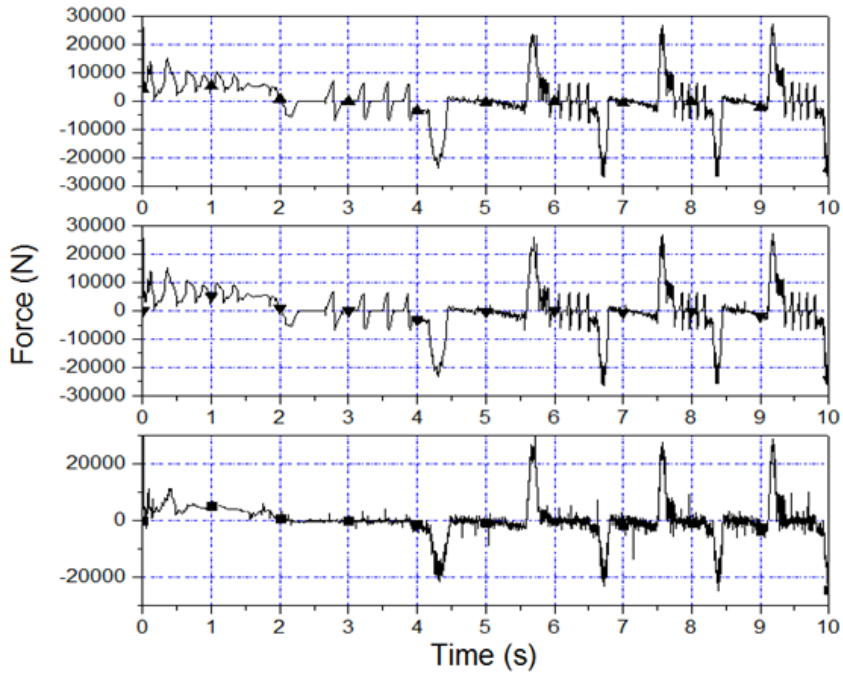

Figure 3.12a: Joint vertical forces
(—▲— Constrained joint model, —▼— Penalty method model k = 1×10^9 N/m, —■— ANCF model)

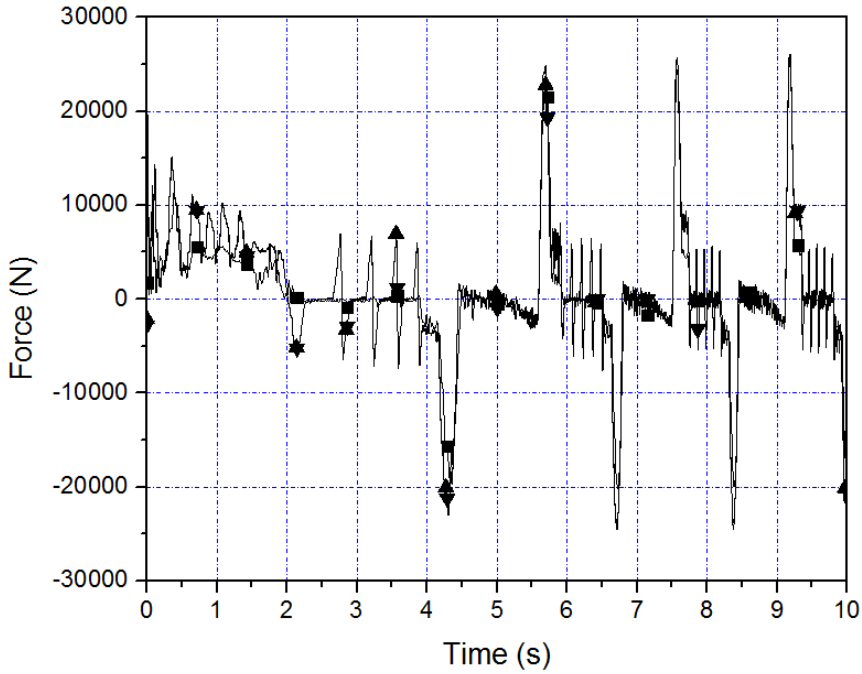

Figure 3.12b: Filtered joint vertical forces using FFT

(—▲— Constrained joint model, —▼— Penalty method model k = 1×10^{9} N/m, —■— ANCF model)

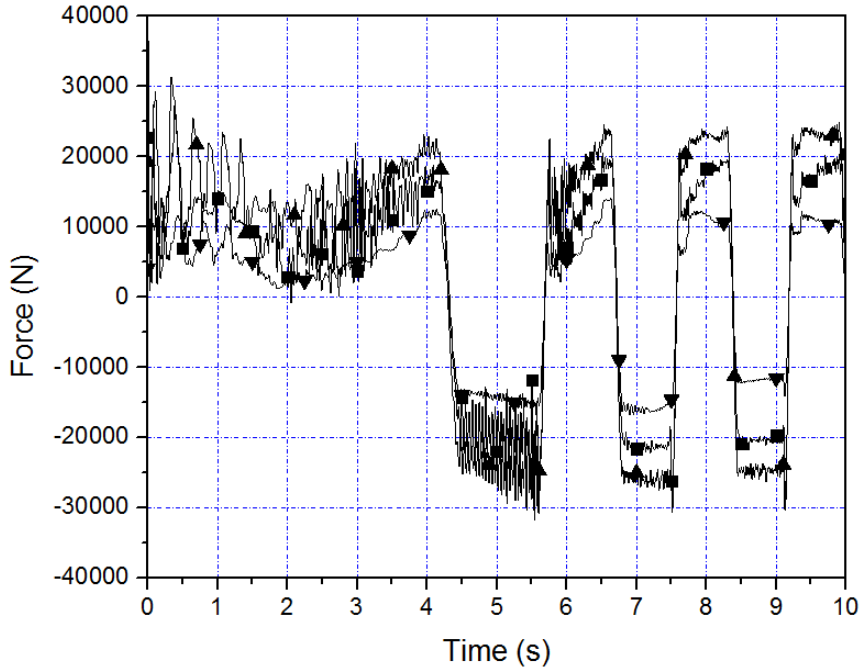

Figure 3.13: Joint Longitudinal forces

(—▲— Constrained joint model, —▼— Penalty method model k = 1×10^{7} N/m, —■—ANCF model)

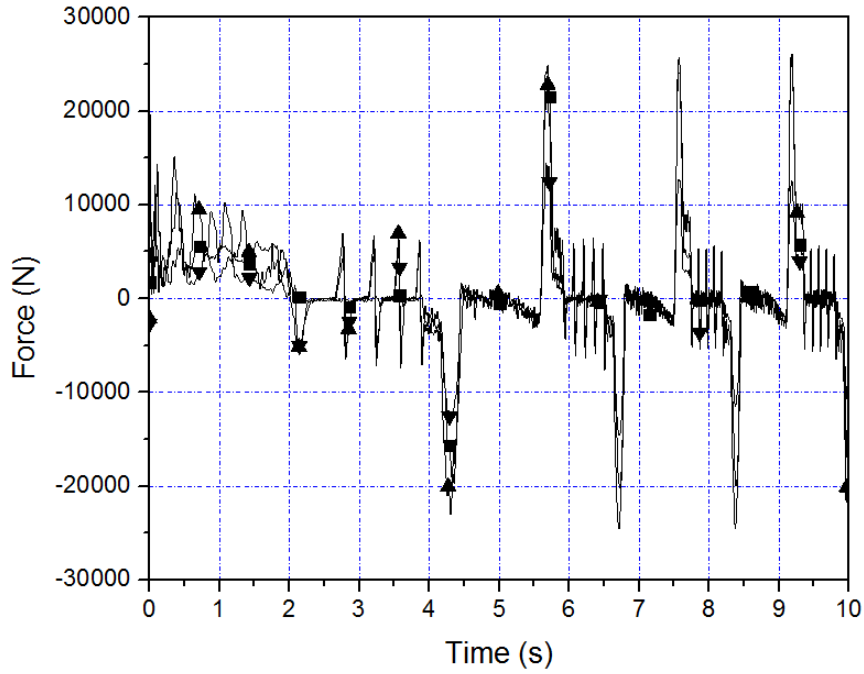

Figure 3.14: Joint vertical forces

(—▲— Constrained joint model, —▼— Penalty method model k = 1×10^{7} N/m, —■— ANCF model)

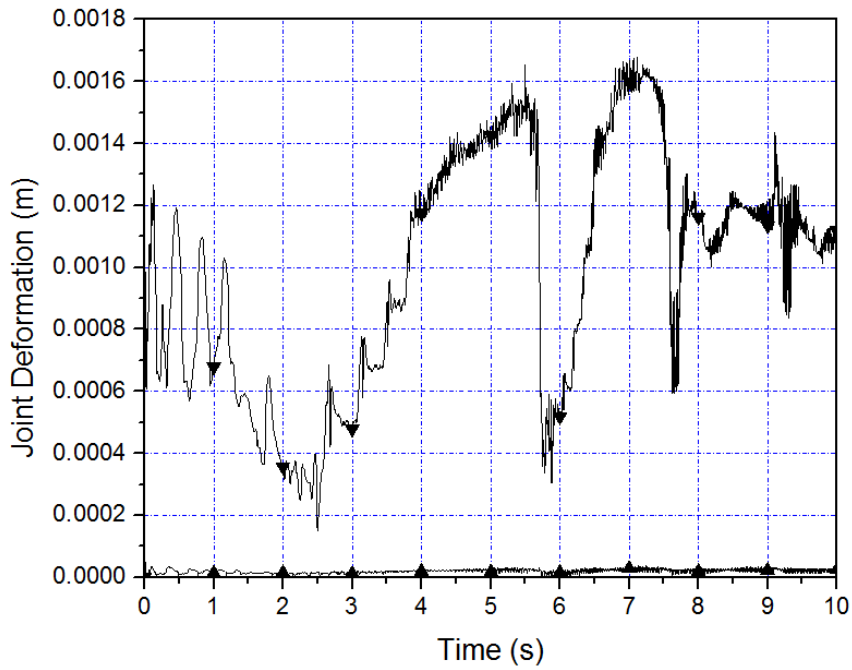

Figure 3.15: Joint constraint violation using penalty model

(—▲— k = 1×10^{9} N/m, —▼— k = 1×10^{7} N/m)

3.7 CONCLUDING REMARKS

In this chapter, different MBS joint formulations are presented and compared using detailed tracked vehicle models. Four main joint formulations are discussed; they are the ideal joint formulation, the penalty method, the compliant discrete element joint formulation, and the compliant continuum-based joint formulation. The ideal joint formulation is developed to eliminate the relative displacement between the two bodies connected by the joint. This can be achieved by enforcing a set of joint algebraic equations using a constrained dynamics approach or by using the penalty method. The constrained dynamics approach eliminates degrees of freedom and ensures that the constraint equations are satisfied at the position, velocity, and acceleration levels. The penalty method, on the other hand, does not reduce the number of degrees of freedom and ensures that the constraint equations are satisfied at the position level only provided that a high stiffness coefficient is used. The compliant discrete element formulation, which allows for joint deformations, can be systematically applied using a standard MBS bushing element that allows for six degrees of freedom of relative motion. The compliant continuum-based approach can be used to develop new joints that capture deformation modes that are not captured by the compliant discrete element joint formulation. ANCF finite elements can be used to systematically develop new joints with distributed elasticity and linear connectivity conditions.

As discussed in this chapter, it is important to choose the proper stiffness and damping coefficients when the penalty method and the bushing elements are used. Numerical results were presented in order to compare between different methods. The ideal joint formulation produces the desired joint kinematics and accurate joint forces. The same is true with the penalty force based joint when large penalty stiffness coefficients are used. Penalty force

based joint construction has been shown to be sensitive to the selection of penalty stiffness with the higher stiffness coefficients leading to better overall results. However, higher penalty stiffness increases CPU time significantly due to higher frequencies. The penalty method and bushing element models each have much larger CPU times than the ideal constrained model due to these high stiffness coefficients. The results presented in this chapter show that the ANCF joint model leads to lower force predictions which can be attributed to the track link flexibility.

CHAPTER 4

ACCURACY EVALUATION IN THE PREDICTION OF THE DYNAMIC STRESSES

(Previously published as Wallin, Michael, Hamed, Ashraf M., Paramsothy, Jayakumar, Gorsich, David J., Letherwood, Michael D., Shabana, Ahmed, A., 2016, "Evaluation of the Accuracy of the Rigid Body Approach in the Prediction of the Dynamic Stresses of Complex Multibody Systems," International Journal of Vehicle Performance, Vol. 2(2), pp. 140-165)

4.1 COUPLED AND DECOUPLED NONLINEAR ANALYSIS

Due to the lack of computational methods that can be used for the direct calculation of the stresses of complex multibody systems such as tracked vehicles, the dynamic stresses of such systems are often evaluated at a post-processing stage using forces obtained from a rigid body analysis. With the recent developments in MBS dynamics, detailed flexible body models of vehicle systems can be developed and used to evaluate, for the first time, the accuracy of the stress prediction based on the rigid body force calculations. It is, therefore, the objective of this chapter to use the finite element absolute nodal coordinate formulation, which automatically accounts for the dynamic coupling between the rigid body motion and the elastic deformation, to obtain the stress results. These results are then used to evaluate the accuracy of the stresses calculated at a post-processing stage using forces determined from a rigid body analysis. ANCF finite elements are used to perform the coupled dynamic analysis and obtain the stresses based on a fully nonlinear flexible body analysis. In order to obtain an accurate representation of the stresses in the case of the rigid body analysis, the floating frame of reference (FFR) formulation

dynamic equations are used to define the inertia and joint reaction forces that must be used in the post-processing stress calculations. To this end, the rigid body accelerations, including the angular accelerations, as well as the joint reaction forces are first predicted using a rigid body analysis. The solution of the rigid body problem is then used to formulate the FFR equations associated with the elastic coordinates. These equations include the effect of the inertia, centrifugal, and Coriolis forces resulting from the rigid body displacements. The resulting linear second order ordinary differential equations associated with the FFR elastic coordinates are solved for the elastic accelerations which are integrated to determine the elastic coordinates and velocities. The obtained elastic coordinates are used to determine the stresses which are compared with the stresses obtained using the fully coupled ANCF analysis. The two approaches described are explained in detail and used in the stress analysis of the track links in a complex three-dimensional tracked vehicle model. One of the most common areas of failure for such tracked vehicles is attributed to the failure of the track link chains, and therefore, performing a detailed fully coupled stress analysis, as the one described in this chapter, is necessary in order to obtain more accurate stress results and avoid failure of such complex vehicle systems.

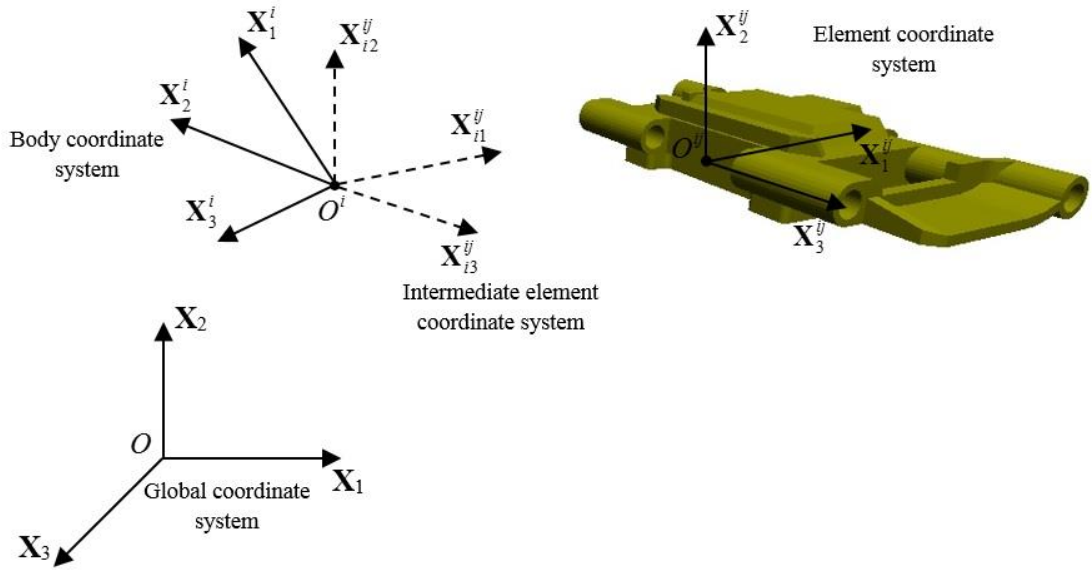

Figure 4.1: Finite element coordinate system

4.2 MOTION DESCRIPTION

Both the ANCF and the FFR formulation will be used in this chapter. ANCF finite elements will be used to develop the fully nonlinear coupled model, while the FFR formulation will be used to define the equations required for the post-processing stress calculations based on forces obtained using rigid body simulations. For this reason, these two formulations are briefly introduced in this section.

The FE/FFR formulation requires the use of four coordinate systems for each finite element, as is shown in Fig. 4.1. The *global coordinate system* $\mathbf{X}_1\mathbf{X}_2\mathbf{X}_3$ is fixed in time and space. Kinematic constraints which can represent mechanical joints and specified motion trajectories are formulated in this coordinate system using a set of nonlinear algebraic equations that depend on the system generalized coordinates and can also be time-dependent. A *body coordinate system* $\mathbf{X}_1^i\mathbf{X}_2^i\mathbf{X}_3^i$, called the floating frame of reference, forms a single set of axes for

the entire assembly of elements in the body i and, as such, serves to express the connectivity of all the elements in the body. Using this coordinate system, the connectivity conditions between elements can be defined using a constant Boolean matrix. The configuration of the body coordinate system is identified by using a set of reference coordinates that define the location and orientation of this rigid frame of reference. The *element coordinate system* $\mathbf{X}_1^{ij}\mathbf{X}_2^{ij}\mathbf{X}_3^{ij}$ for an element j on the deformable body i is rigidly attached to the element. This coordinate system translates and rotates with the element. The final coordinate system, the *intermediate element coordinate system* $\mathbf{X}_{i1}^{ij}\mathbf{X}_{i2}^{ij}\mathbf{X}_{i3}^{ij}$, has its origin rigidly attached to the body coordinate system and does not follow the deformation of the element. This coordinate system is initially oriented to be parallel to the element coordinate system and is represented by the dotted axes lines shown in Fig. 4.1. It is important to note that the use of the intermediate element coordinate system is necessary in order to obtain an exact modeling of the rigid body inertia in the case of complex structures with discontinuities. This concept is similar to the parallel axis theorem used in rigid body mechanics. Furthermore, since this coordinate system has a constant orientation with respect to the body coordinate system, exact modeling of the rigid body inertia in the body coordinate system can be obtained using a constant transformation. Using each of these coordinate systems, the location of an arbitrary point on an element can be defined and used to develop the kinematic and dynamic equations of the elements undergoing large displacement and angular rotation. The FFR formulation will be discussed in more detail in the following section.

While the FFR formulation can be used with finite elements that employ infinitesimal rotations, ANCF finite elements have no infinitesimal or finite rotations as nodal coordinates, and therefore, there are no restrictions on the amount of rotation or deformation within the element. Instead, element nodal coordinates are defined in the inertial frame and used with a

global shape function matrix that has a complete set of rigid body modes. Shown previously in Fig. 3.4 is a beam element consistent with this approach which shows the position vector gradients along each axis as well as the spatial coordinates associated with each node. This element is a fully parameterized element since it has a complete set of parameters, while other elements such as the Euler Bernoulli beam element are called gradient deficient elements since complete set of position vector gradients cannot be defined. Gradient deficient elements such as the Euler-Bernoulli beam element are simpler and more efficient in many applications including chain and belt applications, and for this reason, they will be used in the numerical study presented in this chapter to determine the stresses of the track links of three-dimensional tracked vehicles.

4.3 FFR FORMULATION

The FFR equations account for the dynamic coupling between the rigid body motion and the elastic deformation. The use of these equations will shed light on the approximations made when the forces, determined using a rigid body analysis, are subsequently used at a post-processing stage to solve a linear structural problem for the deformations in order to determine the stresses. Presenting the general form of the FFR dynamic equations of motion will clearly show the terms neglected when determining the stresses using the forces of the rigid body simulations. These stresses will be compared with the stresses determined using a fully coupled ANCF analysis.

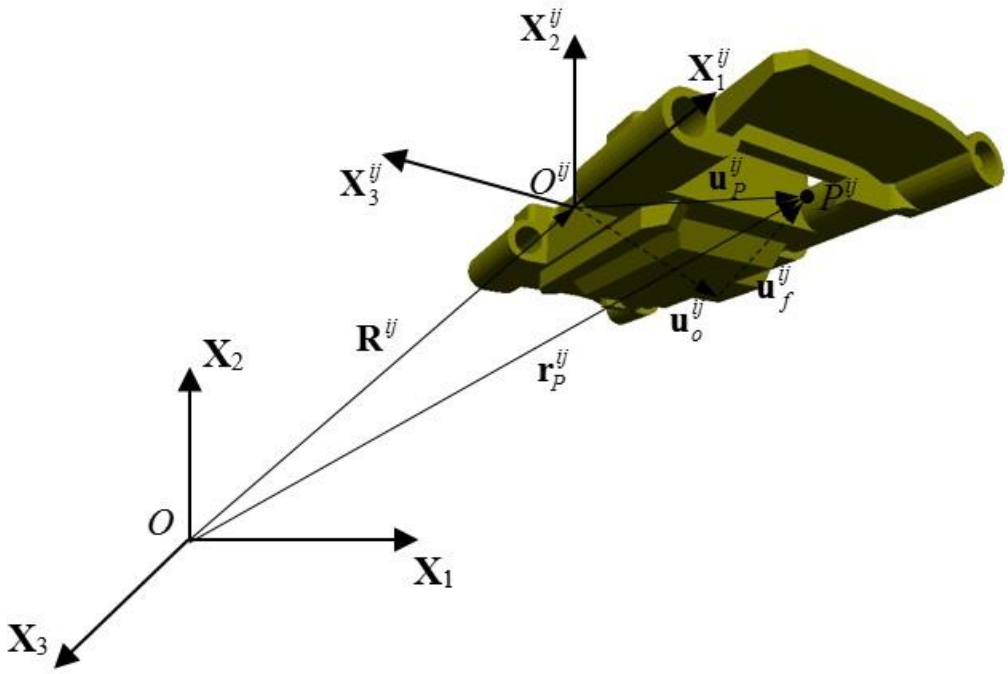

Figure 4.2: Flexible body coordinates

4.3.1 Kinematic Equations

The FE/FFR formulation employs a mixed set of absolute reference and local deformation coordinates (Shabana, 2014). The displacement field for an element i on a deformable body j can be written as $\mathbf{w}^{ij} = \mathbf{S}^{ij}\mathbf{e}^{ij}$, where $\mathbf{e}^{ij}$ is the vector of nodal coordinates which can be split into the vectors of the undeformed coordinates and the elastic nodal coordinates associated with the deformation of the element, $\mathbf{e}_0^{ij}$ and $\mathbf{e}_f^{ij}$, respectively, as $\mathbf{e}^{ij} = \mathbf{e}_0^{ij} + \mathbf{e}_f^{ij}$. The matrix $\mathbf{S}^{ij}$ is the shape function matrix which depends on the element spatial coordinates. For a three-dimensional beam element, the shape function $\mathbf{S}^{ij}$ is defined in the appendix. In the FE/FFR formulation, a deformable body can be divided into more than one finite element in order to obtain more accurate results. Using the element shape function matrix, the global position vector of an arbitrary point P^{ij} on the finite element j of the deformable body i can be written as

$\mathbf{r}^{ij} = \mathbf{R}^{ij} + \mathbf{u}_0^{ij} + \mathbf{u}_f^{ij}$, where $\mathbf{R}^{ij}$ is the position vector of a reference point O^{ij}, and $\mathbf{u}_0^{ij}$ and $\mathbf{u}_f^{ij}$ are the undeformed and deformed local position of the arbitrary point P^{ij}, respectively, as shown in Fig. 4.2. The local position vector of the arbitrary point in the FE/FFR formulation can be written as $\mathbf{u}^{ij} = \mathbf{u}_0^{ij} + \mathbf{u}_f^{ij}$, or equivalently, $\mathbf{u}^{ij} = \mathbf{A}^i \overline{\mathbf{u}}^{ij} = \mathbf{C}^{ij}\mathbf{S}^{ij}\overline{\mathbf{C}}^{ij}\mathbf{B}_1^{ij}\mathbf{q}_n^i = \mathbf{N}^{ij}\mathbf{q}_n^i$, where $\mathbf{A}^i$ is the rotation matrix that defines the orientation of the body reference, $\mathbf{S}^{ij}$ is the shape function matrix, $\mathbf{B}_1^{ij}$ is a constant Boolean matrix describing the element connectivity conditions, $\mathbf{q}_n^i$ is the vector of nodal coordinates of body i, $\mathbf{N}^{\mathbf{ij}} = \mathbf{C}^{ij}\mathbf{S}^{ij}\overline{\mathbf{C}}^{ij}\mathbf{B}_1^{ij}$ is a space dependent matrix, and the element transformation matrices $\mathbf{C}^{ij}$ and $\overline{\mathbf{C}}^{ij}$ are defined in the appendix (Shabana, 2014). One can show that the global position vector can be written as $\mathbf{r}^{ij} = \mathbf{R}^i + \mathbf{A}^i\mathbf{N}^{ij}\left(\mathbf{q}_o^i + \mathbf{B}_2^i\mathbf{q}_f^i\right)$, where the vector of element nodal coordinates can be divided into its undeformed and deformed components $\mathbf{q}_o^i$ and $\mathbf{q}_f^i$, respectively, and $\mathbf{B}_2^i$ is a Boolean matrix representing a linear transformation that arises from imposing the reference conditions that define a unique displacement field. The velocity vector can then be defined as $\dot{\mathbf{r}}^{ij} = \dot{\mathbf{R}}^{ij} + \mathbf{A}^i\left(\overline{\boldsymbol{\omega}}^i \times \overline{\mathbf{u}}^{ij}\right) + \mathbf{A}^i\mathbf{N}^{ij}\mathbf{B}_2^i\dot{\mathbf{q}}_f^i$, where $\overline{\boldsymbol{\omega}}^i$ is the angular velocity vector defined in the local coordinate system, and $\overline{\boldsymbol{\omega}}^i \times \overline{\mathbf{u}}^{ij} = -\tilde{\overline{\mathbf{u}}}^{ij}\overline{\boldsymbol{\omega}}^i$, where $\tilde{\overline{\mathbf{u}}}^{ij}$ is the skew-symmetric matrix associated with the vector $\overline{\mathbf{u}}^{ij}$. The local angular velocity vector $\overline{\boldsymbol{\omega}}^i$ can be written in terms of the reference rotational coordinates of body i as $\overline{\boldsymbol{\omega}}^i = \overline{\mathbf{G}}^i\dot{\boldsymbol{\theta}}^i$, where $\overline{\mathbf{G}}^i$ can be either a 3 $\times$ 4 matrix dependent on the Euler parameters or a 3 $\times$ 3 matrix dependent on the sequence of Euler angles, and $\dot{\boldsymbol{\theta}}^i$ is the vector of rotational coordinates of the body reference. One can then write $\dot{\mathbf{r}}^{ij} = \dot{\mathbf{R}}^{ij} - \mathbf{A}^i\tilde{\overline{\mathbf{u}}}^{ij}\overline{\mathbf{G}}^i\dot{\boldsymbol{\theta}} + \mathbf{A}^i\mathbf{N}^{ij}\mathbf{B}_2^i\dot{\mathbf{q}}_f^i$.

4.3.2 Inertia Forces

One can use the definition of the kinetic energy $T^{ij} = \frac{1}{2}\int_{V^{ij}} \rho^{ij} \dot{\mathbf{r}}^{ij^T} \dot{\mathbf{r}}^{ij} dV^{ij}$ to write $T^{ij} = \frac{1}{2}\dot{\mathbf{q}}^{i^T} \mathbf{M}^{ij} \dot{\mathbf{q}}^{i}$, where the total vector of generalized coordinates of body i is $\mathbf{q}^i = \begin{bmatrix} \mathbf{R}^{i^T} & \boldsymbol{\theta}^{i^T} & \mathbf{q}_f^{i^T} \end{bmatrix}^T$, ρ^{ij} and V^{ij} are, respectively, the element mass density and volume, and $\mathbf{M}^{ij}$ is the symmetric mass matrix of the finite element defined in terms of the vectors and matrices previously introduced in this section as

$$\mathbf{M}^{ij} = \int_{V^{ij}} \rho^{ij} \begin{bmatrix} \mathbf{I} & -\mathbf{A}^i \tilde{\overline{\mathbf{u}}}^{ij} \overline{\mathbf{G}}^i & \mathbf{A}^i \mathbf{N}^{ij} \mathbf{B}_2^i \\ & \overline{\mathbf{G}}^{i^T} \tilde{\overline{\mathbf{u}}}^{ij^T} \tilde{\overline{\mathbf{u}}}^{ij} \overline{\mathbf{G}}^i & \overline{\mathbf{G}}^{i^T} \tilde{\overline{\mathbf{u}}}^{ij} \mathbf{N}^{ij} \mathbf{B}_2^i \\ symmetric & & \mathbf{B}_2^{i^T} \mathbf{N}^{ij^T} \mathbf{N}^{ij} \mathbf{B}_2^i \end{bmatrix} dV^{ij} \tag{4.1}$$

This mass matrix is highly nonlinear in the coordinates and accounts for the dynamic coupling between the rigid body motion and the elastic deformation. It is important to understand the form of this matrix in order to be able to develop a systematic procedure for the post-processing stress calculations in which the effect of the elastic deformation on the rigid body motion is neglected. Because the mass matrix is highly nonlinear, one obtains a complex expression for the vector of Coriolis and centrifugal forces. If the effect of the elastic deformation on the rigid body motion is neglected, the vector of centrifugal and Coriolis forces can be written as (Campanelli et al., 1998)

$$\mathbf{Q}_v^{ij} = \begin{bmatrix} \left(\mathbf{Q}_v^{ij}\right)_R \\ \left(\mathbf{Q}_v^{ij}\right)_\theta \\ \left(\mathbf{Q}_v^{ij}\right)_f \end{bmatrix} = \begin{bmatrix} -\mathbf{A}^i \left[\left(\tilde{\overline{\boldsymbol{\omega}}}^i\right)^2 \int_{V^{ij}} \rho^i \overline{\mathbf{u}}_0^{ij} dV^{ij} \right] \\ -2\dot{\overline{\mathbf{G}}}^{i^T} \overline{\mathbf{I}}_{\theta\theta}^i \overline{\boldsymbol{\omega}}^i \\ -\int_{V^{ij}} \rho^i \mathbf{S}^{ij^T} \left[\left(\tilde{\overline{\boldsymbol{\omega}}}^i\right)^2 \overline{\mathbf{u}}^{ij} + 2\tilde{\overline{\boldsymbol{\omega}}}^i \dot{\overline{\mathbf{u}}}_f^{ij} \right] dV^{ij} \end{bmatrix} \tag{4.2}$$

where $\bar{\mathbf{I}}^i_{\theta\theta} = \int_{V^i} \rho^i \tilde{\bar{\mathbf{u}}}^{i\,T} \tilde{\bar{\mathbf{u}}}^i dV^i \approx \int_{V^i} \rho^i \tilde{\bar{\mathbf{u}}}^{i\,T}_0 \tilde{\bar{\mathbf{u}}}^i_0 dV^i$ is the inertia tensor evaluated by neglecting the effect of the deformation on the mass moments and products of inertia. The vector of centrifugal and Coriolis forces associated with the deformation coordinates can be written as $\left(\mathbf{Q}^i_v\right)_f = -\left(2\tilde{\mathbf{S}}^i_1 \dot{\mathbf{q}}^i_f + \tilde{\mathbf{S}}^i_2 \mathbf{q}^i_f - \tilde{\bar{\mathbf{I}}}^i_o \bar{\boldsymbol{\omega}}^i\right)$, where $\tilde{\mathbf{S}}^i_1$, $\tilde{\mathbf{S}}^i_2$, and $\tilde{\bar{\mathbf{I}}}^i_o$ are defined in the appendix of the thesis. The vector $\left(\mathbf{Q}^i_v\right)_f$ can be simplified to $\left(\mathbf{Q}^i_v\right)_f = \tilde{\bar{\mathbf{I}}}^i_o \bar{\boldsymbol{\omega}}^i$ if the first two terms in this vector are assumed to be much smaller than the third term. Using this assumption, the vector $\left(\mathbf{Q}^i_v\right)_f$ becomes independent of the elastic coordinates. Furthermore, when a centroidal body coordinate system is used $\left(\mathbf{Q}^{ij}_v\right)_R = \mathbf{0}$ since the moment of mass of the body in the initial configuration is equal to zero, that is $\int_{V^{ij}} \rho^i \bar{\mathbf{u}}^{ij}_0 dV^{ij} = \mathbf{0}$.

The expressions of the inertia forces associated with the elastic coordinates must be correctly evaluated and consistently used in the post-processing stress analysis. The last term in the preceding equation, as mentioned above, defines the Coriolis and centrifugal forces associated with the elastic coordinates. This term, which depends on the angular velocity of the body reference (rigid body motion), must be evaluated and used in the equations that are solved for the deformation coordinates used in the stress calculations. Note also that the first term in the preceding equation represents the moment of mass. If the origin of the body coordinate system is selected to be initially attached to the body center of mass, this term will identically equal to zero in the case of the rigid body analysis.

4.3.3 Applied Forces

The vector of generalized forces which includes the external forces $\mathbf{Q}^{ij}_e$, the centrifugal and Coriolis inertia forces $\mathbf{Q}^{ij}_v$, and the constraint forces can be written as $\bar{\mathbf{Q}}^{ij} = \mathbf{Q}^{ij}_e + \mathbf{Q}^{ij}_v - \mathbf{C}^T_{\mathbf{q}^{ij}} \boldsymbol{\lambda}$,

where $\mathbf{C}_{\mathbf{q}^{ij}}$ is the constraint Jacobian matrix, and $\boldsymbol{\lambda}$ is the vector of Lagrange multipliers. Each of the force components in this equation must be determined in terms of undeformed, displacement, rotation, and deformation coordinates, as demonstrated in the case of the vector of Coriolis and centrifugal forces $\mathbf{Q}_v^{ij}$. The vector of generalized external forces, which includes the gravity and contact forces, can be formulated to define the nodal forces. For example, the generalized nodal forces as the results of a force vector $\mathbf{F}_{ext}^{ij}$ acting at a point on the element can be written as $\mathbf{Q}_e^{ij} = \mathbf{S}_m^{ij\,T}\left(\mathbf{A}^{iT}\mathbf{F}_{ext}^{ij}\right)$ where $\mathbf{S}_m^{ij}$ is the shape function matrix defined at the point of application of the force.

4.3.4 Constraint Forces

Tracked vehicle models represent heavily constrained systems that can have a large number of joints, particularly revolute joints. For the post-processing stress analysis in which the effect of deformation on the rigid body motion is neglected, the joint reaction forces are calculated using the rigid body analysis. The effect of these forces in the linear structural problem used to solve for the deformations that define the stresses must be taken into consideration. In general, the vector of generalized constraint forces can be written as the product of the constraint Jacobian matrix and Lagrange multipliers as $\mathbf{Q}_c^i = \mathbf{C}_{\mathbf{q}^i}^T\boldsymbol{\lambda}$. For example, in the case of a revolute joint, the constraint equations can be written as $\mathbf{C} = \left[\left(\mathbf{r}_P^i - \mathbf{r}_P^j\right)^T \quad \mathbf{v}_1^{iT}\mathbf{v}^j \quad \mathbf{v}_2^{i\,T}\mathbf{v}^j\right]^T = \mathbf{0}$, where $\mathbf{r}_P^i$ and $\mathbf{r}_P^j$ are the position vectors of the joint definition points on bodies i and j, respectively, and $\mathbf{v}_1^i$ and $\mathbf{v}_2^i$ are two vectors defined on body i perpendicular to the joint axis vector $\mathbf{v}^j$ defined on body j, as shown previously in Fig. 4.2. Using the revolute joint kinematic equations, one can define the generalized constraint forces as (Campanelli et al., 1998).

$$\mathbf{Q}_c^i = \begin{bmatrix} \mathbf{C}_{\mathbf{R}^i}^T \\ \mathbf{C}_{\boldsymbol{\theta}^i}^T \\ \mathbf{C}_{\mathbf{q}_f^i}^T \end{bmatrix} \boldsymbol{\lambda} = \begin{bmatrix} \mathbf{I} & \mathbf{0} & \mathbf{0} \\ \overline{\mathbf{G}}^{i\,T} \tilde{\overline{\mathbf{u}}}_P^i \mathbf{A}^{i\,T} & \overline{\mathbf{G}}^{i\,T} \tilde{\overline{\mathbf{v}}}_1^i \mathbf{A}^{i\,T} \mathbf{v}^j & \overline{\mathbf{G}}^{i\,T} \tilde{\overline{\mathbf{v}}}_2^i \mathbf{A}^{i\,T} \mathbf{v}^j \\ \mathbf{S}^{i\,T} \mathbf{A}^{i\,T} & \mathbf{S}_{rc}^{i\,T} \tilde{\hat{\mathbf{v}}}_1^i \mathbf{A}^{i\,T} \mathbf{v}^j & \mathbf{S}_{rc}^{i\,T} \tilde{\hat{\mathbf{v}}}_2^i \mathbf{A}^{i\,T} \mathbf{v}^j \end{bmatrix} \boldsymbol{\lambda} \tag{4.3}$$

where $\mathbf{S}_{rc}^i$ is a partition of the shape function matrix which describes the orientation of the intermediate joint coordinate system with respect to the body coordinate system. The virtual work of the constraint forces can then be written as

$$\delta \mathbf{W}_c^i = \mathbf{Q}_c^{i\,T} \delta \mathbf{q}^i = \left(\mathbf{C}_{\mathbf{R}^i}^T \boldsymbol{\lambda}\right)^T \delta \mathbf{R}^i + \left(\mathbf{C}_{\boldsymbol{\theta}^i}^T \boldsymbol{\lambda}\right)^T \delta \boldsymbol{\theta}^i + \left(\mathbf{C}_{\mathbf{q}_f^i}^T \boldsymbol{\lambda}\right)^T \delta \mathbf{q}_f^i = \mathbf{F}_c^{i\,T} \delta \mathbf{r}_c^i + \mathbf{M}_c^{i\,T} \delta \boldsymbol{\psi}_c^i \tag{4.4}$$

where $\delta \mathbf{r}_c^i = \delta \mathbf{R}^i - \mathbf{A}^i \tilde{\overline{\mathbf{u}}}_c^i \overline{\mathbf{G}}^i \delta \boldsymbol{\theta}^i + \mathbf{A}^i \mathbf{S}_c^i \delta \mathbf{q}_f^i$, $\delta \boldsymbol{\psi}_c^i = \mathbf{A}^i \left(\overline{\mathbf{G}}^i \delta \boldsymbol{\theta}^i + \mathbf{S}_{rc}^i \delta \mathbf{q}_f^i\right)$, $\mathbf{S}_c^i$ is the shape function matrix defined at the point of application of the force and $\mathbf{F}_c^i$ and $\mathbf{M}_c^i$ represent the vectors of the actual joint reaction forces and moments acting on body i as a result of the revolute joint connection with body j, respectively. The use of these definitions and the preceding equation of the virtual work leads to the definition of the generalized constraint forces as

$$\mathbf{Q}_c^i = \begin{bmatrix} \mathbf{C}_{\mathbf{R}^i}^T \boldsymbol{\lambda} \\ \mathbf{C}_{\boldsymbol{\theta}^i}^T \boldsymbol{\lambda} \\ \mathbf{C}_{\mathbf{q}_f^i}^T \boldsymbol{\lambda} \end{bmatrix} = \begin{bmatrix} \mathbf{F}_c^i \\ \left(-\mathbf{A}^i \tilde{\overline{\mathbf{u}}}_c^i \overline{\mathbf{G}}^i\right)^T \mathbf{F}_c^i + \left(\mathbf{A}^i \overline{\mathbf{G}}^i\right)^T \mathbf{M}_c^i \\ \left(\mathbf{A}^i \mathbf{S}_c^i\right)^T \mathbf{F}_c^i + \left(\mathbf{A}^i \mathbf{S}_{rc}^i\right)^T \mathbf{M}_c^i \end{bmatrix} \tag{4.5}$$

The vector of generalized constraint forces can be simplified by writing the vector of actual joint moments to be $\mathbf{M}_c^i = \mathbf{A}^i \left(\mathbf{B}_G^i \mathbf{C}_{\theta^i}^T - \tilde{\overline{\mathbf{u}}}_c^i \mathbf{A}^{i\,T} \mathbf{C}_{\mathbf{R}^i}^T\right) \boldsymbol{\lambda}$, where $\mathbf{C}_{\mathbf{R}^i}$ and $\mathbf{C}_{\boldsymbol{\theta}^i}$ represent the partitions of the constraint Jacobian matrix associated with the displacement and rotation coordinates, and the matrix $\mathbf{B}_G^i = \left(\overline{\mathbf{G}}^{i\,T}\right)^{-1}$ when using Euler angles or Rodrigues parameters or $\mathbf{B}_G^i = (1/4)\overline{\mathbf{G}}^i$ when using Euler parameters. This provides a straightforward definition of the generalized constraint forces as

$$\mathbf{Q}_c^i = \begin{bmatrix} \mathbf{C}_{\mathbf{R}^i}^T \boldsymbol{\lambda} \\ \mathbf{C}_{\boldsymbol{\theta}^i}^T \boldsymbol{\lambda} \\ \mathbf{C}_{\mathbf{q}_f^i}^T \boldsymbol{\lambda} \end{bmatrix} = \begin{bmatrix} \mathbf{F}_c^i \\ \overline{\mathbf{G}}^{i\,T} \mathbf{B}_G^i \mathbf{C}_{\boldsymbol{\theta}^i}{}^T \boldsymbol{\lambda} \\ \left(\mathbf{S}_c^i + \tilde{\overline{\mathbf{u}}}_c^i \mathbf{S}_{rc}^i\right)^T \mathbf{A}^{i\,T} \mathbf{C}_{\mathbf{R}^i}^T \boldsymbol{\lambda} + \mathbf{S}_{rc}^i{}^T \mathbf{B}_G^i \mathbf{C}_{\boldsymbol{\theta}^i}^T \boldsymbol{\lambda} \end{bmatrix} \tag{4.6}$$

In the post-processing stress analysis, the vector of Lagrange multipliers $\boldsymbol{\lambda}$ is determined using the rigid body simulation of the model. Using this vector and knowing the reference coordinates, the third element of the constraint force vector in the preceding equation can be evaluated and introduced as an externally applied force to the linear structural problem used to solve for the deformation coordinates that define the stresses.

4.3.4 Post-Processing Stress Analysis

Using the FFR kinematic description, the equations of motion of the elements can be assembled to obtain the equation of motion of the deformable body i which can be written as

$$\begin{bmatrix} \mathbf{m}_{rr}^i & \mathbf{m}_{rf}^i \\ \mathbf{m}_{fr}^i & \mathbf{m}_{ff}^i \end{bmatrix} \begin{bmatrix} \ddot{\mathbf{q}}_r^i \\ \ddot{\mathbf{q}}_f^i \end{bmatrix} + \begin{bmatrix} \mathbf{0} & \mathbf{0} \\ \mathbf{0} & \mathbf{K}_{ff}^i \end{bmatrix} \begin{bmatrix} \mathbf{q}_r^i \\ \mathbf{q}_f^i \end{bmatrix} = \begin{bmatrix} \overline{\mathbf{Q}}_r^i \\ \overline{\mathbf{Q}}_f^i \end{bmatrix} - \begin{bmatrix} \mathbf{C}_{\mathbf{q}_r^i}^T \\ \mathbf{C}_{\mathbf{q}_f^i}^T \end{bmatrix} \boldsymbol{\lambda} \tag{4.7}$$

where the vectors and matrices that appear in this equation are the assembled vectors and matrices of the finite elements. In the post-processing stress analysis, the following assumptions are made:

1. The effect of the elastic deformation on the rigid body motion is neglected.
2. In this case, the mass moments and products of inertia are assumed to be independent of the body deformation.
3. The quadratic velocity vectors reduce to the gyroscopic moments used in the rigid body analysis.

4. The submatrix $\mathbf{m}_{rf}^{i}$ that defines the dynamic coupling between the rigid body motion and the elastic deformation is neglected.

Using these assumptions, one can first solve the nonlinear system of equations $\mathbf{m}_{rr}^{i}\ddot{\mathbf{q}}_{r}^{i} = \bar{\mathbf{Q}}_{r}^{i} - \mathbf{C}_{\mathbf{q}_{r}^{i}}^{T}\boldsymbol{\lambda}$ for the reference coordinates, velocities, and accelerations as well as the vector of Lagrange multipliers using a rigid body analysis approach. Lagrange multipliers can be used to determine the joint reaction forces. Knowing the reference coordinates, velocities, accelerations, and the vector of Lagrange multipliers, the system of linear equations $\mathbf{m}_{ff}^{i}\ddot{\mathbf{q}}_{f}^{i} + \mathbf{K}_{ff}^{i}\mathbf{q}_{f}^{i} = \bar{\mathbf{Q}}_{f}^{i} - \mathbf{m}_{fr}^{i}\ddot{\mathbf{q}}_{r}^{i} - \mathbf{C}_{\mathbf{q}_{f}^{i}}^{T}\boldsymbol{\lambda}$ can be solved for the elastic coordinates which can be used to calculate the stresses. The stresses obtained using this dynamically decoupled procedure will be compared with the stresses obtained using a fully coupled nonlinear ANCF analysis.

4.4 ANCF COUPLED RIGID BODY/DEFORMATION NONLINEAR ANALYSIS

As previously mentioned in this chapter, while the track links of tracked vehicles experience, for the most part, small deformations, the use of the FFR formulation to develop a coupled rigid body/elastic deformation analysis is impractical. This is mainly due to the large number of chain nonlinear constraint equations and the highly nonlinear inertia matrix of the finite elements in the FE/FFR formulation. For this reason, the decoupled rigid body/deformation analysis described in the preceding section has been the only available practical option to evaluate the track link stresses. ANCF finite elements, on the other hand, while developed for large deformations have proven to be very effective in developing efficient small deformation models as in the case of complex tracked vehicle systems. ANCF finite elements can be used to develop linear constraint chain models, allowing for the elimination of the dependent variables at a preprocessing stage.

Furthermore, with the use of the ANCF Cholesky transformation, one obtains a generalized identity inertia matrix. For this reason, ANCF finite elements will be used in this chapter to develop efficient flexible link tracked vehicle models. The use of this approach is justified for the following reasons: (1) By eliminating most of the vehicle constraint equations at a preprocessing stage and by using an identity mass matrix for the vehicle tracks, the problem dimension is significantly reduced and more efficient solution can be obtained; (2) The results obtained by ANCF finite elements and the FFR formulations in the case of small deformation problems agree well as demonstrated in the literature using several examples; (3) In the ANCF approach, no modal reduction techniques are used and a nodal-based model is developed, and therefore, issues such as the choice of the appropriate modes are not relevant when ANCF finite elements are used.

The absolute nodal coordinate formulation (ANCF), which is based on a global position field description, can be used to describe an arbitrary displacement including large rotation and large deformation. ANCF finite elements define a unique rotation field and can be obtained from the position field using a general continuum mechanics description. These finite elements allow for imposing continuity on higher order derivatives without increasing the order of the interpolation or the number of nodal coordinates. Furthermore, one can develop finite element meshes that have linear connectivity and constant inertia, as previously mentioned (Shabana et al., 2012). Figure 4.4 shows an example of the displacement field of an ANCF finite element which can be written as $\mathbf{r}^j\left(x_1,x_2,x_3,t\right)=\mathbf{S}^j\left(x_1,x_2,x_3\right)\mathbf{e}^j\left(t\right)$, where x_1, x_2, and x_3 are the element spatial coordinates; t is time; $\mathbf{S}^j$ is the element shape function matrix, and $\mathbf{e}^j$ is the vector of element nodal coordinates. Using this displacement field, the equations of a pin joint between elements i and j can be written as $\mathbf{r}^i=\mathbf{r}^j$, $\mathbf{r}^i_\alpha=\mathbf{r}^j_\alpha$, where α is the coordinate line

defining the joint axis; α can be x_1, x_2, or x_3, or any other coordinate line. In this chapter, the three-dimensional Euler-Bernoulli beam element is used in the coupled rigid body/deformation analysis of the flexible link track chain. Note that for simulations involving maneuverability, which can involve acts such as cornering, a fully parametrized element that captures all the deformation modes would be more ideal. For the Euler-Bernoulli beam element, the vector of nodal coordinates for element j can be written as $\mathbf{e}^j = \left[\mathbf{r}^{j^T}\left(x_1 = 0\right) \quad \mathbf{r}_{x_1}^{j^T}\left(x_1 = 0\right) \quad \mathbf{r}^{j^T}\left(x_1 = l^j\right) \quad \mathbf{r}_{x_1}^{j^T}\left(x_1 = l^j\right)\right]^T$, where $\mathbf{r}_{x_1}^j = \partial \mathbf{r}^j / \partial x_1$, and l^j is the length of the finite element. It can be shown that the element shape function matrix can be defined as $\mathbf{S}^j = \left[s_1\mathbf{I} \quad s_2\mathbf{I} \quad s_3\mathbf{I} \quad s_4\mathbf{I}\right]$, where $\mathbf{I}$ is a 3×3 identity matrix (Gerstmayr and Shabana, 2006), and the shape functions s_i, for i = 1, 2, 3, 4, are defined as

$$\left.\begin{aligned} s_1 &= 1 - 3\xi^2 + 2\xi^3, \quad s_2 = l^j\left(\xi - 2\xi^2 + \xi^3\right), \\ s_3 &= \quad 3\xi^2 - 2\xi^3, \quad s_4 = l^j\left(-\xi^2 + \xi^3\right) \end{aligned}\right\} \tag{4.8}$$

where $\xi = x_1 / l^j$. The kinetic energy of an element can then be computed as $T^j = \frac{1}{2}\int_{V^j} \rho^j \dot{\mathbf{r}}^{j^T} \dot{\mathbf{r}}^j dV^j = \frac{1}{2}\dot{\mathbf{e}}^{j^T}\mathbf{M}^j\dot{\mathbf{e}}^j$, in which a dot denotes differentiation with respect to time, ρ^j and V^j are, respectively, the mass density and volume of the element, and the constant generalized mass matrix of the element is defined as $\mathbf{M}^j = \int_{V^j} \rho^j \mathbf{S}^{j^T}\mathbf{S}^j dV^j$. It is important to note that the mass matrix is constant and symmetric in both two-dimensional and three-dimensional cases and leads to zero centrifugal and Coriolis forces when the body experiences an arbitrary large deformation and finite rotation. This mass matrix, as previously mentioned, can be converted to an identity generalized mass matrix associated with the ANCF Cholesky

coordinates. The virtual work of the elastic forces of the Euler-Bernoulli beam element can then be defined as $\delta W_s = -\int_0^{l^j} EA\varepsilon_{11}\delta\varepsilon_{11}dx_1 - \int_0^{l^j} EI\kappa\delta\kappa dx_1$ (Shabana, 2008), where E is the modulus of elasticity, A is the element cross section area, I is the second moment of area, and κ is the curvature. The elastic forces of the Euler-Bernoulli beam element can also be evaluated using the following expression for the strain energy $U = \int_0^{l^j} EA(\varepsilon_{11})^2 dx_1 + \int_0^{l^j} EI(\kappa)^2 dx_1$ as $\mathbf{Q}_s = -(\partial U / \partial \mathbf{e})^T$. The axial strain at an arbitrary point on the Euler-Bernoulli beam element can then be defined using the gradient vector evaluated using the element assumed displacement filed as $\varepsilon_{11} = (\mathbf{r}_{x_1}^T \mathbf{r}_{x_1} - 1)/2$. The evaluation of this axial strain using ANCF finite elements in a coupled rigid body/deformation analysis is straight forward and does not require the complexity required by the less accurate post-processing stress analysis that ignores the effect of the elastic deformations on the rigid body motion.

4.5 NUMERICAL RESULTS

In this section, the tracked vehicle model described in the preceding chapter is used to evaluate the accuracy of the stresses calculated using the post-processing approach that neglects the effect of the elastic deformation on the rigid body motion. The accuracy of this approach is measured against the results obtained using a fully coupled ANCF stress analysis.

4.5.1 Initial Configuration and Driving Constraints

This subsection discusses two different tracked vehicle models: one referred to as the “rigid model” which involves rigid track links to later be used in post processing with the simplified

FFR equations and the other referred to as the “ANCF model” which involves flexible ANCF finite element track links. For both models, a relative angular velocity constraint on the sprocket rotation about the lateral axis with respect to the chassis is used to drive the vehicle. The angular velocity profile, which is shown in Figs. 4.3a and 4.3b, starts with the sprocket remaining still for the first second, then increasing for the next seven seconds until it reaches its maximum angular velocity which is then maintained for the final two seconds of the simulation. There are two maximum angular velocities used in this section which represent two different simulation scenarios, one set to 30 rad/sec and the other to 80 rad/sec which, according to Figs. 4.4a, 4.4b, 4.5a, and 4.5b, correspond to maximum forward velocities of 7.27 m/sec (16.26 miles/hour) and 19.62 m/sec (43.90 miles/hour), respectively, for both models.

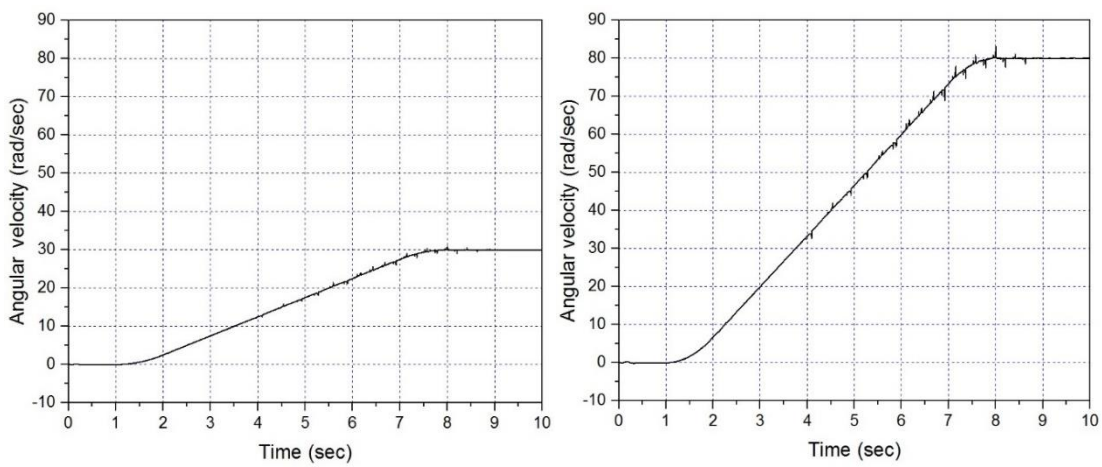

(a) Lower angular velocity (b) Higher angular velocity

Figure 4.3: Sprocket angular velocity profile

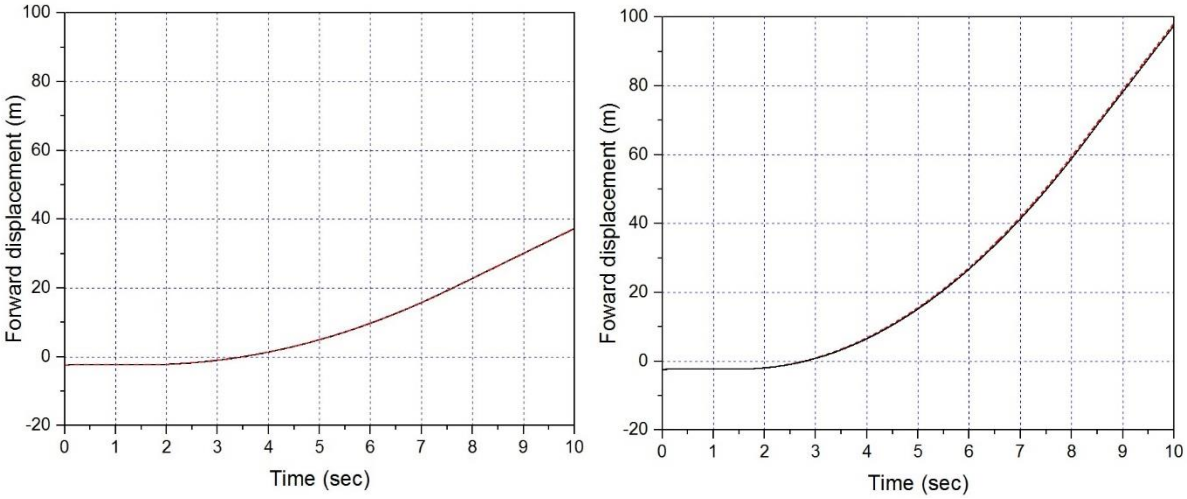

(a) Lower angular velocity (b) Higher angular velocity

Figure 4.4: Chassis forward position

(---- Rigid model, — ANCF model)

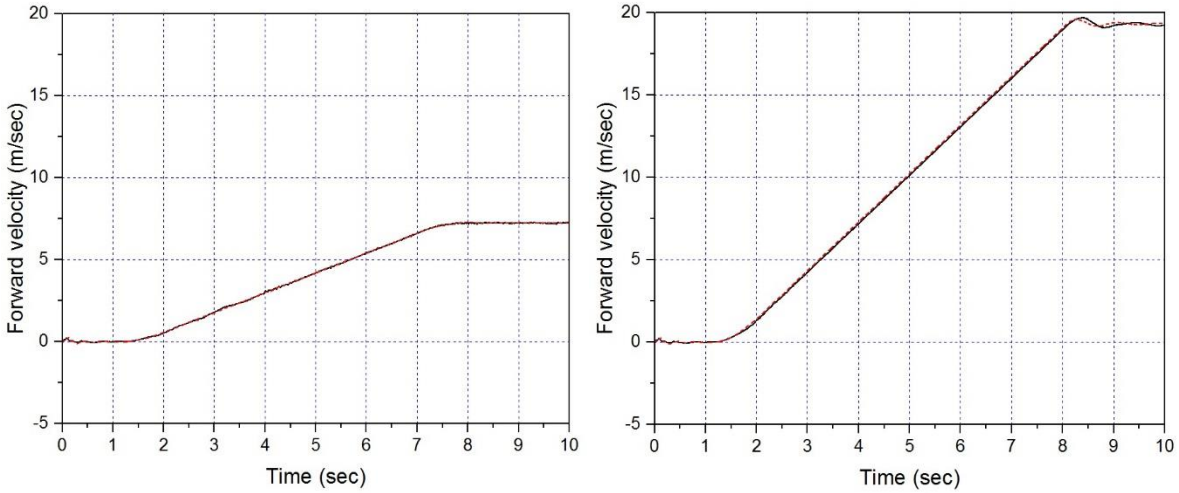

(a) Lower angular velocity (b) Higher angular velocity

Figure 4.5: Chassis forward velocity

(---- Rigid model, — ANCF model)

4.5.2 Axial Stress/Strain Results

This subsection presents specific strain results obtained using the ANCF finite elements and the post processing procedure that employs the simplified FFR equations. Figure 4.6 shows the unfiltered axial strain comparison for a specific track link. The results are obtained using rigid analysis with the post-processing procedure and the fully coupled ANCF analysis in the case of the lower angular velocity profile shown in Fig. 4.3a. It can be seen from Fig. 4.7 that the unfiltered axial strain results have high frequencies due to the high frequencies found in the joint constraint forces. The lower overall magnitude in the ANCF model results can be attributed to the flexibility of the ANCF finite elements that include more modes of deformation. The noise of the unfiltered results makes it impossible to compare anything besides average magnitude of the strain values. Instead, the higher frequencies can be filtered out by using a Fast Fourier Transform (FFT) to compare the results using only the lower frequencies. Figure 4.8 shows the axial strain comparison for the lower velocity simulation using an FFT with a low-pass cut off frequency of 15 Hz. This figure shows a clearer depiction of the axial strain in the track link with each model showing similar results, specifically in trend. The ANCF model in this figure displays a larger range of axial strain values, while the results from post-processing with the rigid model creates a more defined path with lower spikes in frequency. The ANCF model in this case shows a more conservative prediction of the axial strains which can be important when making a general approximation for what strain values could lead to failure in the track chain. Figures 4.9 and 4.10 show, respectively, the unfiltered and filtered axial strain values for the flexible and rigid tracked vehicle models for the higher angular velocity profile shown in Fig. 4.3b. This simulation was performed to examine the effect of larger centrifugal and Coriolis forces due to greater angular velocities on the specific track link. As would be assumed, Figs. 4.9 and 4.10

show larger overall values while Fig. 4.10 still shows a good comparison between models with the vector of centrifugal and Coriolis forces not leading to a significant difference. A closer look at the results of Figs. 4.8 and 4.10 show comparable trend for the two models, while after 8 seconds the results seem to deviate. In Fig. 4.8 at around 9.5 seconds, the post-processing analysis shows an axial strain of about 1.5×10^{-5} while the axial strain of the ANCF model is approximately 0.5×10^{-5}. When each value is multiplied by a Young's Modulus of 200 GPA, it leads to a stress difference of 3 MPA to 1 MPA between the post-processing and the ANCF models. In Fig. 4.10, just before the 10 second mark, a difference of 4.0×10^{-5} to 2.0×10^{-5} can be seen between the rigid and flexible models, respectively. To further investigate these differences, a simulation for the lower angular velocity profile was continued at the same maximum angular velocity. This can be understood as a continuation of Fig. 4.8 for another 10 seconds. Figure 4.11 shows this as a more definitive difference with the ANCF model having a larger average axial strain value. Figure 4.12 shows the stresses calculated from the axial strain values in Fig. 4.11 which can have differences of over 2 MPa.

Simulation times varied between the two models. The rigid-linked model took approximately a third of the time as the flexible-linked model for its initial simulation. When the second step of the stress analysis is added on, the overall post processing CPU time becomes double that of the one-step ANCF model. Each step utilizes the same step size of 10^{-3}.

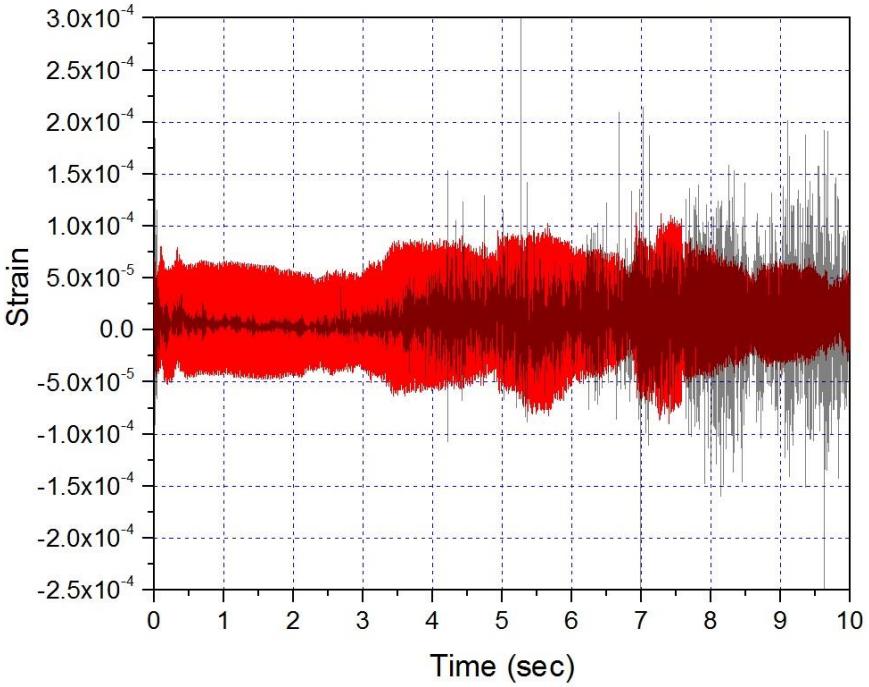

Figure 4.6: Unfiltered axial strain (Lower angular velocity)

(— FFR post processing, — ANCF)

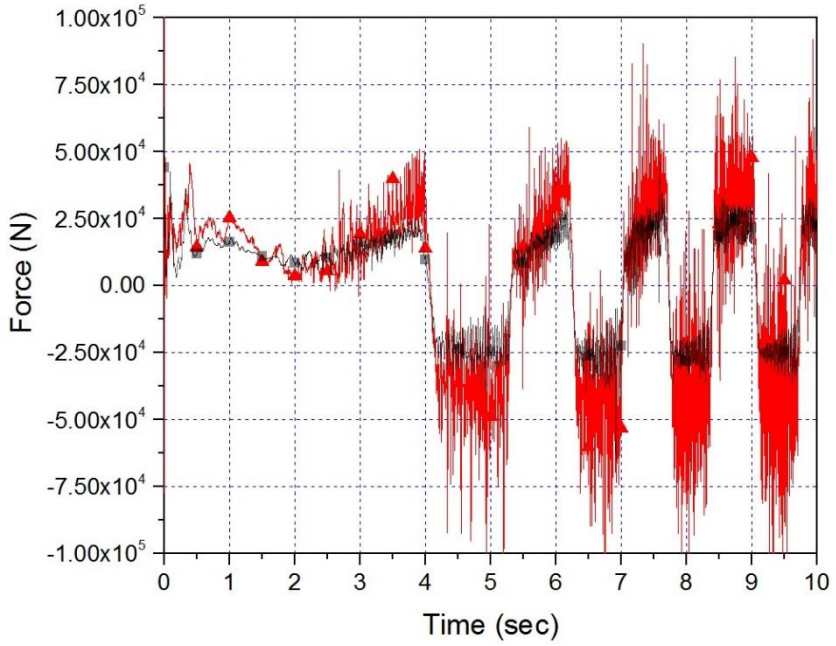

Figure 4.7: Joint longitudinal forces (Lower angular velocity)

(—▲— Rigid model, —■— ANCF model)

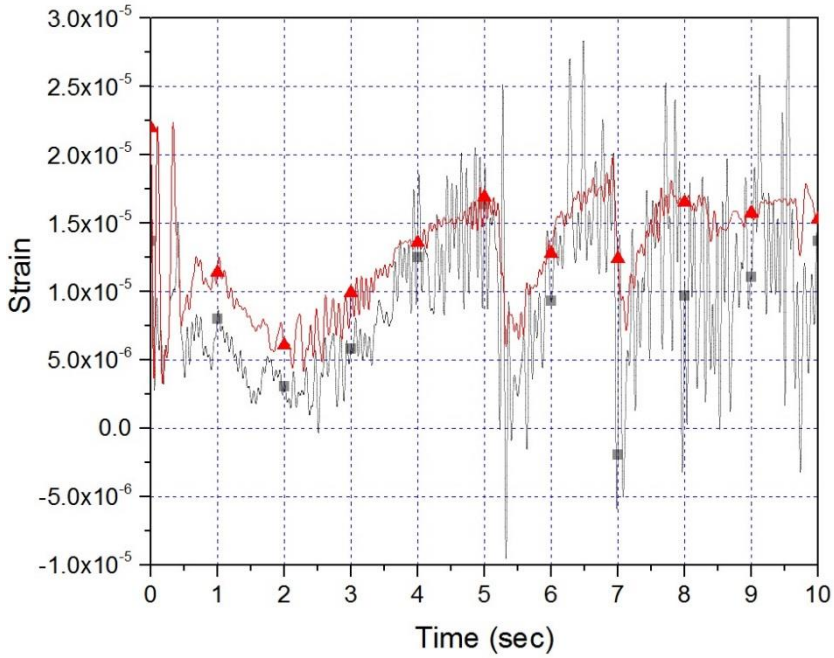

Figure 4.8: Filtered axial strain (Lower angular velocity)

(–▲– FFR post processing, –■– ANCF)

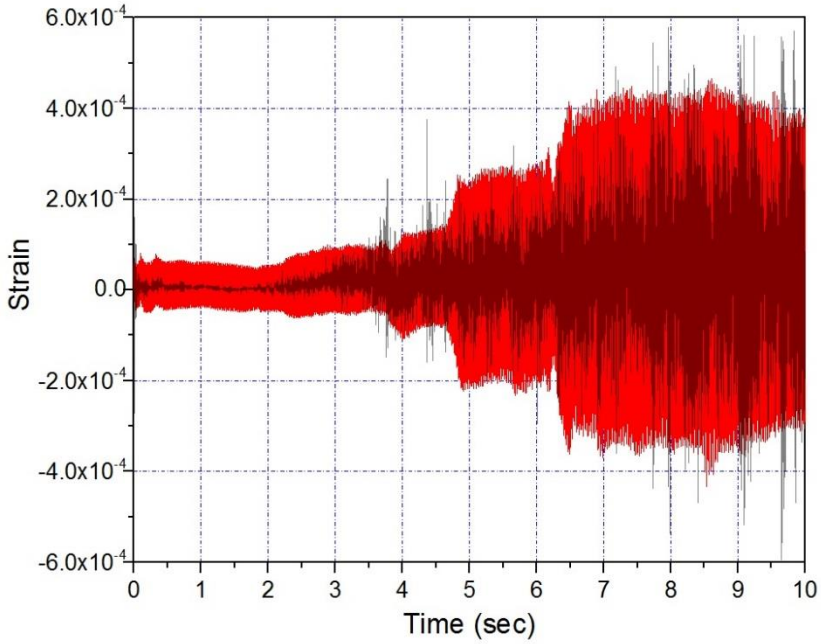

Figure 4.9: Unfiltered axial strain (Higher angular velocity)

(— FFR post processing, — ANCF)

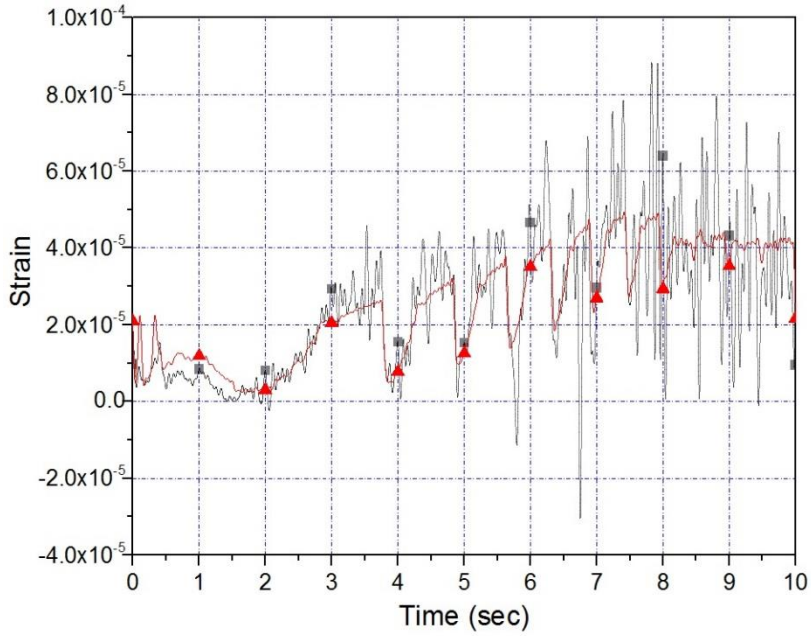

Figure 4.10: Filtered axial strain (Higher angular velocity)

(–▲– FFR post processing, –■– ANCF)

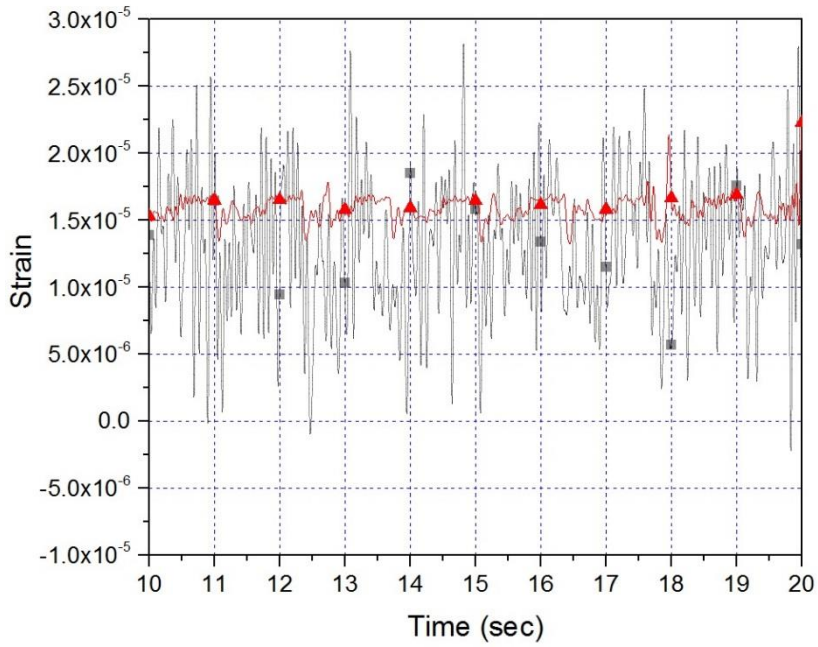

Figure 4.11: Filtered axial strain (Lower angular velocity)

(–▲– FFR post processing, –■– ANCF)

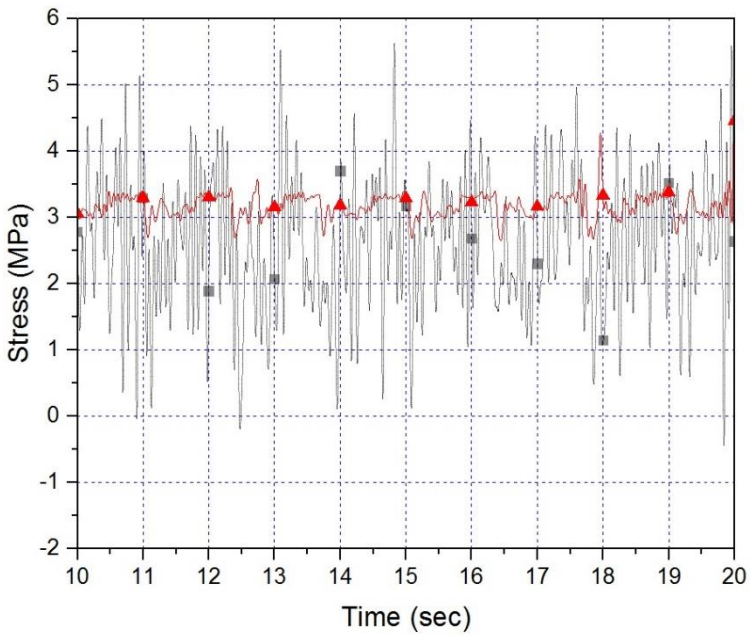

Figure 4.12: Filtered axial stress (Lower angular velocity)

(–▲– FFR post processing, –■– ANCF)

4.6 CONCLUDING REMARKS

In this chapter, two different formulations are described and used to examine the accuracy of the stress prediction when neglecting the effect of the elastic deformation on the rigid body motion in the case of complex tracked vehicle systems. The FFR formulation, which uses a mixed set of absolute reference and local deformation coordinates, was used to obtain simplified equations that are used to perform the rigid body analysis to determine the inertia and joint forces which are entered to a linear structural analysis problem to determine the strain and stresses. The results of this decoupled procedure are compared with the results obtained using a fully coupled analysis using ANCF finite elements. In the ANCF approach, no infinitesimal or finite rotations are used as nodal coordinates, meaning there are no restrictions on the amount of rotation or deformation

within an element. Instead, element nodal coordinates are defined in the inertial frame and used with a global shape function covering a complete set of rigid body modes.

The results presented in the preceding section show that both the simplified FFR formulation and ANCF can be used to predict the stresses of complex tracked vehicle models. Rigid and flexible simulations showed almost exact values in terms of tracked vehicle positions and velocities while axial strain results found using each formulation showed comparable trends, but different strain values. Differences in magnitude become more apparent as the simulation continues. This can be attributed to differences between the formulations such as the online computations used in the ANCF versus a two-step process using the post-processing analysis. The two-step process includes the inherent error of decoupling the equations and using an integrator for each step when determining the deformation coordinates. The post-processing analysis assumptions were clearly stated in Section 4.3.

In this chapter, the ANCF and post-processing procedures were each shown to carry their own benefits. The ANCF showed a more conservative approximation of the axial strain values calculated with less efforts, while the post-processing procedure showed a more defined result pattern with lower overall frequencies and simpler rigid body simulation. In terms of failure and fatigue analysis, safety precautions dictate using the highest and lowest calculated stress values, which were found using the ANCF analysis. Additionally, using a one-step, online process can eliminate further error accumulation and lead to a more efficient evaluation process.

It is important to note that while validation hasn't been accomplished, the results obtained from the flexible-linked chain have been verified by comparing results obtained using fully parameterized ANCF beam elements with the elastic forces formulated using a general continuum mechanics approach and the elastic line approach (Hamed, 2015).

CHAPTER 5

SUMMARY AND CONCLUSIONS

The second chapter of this thesis highlights some issues on the interpolation of rotations in the analysis of large deformation of bodies in flexible multibody system dynamics and presents results of the large rotation vector formulation. The focus of this chapter was on the geometry issues arising from the use of two interpolation meshes: the position mesh and the rotation mesh. These two meshes lead to different space curves that can differ by an arbitrary rigid body displacement and have different geometric properties. The examples demonstrate the known fact that the rotation mesh of the LRVF is inextensible and that the material points of a rotation-based position mesh occupy different positions from the material points of the position mesh. The consequences of the redundancy in the geometry definition can negatively affect the accuracy of the strain energy and the inertia of the bodies. These inconsistencies become more apparent in the case of larger deformations and are not circumvented by the inclusion of elastic forces or imposing kinematic constraints. This is mainly due to the fact that two different assumed displacement fields cannot, in general, be brought to the same configuration as previously illustrated. This chapter was concentrated on a fundamental issue related to the use of the large rotation vector formulation. It was not intended to provide a comparison of the LRVF with other formulations. Nonetheless, it is worth mentioning that several other approaches have been used in the large displacement analysis of structural systems. These formulations include the ANCF and methods based on B-spline representation.

In the third chapter of this thesis, different MBS joint formulations are presented and compared using detailed tracked vehicle models. Four main joint formulations were discussed: the ideal joint formulation, the penalty method, the compliant discrete element joint formulation, and the compliant continuum-based joint formulation. The ideal joint formulation is developed to eliminate the relative displacement between the two bodies connected by the joint. This can be achieved by enforcing a set of joint algebraic equations using a constrained dynamics approach or by using the penalty method. The constrained dynamics approach eliminates degrees of freedom and ensures that the constraint equations are satisfied at the position, velocity, and acceleration levels. The penalty method, on the other hand, does not reduce the number of degrees of freedom and ensures that the constraint equations are satisfied at the position level only provided that a high stiffness coefficient is used. The compliant discrete element formulation, which allows for joint deformations, can be systematically applied using a standard MBS bushing element that allows for six degrees of freedom of relative motion. The compliant continuum-based approach can be used to develop new joints that capture deformation modes that are not captured by the compliant discrete element joint formulation. ANCF finite elements can be used to systematically develop new joints with distributed elasticity and linear connectivity conditions.

As discussed in the third chapter, it is important to choose the proper stiffness and damping coefficients when the penalty method and the bushing elements are used. Numerical results were presented in order to compare between different methods. The ideal joint formulation produces the desired joint kinematics and accurate joint forces. The same is true with the penalty force based joint when large penalty stiffness coefficients are used. Penalty force based joint construction has been shown to be sensitive to the selection of penalty

stiffness with the higher stiffness coefficients leading to better overall results. However, higher penalty stiffness increases CPU time significantly due to higher frequencies. The penalty method and bushing element models each have much larger CPU times than the ideal constrained model due to these high stiffness coefficients. The results presented showed that the ANCF joint model leads to lower force predictions which can be attributed to the track link flexibility.

In the fourth chapter, two different formulations are described and used to examine the accuracy of the stress prediction when neglecting the effect of the elastic deformation on the rigid body motion in the case of complex tracked vehicle systems. The FFR formulation, which uses a mixed set of absolute reference and local deformation coordinates, was used to obtain simplified equations that are used to perform the rigid body analysis to determine the inertia and joint forces which are entered into a linear structural analysis problem to determine the strain and stresses. The results of this decoupled procedure were compared with the results obtained using a fully coupled analysis using ANCF finite elements. In the ANCF approach, no infinitesimal or finite rotations are used as nodal coordinates, meaning there are no restrictions on the amount of rotation or deformation within an element. Instead, element nodal coordinates are defined in the inertial frame and used with a global shape function covering a complete set of rigid body modes.

The results presented showed that both the simplified FFR formulation and ANCF can be used to predict the stresses of complex tracked vehicle models. Rigid and flexible simulations showed almost exact values in terms of tracked vehicle positions and velocities while axial strain results found using each formulation showed comparable trends, but different strain values. Differences in magnitude become more apparent as the simulation continues. This can be

attributed to differences between the formulations such as the online computations used in the ANCF versus a two-step process using the post-processing analysis. The two-step process includes the inherent error of decoupling the equations and using an integrator for each step when determining the deformation coordinates.

The ANCF and post-processing procedures were each shown to carry their own benefits. The ANCF showed a more conservative approximation of the axial strain values calculated with less efforts, while the post-processing procedure showed a more defined result pattern with lower overall frequencies and simpler rigid body simulation. In terms of failure and fatigue analysis, safety precautions dictate using the highest and lowest calculated stress values, which were found using the ANCF analysis. Additionally, using a one-step, online process can eliminate further error accumulation and lead to a more efficient evaluation process.

It is important to note that while validation hasn't been accomplished on the tracked vehicle model, the results obtained from the flexible-linked chain have been verified by comparing results obtained using fully parameterized ANCF beam elements with the elastic forces formulated using a general continuum mechanics approach and the elastic line approach (Hamed, 2015).

APPENDIX

For the three-dimensional beam element used in the post-processing procedure, the shape function matrix is defined as (Przemieniecki, 1968; Shabana, 2014)

$$\mathbf{S}^{ij^T} = \begin{bmatrix} 1-\xi & 0 & 0 \\ 6\left(\xi-\xi^2\right)\eta & 1-3\xi^2+2\xi^3 & 0 \\ 6\left(\xi-\xi^2\right)\zeta & 0 & 1-3\xi^2+2\xi^3 \\ 0 & -\left(1-\xi\right)l\zeta & \left(1-\xi\right)l\eta \\ \left(1-4\xi+3\xi^2\right)l\zeta & 0 & \left(-\xi+2\xi^2-\xi^3\right)l \\ \left(-1+4\xi-3\xi^2\right)l\eta & \left(\xi-2\xi^2+\xi^3\right)l & 0 \\ \xi & 0 & 0 \\ 6\left(-\xi+\xi^2\right)\eta & 3\xi^2-2\xi^3 & 0 \\ 6\left(-\xi+\xi^2\right)\zeta & 0 & 3\xi^2-2\xi^3 \\ 0 & -l\xi\zeta & l\xi\eta \\ \left(-2\xi+3\xi^3\right)l\zeta & 0 & \left(\xi^2-\xi^3\right)l \\ \left(2\xi-3\xi^3\right)l\eta & \left(-\xi^2+\xi^3\right)l & 0 \end{bmatrix}^{ij} \tag{A.1}$$

in which $\xi^{ij} = x_1^{ij} / l^{ij}$, $\eta^{ij} = x_2^{ij} / l^{ij}$, $\zeta^{ij} = x_3^{ij} / l^{ij}$ and l^{ij} is the length of element ij, and x_1^{ij}, x_2^{ij}, and x_3^{ij} are the spatial coordinates along the element axes. This matrix is essential in defining the mass matrix, as well as the element transformation matrices $\mathbf{C}^{ij}$ and $\overline{\mathbf{C}}^{ij}$ which are defined as

$$\mathbf{C}^{ij} = \begin{bmatrix} c_1 & \dfrac{-c_1c_2}{\sqrt{\left(c_1\right)^2+\left(c_3\right)^2}} & \dfrac{-c_3}{\sqrt{\left(c_1\right)^2+\left(c_3\right)^2}} \\ c_2 & \sqrt{\left(c_1\right)^2+\left(c_3\right)^2} & 0 \\ c_3 & \dfrac{-c_2c_3}{\sqrt{\left(c_1\right)^2+\left(c_3\right)^2}} & \dfrac{c_1}{\sqrt{\left(c_1\right)^2+\left(c_3\right)^2}} \end{bmatrix}^{ij}, \overline{\mathbf{C}}^{ij} = \begin{bmatrix} \mathbf{C}^{ij} & \mathbf{0} & \mathbf{0} & \mathbf{0} \\ \mathbf{0} & \mathbf{C}^{ij} & \mathbf{0} & \mathbf{0} \\ \mathbf{0} & \mathbf{0} & \mathbf{C}^{ij} & \mathbf{0} \\ \mathbf{0} & \mathbf{0} & \mathbf{0} & \mathbf{C}^{ij} \end{bmatrix}^T \tag{A.2}$$

where $c_1^{ij} = (b_1 - a_1)/l^{ij}$, $c_2^{ij} = (b_2 - a_2)/l^{ij}$, and $c_3^{ij} = (b_3 - a_3)/l^{ij}$; the length of element ij can be defined as $l^{ij} = \sqrt{(b_1 - a_1)^2 + (b_2 - a_2)^2 + (b_3 - a_3)^2}$; (a_1, a_2, a_3) and (b_1, b_2, b_3) are the locations of each node on element ij. Equation A.2 is valid for all cases except when c_1 and c_3 are equal to zero, a case which occurs when the element $\mathbf{X}_1^{ij}$ axis coincides with the body $\mathbf{X}_2^{i}$ axis, in which case $\mathbf{C}^{ij}$ is given as

$$\mathbf{C}^{ij} = \begin{bmatrix} 0 & -c_2 & 0 \\ c_2 & 0 & 0 \\ 0 & 0 & 1 \end{bmatrix}^{ij} \tag{A.3}$$

The matrices used in defining the vector of centrifugal and Coriolis forces can be defined as

$$\tilde{\mathbf{S}}_1^i = \mathbf{B}_2^{i\,T} \left\{ \sum_{j=1}^{n} \mathbf{B}_1^{ij\,T} \overline{\mathbf{C}}^{ij\,T} \left[\int_{V^{ij}} \rho^{ij} \mathbf{N}^{ij\,T} \mathbf{C}^{ij\,T} \tilde{\overline{\boldsymbol{\omega}}}^i \mathbf{C}^{ij} \mathbf{N}^{ij} \overline{\mathbf{C}}^{ij\,T} dV^{ij} \right] \overline{\mathbf{C}}^{ij} \mathbf{B}_1^{ij} \right\} \mathbf{B}_2^i \tag{A.4a}$$

$$\tilde{\mathbf{S}}_2^i = \mathbf{B}_2^{i\,T} \left\{ \sum_{j=1}^{n} \mathbf{B}_1^{ij\,T} \overline{\mathbf{C}}^{ij\,T} \left[\int_{V^{ij}} \rho^{ij} \mathbf{N}^{ij\,T} \mathbf{C}^{ij\,T} \left(\tilde{\overline{\boldsymbol{\omega}}}^i \right)^2 \mathbf{C}^{ij} \mathbf{N}^{ij} \overline{\mathbf{C}}^{ij\,T} dV^{ij} \right] \overline{\mathbf{C}}^{ij} \mathbf{B}_1^{ij} \right\} \mathbf{B}_2^i \tag{A.4b}$$

$$\tilde{\overline{\mathbf{I}}}_0^i = \mathbf{B}_2^{i\,T} \left\{ \sum_{j=1}^{n} \mathbf{B}_1^{ij\,T} \overline{\mathbf{C}}^{ij\,T} \left[\int_{V^{ij}} \rho^{ij} \mathbf{N}^{ij\,T} \mathbf{C}^{ij\,T} \tilde{\overline{\boldsymbol{\omega}}}^i \tilde{\overline{\mathbf{u}}}_0^{ij} dV^{ij} \right] \right\} \tag{A.4c}$$

where n is the total number of elements in body i. It is important to note that matrices $\tilde{\mathbf{S}}_1^i$ and $\tilde{\mathbf{S}}_2^i$ are much smaller than $\tilde{\overline{\mathbf{I}}}_0^i$ and therefore are neglected in the calculation of quadratic velocity vector shown in Chapter 3. The stiffness matrix $\mathbf{K}_{ff}^{ij}$ of the element of uniform cross-sectional area is defined as (Przemieniecki, 1968)

$$
\overline{\mathbf{K}}_{ff}^{ij} = \begin{bmatrix}
\frac{Ea}{l} & & & & & & & & & & & \\
0 & \frac{12EI_3}{l^3} & & & & & & & & & & \\
0 & 0 & \frac{12EI_2}{l^3} & & & & & & symmetric & & & \\
0 & 0 & 0 & \frac{GI_1}{l} & & & & & & & & \\
0 & 0 & -\frac{6EI_2}{l^2} & 0 & \frac{4EI_2}{l} & & & & & & & \\
0 & -\frac{6EI_2}{l^2} & 0 & 0 & 0 & \frac{4EI_3}{l} & & & & & & \\
-\frac{Ea}{l} & 0 & 0 & 0 & 0 & 0 & \frac{aE}{l} & & & & & \\
0 & -\frac{12EI_3}{l^3} & 0 & 0 & 0 & -\frac{6EI_3}{l^2} & 0 & \frac{12EI_3}{l^3} & & & & \\
0 & 0 & -\frac{12EI_2}{l^3} & 0 & \frac{6EI_2}{l^2} & 0 & 0 & 0 & \frac{12EI_2}{l^3} & & & \\
0 & 0 & 0 & -\frac{GI_1}{l} & 0 & 0 & 0 & 0 & 0 & \frac{GI_1}{l} & & \\
0 & 0 & -\frac{6EI_2}{l^2} & 0 & \frac{2EI_2}{l} & 0 & 0 & 0 & \frac{6EI_2}{l^2} & 0 & \frac{4EI_2}{l} & \\
0 & \frac{6EI_3}{l^2} & 0 & 0 & 0 & \frac{2EI_3}{l} & 0 & -\frac{6EI_3}{l^2} & 0 & 0 & 0 & \frac{4EI_3}{l}
\end{bmatrix}^{ij} \quad \text{(A.5)}
$$

where ρ^{ij}, l^{ij}, and a^{ij} are the mass density, length, and cross-sectional area of element ij, E^{ij} and G^{ij} are, respectively, the elasticity and rigidity moduli, and I_1^{ij}, I_2^{ij}, and I_3^{ij} are the second moments of areas about the $\mathbf{X}_1^{ij}$, $\mathbf{X}_2^{ij}$, and $\mathbf{X}_3^{ij}$ element axes, respectively. This matrix can be defined in the body coordinate system using the transformation $\mathbf{K}_{ff}^{ij} = \overline{\mathbf{C}}^{ij\,T} \overline{\mathbf{K}}_{ff}^{ij} \overline{\mathbf{C}}^{ij}$.

COPYRIGHT PERMISSION

Springer License for the manuscript "A Comparative Study of Joint Formulations: Application to Multibody System Tracked Vehicles":

SPRINGER LICENSE
TERMS AND CONDITIONS

Jul 07, 2016

This Agreement between Michael Wallin ("You") and Springer ("Springer") consists of your license details and the terms and conditions provided by Springer and Copyright Clearance Center.

License Number	3903831187821
License date	Jul 07, 2016
Licensed Content Publisher	Springer
Licensed Content Publication	Nonlinear Dynamics
Licensed Content Title	A comparative study of joint formulations: application to multibody system tracked vehicles
Licensed Content Author	Michael Wallin
Licensed Content Date	Jan 1, 2013
Licensed Content Volume Number	74
Licensed Content Issue Number	3
Type of Use	Thesis/Dissertation
Portion	Full text
Number of copies	1
Author of this Springer article	Yes and you are the sole author of the new work
Order reference number	
Title of your thesis / dissertation	FULLY COUPLED ANALYSIS OF LARGE SCALE TRACKED VEHICLE SYSTEMS WITH FLEXIBLE LINK CHAINS
Expected completion date	Jul 2016
Estimated size(pages)	120
Requestor Location	Michael Wallin 1754 E Lincoln Ave. DES PLAINES, IL 60018 United States Attn: Michael Wallin
Billing Type	Invoice
Billing Address	Michael Wallin 1754 E Lincoln Ave. DES PLAINES, IL 60018 United States Attn: Michael Wallin
Total	0.00 USD
Terms and Conditions	

Introduction

The publisher for this copyrighted material is Springer. By clicking "accept" in connection with completing this licensing transaction, you agree that the following terms and conditions apply to this transaction (along with the Billing and Payment terms and conditions established by Copyright Clearance Center, Inc. ("CCC"), at the time that you opened your Rightslink account and that are available at any time at http://myaccount.copyright.com).

Limited License

With reference to your request to reuse material on which Springer controls the copyright, permission is granted for the use indicated in your enquiry under the following conditions:

- Licenses are for one-time use only with a maximum distribution equal to the number stated in your request.
- Springer material represents original material which does not carry references to other sources. If the material in question appears with a credit to another source, this permission is not valid and authorization has to be obtained from the original copyright holder.
- This permission
• is non-exclusive
• is only valid if no personal rights, trademarks, or competitive products are infringed.
• explicitly excludes the right for derivatives.
- Springer does not supply original artwork or content.
- According to the format which you have selected, the following conditions apply accordingly:
• **Print and Electronic:** This License include use in electronic form provided it is password protected, on intranet, or CD-Rom/DVD or E-book/E-journal. It may not be republished in electronic open access.
• **Print:** This License excludes use in electronic form.
• **Electronic:** This License only pertains to use in electronic form provided it is password protected, on intranet, or CD-Rom/DVD or E-book/E-journal. It may not be republished in electronic open access.

For any electronic use not mentioned, please contact Springer at permissions.springer@spi-global.com.

- Although Springer controls the copyright to the material and is entitled to negotiate on rights, this license is only valid subject to courtesy information to the author (address is given in the article/chapter).
- If you are an STM Signatory or your work will be published by an STM Signatory and you are requesting to reuse figures/tables/illustrations or single text extracts, permission is granted according to STM Permissions Guidelines: http://www.stm-assoc.org/permissions-guidelines/

For any electronic use not mentioned in the Guidelines, please contact Springer at permissions.springer@spi-global.com. If you request to reuse more content than stipulated in the STM Permissions Guidelines, you will be charged a permission fee for the excess content.

Permission is valid upon payment of the fee as indicated in the licensing process. If permission is granted free of charge on this occasion, that does not prejudice any rights we might have to charge for reproduction of our copyrighted material in the future.

-If your request is for reuse in a Thesis, permission is granted free of charge under the following conditions:

This license is valid for one-time use only for the purpose of defending your thesis and with a maximum of 100 extra copies in paper. If the thesis is going to be published, permission needs to be reobtained.

- includes use in an electronic form, provided it is an author-created version of the thesis on his/her own website and his/her university's repository, including UMI (according to the definition on the Sherpa website: http://www.sherpa.ac.uk/romeo/);
- is subject to courtesy information to the co-author or corresponding author.

Geographic Rights: Scope
Licenses may be exercised anywhere in the world.
Altering/Modifying Material: Not Permitted
Figures, tables, and illustrations may be altered minimally to serve your work. You may not alter or modify text in any manner. Abbreviations, additions, deletions and/or any other alterations shall be made only with prior written authorization of the author(s).
Reservation of Rights
Springer reserves all rights not specifically granted in the combination of (i) the license details provided by you and accepted in the course of this licensing transaction and (ii) these terms and conditions and (iii) CCC's Billing and Payment terms and conditions.
License Contingent on Payment
While you may exercise the rights licensed immediately upon issuance of the license at the end of the licensing process for the transaction, provided that you have disclosed complete and accurate details of your proposed use, no license is finally effective unless and until full payment is received from you (either by Springer or by CCC) as provided in CCC's Billing and Payment terms and conditions. If full payment is not received by the date due, then any license preliminarily granted shall be deemed automatically revoked and shall be void as if never granted. Further, in the event that you breach any of these terms and conditions or any of CCC's Billing and Payment terms and conditions, the license is automatically revoked and shall be void as if never granted. Use of materials as described in a revoked license, as well as any use of the materials beyond the scope of an unrevoked license, may constitute copyright infringement and Springer reserves the right to take any and all action to protect its copyright in the materials.
Copyright Notice: Disclaimer
You must include the following copyright and permission notice in connection with any reproduction of the licensed material:
"Springer book/journal title, chapter/article title, volume, year of publication, page, name(s) of author(s), (original copyright notice as given in the publication in which the material was originally published) "With permission of Springer"
In case of use of a graph or illustration, the caption of the graph or illustration must be included, as it is indicated in the original publication.
Warranties: None
Springer makes no representations or warranties with respect to the licensed material and adopts on its own behalf the limitations and disclaimers established by CCC on its behalf in its Billing and Payment terms and conditions for this licensing transaction.
Indemnity
You hereby indemnify and agree to hold harmless Springer and CCC, and their respective officers, directors, employees and agents, from and against any and all claims arising out of your use of the licensed material other than as specifically authorized pursuant to this license.
No Transfer of License
This license is personal to you and may not be sublicensed, assigned, or transferred by you without Springer's written permission.
No Amendment Except in Writing
This license may not be amended except in a writing signed by both parties (or, in the case of Springer, by CCC on Springer's behalf).
Objection to Contrary Terms
Springer hereby objects to any terms contained in any purchase order, acknowledgment, check endorsement or other writing prepared by you, which terms are inconsistent with these terms and conditions or CCC's Billing and Payment terms and conditions. These terms and conditions, together with CCC's Billing and Payment terms and conditions (which are incorporated herein), comprise the entire agreement between you and Springer (and CCC) concerning this licensing transaction. In the event of any conflict between your obligations

established by these terms and conditions and those established by CCC's Billing and Payment terms and conditions, these terms and conditions shall control.

Jurisdiction

All disputes that may arise in connection with this present License, or the breach thereof, shall be settled exclusively by arbitration, to be held in the Federal Republic of Germany, in accordance with German law.

Other conditions:

V 12AUG2015

Questions? customercare@copyright.com or +1-855-239-3415 (toll free in the US) or +1-978-646-2777.

According to the Inderscience Copyright and Author Rights and Responsibilities, the author has the right to incorporate the content of the Article in other works of which you are the Author while Inderscience retains the copyright of the Article ("Evaluation of the Accuracy of the Rigid Body Approach in the Prediction of the Dynamic Stresses of Complex Multibody Systems"):

Inderscience: Copyright and Author Rights and Responsibilities

Inderscience is wholly committed to the highest standards of publishing, founded on rigorous double-blind peer review. In all that we do, we work to ensure the widest possible access to the Articles that we publish, to enhance the reputation of the Author, the Journal, its Editor and Editorial Board, and the value that we add as Publisher in both printed and online form.

In order that we can do this properly and professionally, we ask Authors of Articles accepted for publication to sign our Author Copyright Agreement assigning (or transferring) copyright to Inderscience.

The transfer of copyright is standard practice in journal publishing. This enables us, as the Publisher, to negotiate subsidiary licences to database aggregators and document supply companies, and allows permissions to reproduce Articles in books, course packs, electronic reserve or for library loan to be handled efficiently and with sensitivity to changing library and reader needs.

This relieves Authors of a time-consuming and costly administrative burden. It also enable us to defend and enforce Authors' rights against plagiarism, copyright infringement, unauthorised use and, most important for Authors' professional reputation, breach of Authors' moral rights.

What rights do Authors retain?

There is often confusion about what rights Authors retain after assigning copyright to us. When copyright is assigned to Inderscience, you can continue to enjoy the following rights:

1. Patent and trademark rights.
2. The right to be identified as the Author (i.e. you assert your moral rights under copyright law).

   After publication, you have the right to:

3. The right to share with colleagues the Authors Original*.
4. The right to post the Author's Original* or Accepted Manuscript* on the Author's personal web pages and/or institutional repositories and/or subject repositories without embargo, or the Proof* upon condition that it shall not be accessible until after six months from Inderscience's publication date. For open [freely available] repositories, if the manuscript was funded by either RCUK or the Wellcome Trust, use the CC-BY-NC: Creative Commons Attribution-NoDerivs 4.0 licence. Otherwise, follow the licensing restrictions applied to all material copyrighted by Inderscience;
5. The right to post the Version of Record* to a subject-based repository such as PubMed Central only in cases where a funding agency providing the grant for the research on which the Article is based requires this of the Author, upon condition that it shall not be accessible until after six months from Inderscience's publication date;
6. The right to use the Article in your research, and in courses that you are teaching.
7. The right to incorporate the content of the Article in other works of which you are the Author.

* Versions of a paper defined as

- **Author's Original** = Author's manuscript prior to peer review
- **Accepted Manuscript** = Accepted version of Author's manuscript
- **Proof** = Author's version of corrected accepted version
- **Version of Record** = Publisher's version of finished Article

In the case of 3 to 7 above, these rights are intended to help you in your academic and professional work, and are subject to two conditions:

a. These rights may not be used for commercial purposes; and
b. Acknowledgement in the form of a full citation must be given to the Journal as the original source of publication, together with a link to the Journal web page and/or DOI as soon as they are available.

You must obtain written permission beforehand from Inderscience for the following:

1. Copies of your Article in a course pack for onward commercial sale by a third party.
2. Except as specifically provided above, distribution in print or electronic form by any third party such as the convenor of a conference, database aggregator, website, blog or listserv;
3. Any other commercial use.

What happens when the Author does not own copyright in the Article?

If you have written the Article in the course of your employment, your employer may consider that it owns the copyright and is considered the legal Author. This is often referred to as 'Work for Hire'. In such cases, your employer should sign the Author Copyright Agreement. This does NOT apply to faculty and researchers working in a university and submitting the Article as a normal part of research activity.

If you are a government employee, the following applies:

1. *If you are a UK, Canadian or Australian Government employee*

   Crown Copyright applies to your Article, and it should be cleared for publication by your Head of Department. This applies in the UK, Australia, Canada, New Zealand and eleven other Commonwealth countries. For full information, see the Office of Public Sector Information guidelines: http://www.opsi.gov.uk/advice/crown-copyright/copyright-guidance/publication-of-articles-written-by-ministers-and-civil-servants

2. *If you are an officer or employee of the US Government*

   An Article prepared by an officer or employee of the US Federal Government does not enjoy copyright protection under US law; it is 'non-copyright', so there is no copyright to transfer. It is your responsibility to make the necessary enquiries and provide Inderscience with any form of words that is required for publication. Please note that this applies only to Federal, and not to state or local government employees.

If your research has been funded by a grant from a research funding agency, the funding grant may have had conditions attached to it that affect the transfer of copyright to Inderscience, or require you to post you Article to a repository. It is your responsibility to advise Inderscience of any such conditions and provide any documentation that may be required before publication.

Springer License for the manuscript "Use of Independent Rotation Field in the Large Displacement Analysis of Beams":

SPRINGER LICENSE
TERMS AND CONDITIONS

Jul 07, 2016

This Agreement between Michael Wallin ("You") and Springer ("Springer") consists of your license details and the terms and conditions provided by Springer and Copyright Clearance Center.

License Number	3903840039724
License date	Jul 07, 2016
Licensed Content Publisher	Springer
Licensed Content Publication	Nonlinear Dynamics
Licensed Content Title	Use of independent rotation field in the large displacement analysis of beams
Licensed Content Author	Jieyu Ding
Licensed Content Date	Jan 1, 2014
Licensed Content Volume Number	76
Licensed Content Issue Number	3
Type of Use	Thesis/Dissertation
Portion	Full text
Number of copies	1
Author of this Springer article	Yes and you are the sole author of the new work
Order reference number	
Title of your thesis / dissertation	FULLY COUPLED ANALYSIS OF LARGE SCALE TRACKED VEHICLE SYSTEMS WITH FLEXIBLE LINK CHAINS
Expected completion date	Jul 2016
Estimated size(pages)	120
Requestor Location	Michael Wallin 1754 E Lincoln Ave. DES PLAINES, IL 60018 United States Attn: Michael Wallin
Billing Type	Invoice
Billing Address	Michael Wallin 1754 E Lincoln Ave. DES PLAINES, IL 60018 United States Attn: Michael Wallin
Total	0.00 USD
Terms and Conditions	

Introduction

The publisher for this copyrighted material is Springer. By clicking "accept" in connection with completing this licensing transaction, you agree that the following terms and conditions apply to this transaction (along with the Billing and Payment terms and conditions established by Copyright Clearance Center, Inc. ("CCC"), at the time that you opened your Rightslink account and that are available at any time at http://myaccount.copyright.com).

Limited License

With reference to your request to reuse material on which Springer controls the copyright, permission is granted for the use indicated in your enquiry under the following conditions:

- Licenses are for one-time use only with a maximum distribution equal to the number stated in your request.
- Springer material represents original material which does not carry references to other sources. If the material in question appears with a credit to another source, this permission is not valid and authorization has to be obtained from the original copyright holder.
- This permission
• is non-exclusive
• is only valid if no personal rights, trademarks, or competitive products are infringed.
• explicitly excludes the right for derivatives.
- Springer does not supply original artwork or content.
- According to the format which you have selected, the following conditions apply accordingly:
• **Print and Electronic:** This License include use in electronic form provided it is password protected, on intranet, or CD-Rom/DVD or E-book/E-journal. It may not be republished in electronic open access.
• **Print:** This License excludes use in electronic form.
• **Electronic:** This License only pertains to use in electronic form provided it is password protected, on intranet, or CD-Rom/DVD or E-book/E-journal. It may not be republished in electronic open access.

For any electronic use not mentioned, please contact Springer at permissions.springer@spi-global.com.

- Although Springer controls the copyright to the material and is entitled to negotiate on rights, this license is only valid subject to courtesy information to the author (address is given in the article/chapter).
- If you are an STM Signatory or your work will be published by an STM Signatory and you are requesting to reuse figures/tables/illustrations or single text extracts, permission is granted according to STM Permissions Guidelines: http://www.stm-assoc.org/permissions-guidelines/

For any electronic use not mentioned in the Guidelines, please contact Springer at permissions.springer@spi-global.com. If you request to reuse more content than stipulated in the STM Permissions Guidelines, you will be charged a permission fee for the excess content.

Permission is valid upon payment of the fee as indicated in the licensing process. If permission is granted free of charge on this occasion, that does not prejudice any rights we might have to charge for reproduction of our copyrighted material in the future.

-If your request is for reuse in a Thesis, permission is granted free of charge under the following conditions:

This license is valid for one-time use only for the purpose of defending your thesis and with a maximum of 100 extra copies in paper. If the thesis is going to be published, permission needs to be reobtained.

- includes use in an electronic form, provided it is an author-created version of the thesis on his/her own website and his/her university's repository, including UMI (according to the definition on the Sherpa website: http://www.sherpa.ac.uk/romeo/);
- is subject to courtesy information to the co-author or corresponding author.

Geographic Rights: Scope
Licenses may be exercised anywhere in the world.
Altering/Modifying Material: Not Permitted
Figures, tables, and illustrations may be altered minimally to serve your work. You may not alter or modify text in any manner. Abbreviations, additions, deletions and/or any other alterations shall be made only with prior written authorization of the author(s).
Reservation of Rights
Springer reserves all rights not specifically granted in the combination of (i) the license details provided by you and accepted in the course of this licensing transaction and (ii) these terms and conditions and (iii) CCC's Billing and Payment terms and conditions.
License Contingent on Payment
While you may exercise the rights licensed immediately upon issuance of the license at the end of the licensing process for the transaction, provided that you have disclosed complete and accurate details of your proposed use, no license is finally effective unless and until full payment is received from you (either by Springer or by CCC) as provided in CCC's Billing and Payment terms and conditions. If full payment is not received by the date due, then any license preliminarily granted shall be deemed automatically revoked and shall be void as if never granted. Further, in the event that you breach any of these terms and conditions or any of CCC's Billing and Payment terms and conditions, the license is automatically revoked and shall be void as if never granted. Use of materials as described in a revoked license, as well as any use of the materials beyond the scope of an unrevoked license, may constitute copyright infringement and Springer reserves the right to take any and all action to protect its copyright in the materials.
Copyright Notice: Disclaimer
You must include the following copyright and permission notice in connection with any reproduction of the licensed material:
"Springer book/journal title, chapter/article title, volume, year of publication, page, name(s) of author(s), (original copyright notice as given in the publication in which the material was originally published) "With permission of Springer"
In case of use of a graph or illustration, the caption of the graph or illustration must be included, as it is indicated in the original publication.
Warranties: None
Springer makes no representations or warranties with respect to the licensed material and adopts on its own behalf the limitations and disclaimers established by CCC on its behalf in its Billing and Payment terms and conditions for this licensing transaction.
Indemnity
You hereby indemnify and agree to hold harmless Springer and CCC, and their respective officers, directors, employees and agents, from and against any and all claims arising out of your use of the licensed material other than as specifically authorized pursuant to this license.
No Transfer of License
This license is personal to you and may not be sublicensed, assigned, or transferred by you without Springer's written permission.
No Amendment Except in Writing
This license may not be amended except in a writing signed by both parties (or, in the case of Springer, by CCC on Springer's behalf).
Objection to Contrary Terms
Springer hereby objects to any terms contained in any purchase order, acknowledgment, check endorsement or other writing prepared by you, which terms are inconsistent with these terms and conditions or CCC's Billing and Payment terms and conditions. These terms and conditions, together with CCC's Billing and Payment terms and conditions (which are incorporated herein), comprise the entire agreement between you and Springer (and CCC) concerning this licensing transaction. In the event of any conflict between your obligations

established by these terms and conditions and those established by CCC's Billing and Payment terms and conditions, these terms and conditions shall control.

Jurisdiction

All disputes that may arise in connection with this present License, or the breach thereof, shall be settled exclusively by arbitration, to be held in the Federal Republic of Germany, in accordance with German law.

Other conditions:

V 12AUG2015

Questions? customercare@copyright.com or +1-855-239-3415 (toll free in the US) or +1-978-646-2777.

REFERENCES

1. Abbas, L. K., Rui, X., and Hammoudi, Z. S., 2010, "Plate/Shell Element of Variable Thickness Based on the Absolute Nodal Coordinate Formulation," *IMechE Journal of Multibody Dynamics*, Vol. 224, Part K, pp. 127-141.
2. Bando, K., Yoshida, K., Hori, K., 1991, "The Development of the Rubber Track for Small Size Bulldozers," International Off-Highway & Powerplant Congress & Exposition, Milwaukee, WI.
3. Bauchau, O. A., Damilano, G., Theron, N. J., 1995, "Numerical Integration of Nonlinear Elastic Multi-body Systems," *International Journal of Numerical Methods in Engineering*, Vol. 38, pp. 2727–2751.
4. Bauchau, O. A., Epple, A., Heo, S., 2008, "Interpolation of Finite Rotations in Flexible Multi-body Dynamics Simulations," *Journal of Multibody Dynamics*, Vol. 222, pp. 353–366.
5. Bauchau, O. A., Theron, N. J., 1996, "Energy Decaying Scheme for Non-linear Beam Models," *Computer Methods in Applied Mechanics and Engineering*, Vol. 134, pp. 37–56.
6. ayoumy, A. H., Nada, A. A., Megahed, S. M., 2013, "A Continuum Based Three-Dimensional Modeling of Wind Turbine Blades," *Journal of Computational and Nonlinear Dynamics*, Vol. 8(3), pp. 031004.
7. Belytschko, T., Schwer, L., Klein, M. L., 1977, "Large Displacement, Transient Analysis of Space Frames," *International Journal of Numerical Methods in Engineering*, Vol. 11(1), pp. 65-84.

8. Campanelli, M., Choi, J. C., and Shabana, A. A., 1998, “Chain Vibration and Dynamic Stress in Three-Dimensional Multibody Tracked Vehicles,” *Multibody System Dynamics*, Vol. 2, pp. 277-316.
9. Choi J. H., Lee H. C., and Shabana A. A., 1998, “Spatial Dynamics of Multibody Tracked Vehicles,” *Vehicle System Dynamics*, Vol. 29, pp. 27–49.
10. Crisfield, A. A., Jelenic, G., 1999, “Objectivity of Strain Measures in the Geometrically Exact Three-Dimensional Beam Theory and its Finite-Element Implementation,” *Proceedings of the Royal Society*, Vol. 455, pp. 1125–1147.
11. Dibold, M., Gerstmayr, J., and Irschik, H., 2009, “A Detailed Comparison of the Absolute Nodal Coordinate Formulation and Floating Frame of Reference Formulation in Deformable Multibody Systems,” *Journal of Computational and Nonlinear Dynamics*, Vol. 4, pp. 021006-1-021006-10.
12. Ding, Jieyu, Wallin, Michael, Wei, Cheng, Recuero, Antonio M., Shabana, Ahmed A., 2014, “Use of Independent Rotation Field in the Large Displacement Analysis of Beams,” *Journal of Computational and Nonlinear Dynamics*, Vol. 76(3), pp. 1829-1843.
13. Galaitsis, A. G., 1984, “Traxion: A Model for Predicting Dynamic Track Loads in Military Vehicles,” *Journal of Vibration, Stress and Reliability in Design*, Vol. 106, pp. 2816–291.
14. Gantoi, F. M., Shabana, A. A., Brown, M. A., 2013, “Finite Element Modeling of the Contact Geometry and Deformation in Biomechanics Applications,” *Journal of Computational and Nonlinear Dynamics*, Vol. 8(4), pp. 041013-01-041013-11.
15. Gerstmayr, J. and Shabana, A. A., 2006, "Analysis of Thin Beams and Cables Using the Absolute Nodal Coordinate Formulation," *Nonlinear Dynamics*, Vol. 45, pp. 109-30.

16. Gerstmayr, J., Sugiyama, H., Mikkola, A., 2013, "Review on the Absolute Nodal Coordinate Formulation for Large Deformation Analysis of Multibody Systems," *Journal of Computational and Nonlinear Dynamics*, Vol. 8(3), pp. 031016-01-031016-12.
17. Hamed, A. M., 2014, "New Finite Element Mesh for Efficient Modeling of Spatial Flexible Link Articulated Systems," PhD Dissertation, University of Illinois at Chicago, Chicago, IL.
18. Hamed, A. M., Jayakumar, P., Letherwood, M. D., Gorsich, D. J., Recuero, A. M., Shabana, A. A., 2015, "Ideal Compliant Joints and Integration of Computer Aided Design and Analysis," *Journal of Computational and Nonlinear Dynamics*, Vol. 10, pp. 021015-1-021015-14.
19. Irschik, H., Gerstmayr, J., 2009, "A Continuum Mechanics Based Derivation of Reissner's Large-Displacement Finite-Strain Beam Theory: The Case of Plane Deformations of Originally Straight Bernoulli–Euler Beams," *Acta Mechanica*, Vol. 206(1–2), pp. 1–21.
20. Irschik, H., Nader, M., Stangl, M., von Garssen, H.G., 2009, "A Floating Frame-of-Reference Formulation for Deformable Rotors using the Properties of Free Elastic Vibration Modes," Proceedings of the ASME 2009 International Design Engineering Technical Conferences and Computers and Information in Engineering Conference, ASME, San Diego, CA, US, DETC2009-86660.
21. Liu, C., Tian, Q., Hu, H. Y., 2011, "Dynamics of Large Scale Rigid-Flexible Multibody System Composed of Composite Laminated Plates," *Multibody System Dynamics*, Vol. 26, pp. 283-305.
22. M113: Image, A Troop 4/12 CAV, 2003,Web, 11 July 2012, http://www.atroop412cav.com/tools/ACAV/images/M113-drawing.gif

23. M113 Vehicle Family Rubber Track Installation Instructions: Litho'd, in Canada, 2003, 16 July 2012, www.combatreform.org/SoucyBandTrackInstallationA-654RB.pdf

24. Mohamed, A. A., 2013, "Three-Dimensional Fully Parameterized Triangular Plate Element Based on the Absolute Nodal Coordinate Formulation," *Journal of Computational and Nonlinear Dynamics*, Vol. 8(4), pp. 041016-01-041016-20.

25. Murray, M., Canfield, T. R., 1992, "Modeling of a Flexible Link Power Transmission System," Proceedings of the 6th ASME International Power Transmission and Gearing Conference, Scottsdale, Arizona.

26. Nachbaguaer, K., 2012, "Development of Shear and Cross Section Deformable Beam Finite Elements Applied to Large Deformation and Dynamics Problems," PhD Dissertation, Johannes Kepller University, Linz, Austria.

27. Nada, A. A., Hussein, B. A., Megahed, S. M., and Shabana, A. A., 2009, "Use of the Floating Frame of Reference Formulation in the Large Deformation Analysis: Experimental and Numerical Validation," *Journal of Multi-body Dynamics*, Vol. 224, pp. 45-58.

28. Nakanishi, T., Shabana, A.A., 1994, "Contact Forces in the Nonlinear Dynamic Analysis of Tracked Vehicles," *International Journal of Numerical Methods in Engineering*, Vol. 37, pp. 1251–1275.

29. Ozaki, T., Shabana, A. A., 2003, "Treatment of Constraints in Multibody Systems, Part I: Methods of Constrained Dynamics," *International Journal of Multiscale Computational Engineering*, Vol. 1, pp. 235–252.

30. Ozaki, T., Shabana, A. A., 2003, "Treatment of Constraints in Multibody Systems, Part II: Application to Tracked Vehicles," *International Journal of Multiscale Computational Engineering*, Vol. 1, pp. 253–276.

31. Olshevskiy, A., Dmitrochenko, O. and Kim, C. W., 2013, "Three-Dimensional Solid Brick Element Using Slopes in the Absolute Nodal Coordinate Formulation," *ASME Journal of Computational and Nonlinear Dynamics*, Vol. 9(2), pp. 021001-01-021001-10.
32. Przemieniecki, J. S., 1968, *Theory of Matrix Structural Analysis*, McGraw-Hill, New York.
33. Qin, H., 1996, "D-NURBS: A Physics-Based Framework for Geometric Design," *IEEE Transactions on Visualization and Computer Graphics*, Vol. 2(1), pp. 85–96.
34. Rathod, C., Shabana, A. A., 2006, "Rail Geometry and Euler Angles," *Journal of Computational and Nonlinear Dynamics*, Vol. 1, pp. 264–268.
35. Reissner, E., 1972, "On One-Dimensional Finite-Strain Seam Theory: The Plane Problem," *Journal of Applied Mathematics and Physics*, Vol. 23, pp. 795–804.
36. Reissner, E., 1973, "On a One-Dimensional Large-Displacement, Finite-Strain Beam Theory," *Studies in Applied Mathematics*, Vol. 52, pp. 87–95.
37. Roberson, R. E., and Schertassek, R., 1988, *Dynamics of Multibody Systems*, Springer, Berlin.
38. Romero, I., 2004, "The Interpolation of Rotations and its Application to Finite Element Models of Geometrically Exact Rods," *Computational Mechanics*, Vol. 34, pp. 121–133.
39. Romero, I., Armero, F., 2004, "An Objective Finite Element Approximation of the Kinematics of Geometrically Exact Rods and its use in the Formulation of an Energy–Momentum Conserving Scheme in Dynamics," *International Journal of Numerical Methods in Engineering*, Vol. 54, pp. 1683–1716.
40. Rubinstein, D., Hitron, R., 2004, "A Detailed Multi-body Model for Dynamic Simulation of Off-Road Tracked Vehicles," *Journal of Terramechanics*, Vol. 41, 163–173.

41. Ryu, H. S., Bae, D. S., Choi, J. H., and Shabana, A. A., 2000, "A Compliant Track Link Model for High-Speed, High-Mobility Tracked Vehicles," *International Journal for Numerical Methods in Engineering*, Vol. 48, pp. 1481-1502.

42. Ryu, H. S., Huh, K. S., Bae, D. S., and Choi, J. H., 2003, "Development of a Multibody Dynamics Simulation Tool for Tracked Vehicles Part I: Efficient Contact and Nonlinear Dynamics Modeling," *JSME International Journal*, Vol. 46(2), pp. 540-549.

43. Shabana, A.A., 1996, "Finite Element Incremental Approach and Exact Rigid Body Inertia," *Journal of Mechanical Design*, Vol. 118, pp. 171–178.

44. Shabana, A. A., 2012, *Computational Continuum Mechanics*, Cambridge University Press, New York.

45. Shabana, A. A., 2010, *Computational Dynamics*, Wiley, New York.

46. Shabana, A. A., 2010, "Uniqueness of the Geometric Representation in Large Rotation Finite Element Formulations," *Journal of Computational and Nonlinear Dynamics*, Vol. 5(4), pp. 044501-1–044501-5.

47. Shabana, A. A., 2014, *Dynamics of Multibody Systems*, Fourth Edition, Cambridge University Press, New York.

48. Shabana, A.A. and Schwertassek, R., 1998, "Equivalence of the Floating Frame of Reference Approach and Finite Element Formulations," *International Journal of Non-Linear Mechanics*, Vol. 33, pp. 417-432.

49. Shabana, A. A., Hamed, A. M., Mohamed, A. A., Jayakumar, P., and Letherwood, M. D. 2012, "Use of B-Spline in the Finite Element Analysis: Comparison with ANCF Geometry," *Journal of Computational and Nonlinear Dynamics*, Vol. 7, pp. 81-88.

50. Shabana, A. A., Zaazaa, K. E., Sugiyama, H., 2008, "Railroad Vehicle Dynamics: A Computational Approach," Taylor & Francis/CRC, Boca Raton.

51. Sherif, K., Irschik, H., Witteveen, W., 2012, "Transformation of Arbitrary Elastic Mode Shapes into Pseudo-Free-Surface and Rigid Body Modes for Multibody Dynamic Systems," *ASME Journal of Computational and Nonlinear Dynamics*, Vol. 7(2), pp. 021008-01-021008-10.

52. Sherif, K., Witteveen, W., Irschik, H., Holl, H., Mayrhofer, K., 2011, "On the Extension of Global Vibration Modes with Ritz-Vectors Needed for Local Effects," In: T. Proulx (ed.) Linking Models and Experiments, Volume 2, Proceedings of the 29th IMAC, A Conference on Structural Dynamics 2011, Vol. 4, pp. 37–46.

53. Sherif, K., Witteveen, W., Mayrhofer, K., 2012, "Quasi-Static Consideration of High Frequency Modes for more Efficient Flexible Multibody Simulations," *Acta Mechanica*, Vol. 223, pp. 1285–1305.

54. Simo, J.C., Vu-Quoc, L., 1986, "On the Dynamics of Flexible Beams under Large Overall Motions: The Plane Case, Part I and II," *Journal of Applied Mechanics*, Vol. 53, pp. 849–863.

55. Stanciulescu, I., Khude, N., Negrut, D., Melanz, D., 2013, "Efficient Parallel Simulation of Large Flexible Body Systems with Multiple Contacts," *Journal of Computational and Nonlinear Dynamics*, Vol. 8(4), pp. 041003-01-041003-11.

56. Theetten, A., Grisoni, L., Andriot, C., Barsky, B., 2008, "Geometrically Exact Dynamic Splines," *Computer Aided Design*, Vol. 40, pp. 35–48.

57. Tian, Q., Chen, L.P., Zhang, Y.Q., Yang, J.Z., 2009, “An Efficient Hybrid Method for Multibody Dynamics Simulation Based on Absolute Nodal Coordinate Formulation,” *ASME Journal of Computational and Nonlinear Dynamics*, Vol. 4, pp. 021009-1-021009-14.

58. Tian, Q., Zhang, Y., Chen, L., and Yang, J., 2010, “Simulation of Planar Flexible Multibody Systems with Clearance and Lubricated Revolute Joints,” *Nonlinear Dynamics*, Vol. 60, pp. 489-511.

59. Valentini, P. P., Pennestri, E., 2011, “Modeling Elastic Beams using Dynamic Splines,” *Multibody System Dynamics*, Vol. 25, pp. 271–284.

60. von Dombrowski. S., 1997, “Modellierung von Balken bei grossen Verformungen fur ein kraftreflektierendes Eingabegerat,” Diploma thesis, University Stuttgart, Stuttgart, Germany.

61. Wallin, Michael, Aboubakr, Ahmed K., Jayakumar, Paramsothy, Letherwood, Michael D., Gorsich, David J., Hamed, Ashraf, Shabana, Ahmed A., 2013, "A Comparative Study of Joint Formulations: Application to Multibody System Tracked Vehicles," Journal of Computational and Nonlinear Dynamics, Vol. 74(3), pp. 783-800.

62. Wallin, Michael, Hamed, Ashraf M., Paramsothy, Jayakumar, Gorsich, David J., Letherwood, Michael D., Shabana, Ahmed, A., 2016, “Evaluation of the Accuracy of the Rigid Body Approach in the Prediction of the Dynamic Stresses of Complex Multibody Systems,” *International Journal of Vehicle Performance*, Vol. 2(2), pp. 140-165.

63. Yamakawa, J. and Watanabe, K., 2004, “A Spatial Motion Analysis Model of Tracked Vehicles with Torsion Bar Type Suspension,” *Journal of Terramechanics*, Vol. 41, pp. 113-126.

64. Yoo, W. S., Dmitrochenko, O., and Pogorelov, D. Y. , 2005, “Review of Finite Elements using Absolute Nodal Coordinates for Large-Deformation Problems and Matching Physical

Experiments," Proceedings of the ASME International DETC and CIE Conference, 6:1285–1294.

65. Yoo, W. S., Lee, J. H., Sohn, S.J, Park, J. H., Pogorelov, D., and Dmitrochenko, O., 2004, "Large Deflection of a Thin Plate: Computer Simulation and Experiments," *Multibody System Dynamics*, Vol. 11, pp.185–208.

VITA

MICHAEL WALLIN

EDUCATION

- **Doctor of Philosophy, Mechanical Engineering, June 2016 (Expected),** University of Illinois at Chicago
- **Bachelor of Science, Mechanical Engineering, December 2011,** University of Illinois at Chicago

---

PROFESSIONAL EXPERIENCE

- **Research and Development Engineer | Computational Dynamics Inc., Berwyn, IL**
  March 2014 - Present

  Principal investigator work included supervising and meeting with other engineers, mapping current and future projects, contacting the contracting office, and applying for grants while working with the complex multibody software Sigma/Sams. Major multibody work included visualization of flexible bodies and post processing stress analysis including visualization of stresses and strains using the absolute nodal coordinate formulation (ANCF). Other work included parallelization within FORTRAN subroutines to increase computational efficiency and interface usability upgrades.
- **Research Assistant | Dynamic Simulations Laboratory, UIC, Chicago, IL**
  January 2010 – February 2014

  Developed and tested a complex multibody tracked vehicle model using different software codes including Sigma/Sams, RecurDyn, and ANSYS. Multiple tracked vehicles were developed with varying connections between track links such as ideal constrained, penalty method, compliant discrete element (bushing elements), and compliant continuum-based joints. The compliant continuum-based approach used flexible track links made up of ANCF finite elements. Compared uncoupled post-processing FFR stress analysis with the online fully couple ANCF stress analysis for a track link simulating through the track system of the same tracked vehicle model.
- **Teaching Assistant | UIC, Chicago, IL**
  January 2010 - May 2010

  Taught students subjects dealing with the design of machinery including: linkages, cams, gear trains and overall efficiency. Graded homework assignments and assisted students work with a simple multibody software dealing with 4-bar mechanisms.

PROFESSIONAL SERVICE

- Conference Reviewer | ASME IDETC/CIE 2014 **August 2014**
- Chairperson | CNDI 2016 **May 2016**

JOURNAL PUBLICATIONS

- Wallin, Michael, Aboubakr, Ahmed K., Jayakumar, Paramsothy, Letherwood, Michael D., Gorsich, David J., Hamed, Ashraf, Shabana, Ahmed A., 2013, "A Comparative Study of Joint Formulations: Application to Multibody System Tracked Vehicles," *Journal of Computational and Nonlinear Dynamics*, Vol. 74(3), pp. 783-800.
- Ding, Jieyu, Wallin, Michael, Wei, Cheng, Recuero, Antonio M., Shabana, Ahmed A., 2014, "Use of Independent Rotation Field in the Large Displacement Analysis of Beams," *Journal of Computational and Nonlinear Dynamics*, Vol. 76(3), pp. 1829-1843.
- Wallin, Michael, Hamed, Ashraf M., Paramsothy, Jayakumar, Gorsich, David J., Letherwood, Michael D., Shabana, Ahmed, A., 2016, "Evaluation of the Accuracy of the Rigid Body Approach in the Prediction of the Dynamic Stresses of Complex Multibody Systems," *International Journal of Vehicle Performance*, Vol. 2(2), pp. 140-165.

CONFERENCE REPORTS

- Wallin, Michael, Aboubakr, Ahmed K., Jayakumar, Paramsothy, Letherwood, Michael D., Shabana, Ahmed A., *Chain Dynamic Formulations for Multibody System Tracked Vehicles*: Presented at the Modeling and Simulation, Testing and Validation symposium at the Ground Vehicle Systems Engineering and Technology Symposium (GVSETS), Dearborn, MI, August 2012.
- Ding, Jieyu, Wallin, Michael, Wei, Cheng, Recuero, Antonio M., Shabana, Ahmed A., *On the Use of the Rotation Parameters in the Large Displacement Analysis of Beams*: European Congress on Computational Methods in Applied Sciences and Engineering (ECCOMAS), University of Zagreb, Croatia, July 1-4, 2013.
- Wallin, Michael, Aboubakr, Ahmed K., Jayakumar, Paramsothy, Letherwood, Michael D., Hamed, Ashraf, Shabana, Ahmed A., *Evaluation of Compliant Mechanical Joint Models: A Comparative Study*: European Congress on Computational Methods in Applied Sciences and Engineering (ECCOMAS), University of Zagreb, Croatia, July 1-4, 2013.
- Wallin, Michael, Hamed, Ashraf M., Jayakumar, Paramsothy, Letherwood, Michael, Gorsich, David J., Shabana, Ahmed A., *A Multibody System Approach for Modeling Rigid- and Flexible-Link Chain and Belt Drives*: Presented at the Society of Automotive Engineers Commercial Vehicle Engineering Congress (SAE COMVEC), Rosemont, IL, October, 2014.

CONFERENCE PUBLICATIONS

- Wallin, Michael, Aboubakr, Ahmed K., Jayakumar, Paramsothy, Letherwood, Michael D., Shabana, Ahmed A., *Chain Dynamic Formulations for Multibody System Tracked Vehicles*: published in the 2012 NDIA Ground Vehicle Systems Engineering and Technology Symposium (GVSETS), Dearborn, MI, August 2012.

TECHNICAL ACUMEN

- Multibody Simulation: Sigma/Sams, RecurDyn
- Finite Element Analysis: ANSYS, ABAQUS
- Computer Aided Design/Manufacturing: Pro/Engineer, SolidWorks, Autodesk 3DS Max
- Microsoft Office Suite: Word, Excel, PowerPoint
- Programming Languages: FORTRAN, VB.NET, MatLab, C++, OpenGL (drawing)

CITIZENSHIP

- US-born citizen